DOKUZ EYLÜL UNIVERSITY
GRADUATE SCHOOL OF NATURAL AND APPLIED SCIENCES

ANALYSIS OF OSCILLATORY DYNAMICS OF P53 NETWORK BASED ON REDUCED 2-D MODELS TO IDENTIFY THERAPEUTIC TARGETS FOR DEFICIENT P53 DYNAMICS

by

Gökhan DEMİRKIRAN

November, 2017

İZMİR

ANALYSIS OF OSCILLATORY DYNAMICS OF P53 NETWORK BASED ON REDUCED 2-D MODELS TO IDENTIFY THERAPEUTIC TARGETS FOR DEFICIENT P53 DYNAMICS

A Thesis Submitted to the
Graduate School of Natural and Applied Sciences of Dokuz Eylül University
In Partial Fulfillment of the Requirements for the Degree of Doctor of
Philosophy in Electrical and Electronics Engineering

by
Gökhan DEMİRKIRAN

November, 2017
İZMİR

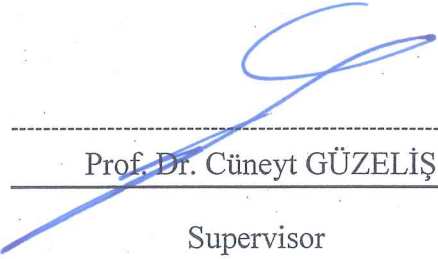## Ph.D. THESIS EXAMINATION RESULT FORM

We have read the thesis entitled **"ANALYSIS OF OSCILLATORY DYNAMICS OF P53 NETWORK BASED ON REDUCED 2-D MODELS TO IDENTIFY THERAPEUTIC TARGETS FOR DEFICIENT P53 DYNAMICS"** completed by **GÖKHAN DEMİRKIRAN** under supervision of **ASSIST. PROF. DR. GÜLESER KALAYCI DEMİR** and **PROF. DR. CÜNEYT GÜZELİŞ** we certify that in our opinion it is fully adequate, in scope and in quality, as a thesis for the degree of Doctor of Philosophy.

Assist. Prof. Dr. Güleser KALAYCI DEMİR

Supervisor

Prof. Dr. Cüneyt GÜZELİŞ

Supervisor

Prof. Dr. Levent Çavaş

Thesis Committee Member

Doç. Dr. Olcay Akay
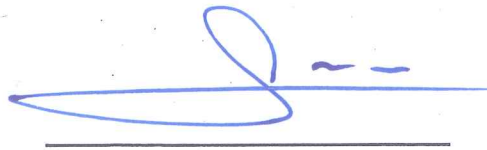
Thesis Committee Member

Doç. Dr. Barış Atakan

Examining Committee Member

Prof. Dr. Uğur Sezerman

Examining Committee Member

Prof. Dr. Kadriye ERTEKİN
Director
Graduate School of Natural and Applied Sciences

ACKNOWLEDGEMENTS

ANALYSIS OF OSCILLATORY DYNAMICS OF P53 NETWORK BASED ON REDUCED 2-D MODELS TO IDENTIFY THERAPEUTIC TARGETS FOR DEFICIENT P53 DYNAMICS

ABSTRACT

We propose a reduced 2-dimensional (2-D) oscillator model embedded inherently in the two-phase dynamics model and investigate the impact of p53 and its regulators on the decision of cell fate based on this reduced model. We show that the introduced 2-D model is an excitable relaxation oscillator and modes of this oscillator has the central role in determining the cell fate. By using the proposed 2-D model, we show that obstacles in using p53 inhibitors, e.g. Mdm2, to activate apoptotic pathway as a cancer therapeutic strategy may rise from the structure underlying relaxation oscillator. So, alternative approaches are suggested: Via computational studies, we identify Wip1 and P53DINP1 as targets of therapies for cancer caused by deficient p53 dynamics, which is in agreement with biological findings. We point out that most sensitive parameters correspond to well-known mutations of p53 network, such as ATM deficiency and Wip1 overexpression, indicating the novelty of the 2-D model. We also developed a novel canonical polynomial type 2-D relaxation oscillator model for p53 network such that analytical conditions on the parameters underlying each mode of the oscillator, accordingly outcomes of cell fate, is given. With the help of a developed coupling framework, we investigate the intercellular synchronization properties of p53 network using the proposed 2-D oscillator models and show that synchronization confers robustness against noise and genetic heterogeneity. We also developed a coupling framework between p53 network and circadian clock (CC) model. Using the framework, we show that CC has a positive effect on DNA damage response of the cell. A thorough understanding of the coupling between p53 network and CC is crucial in developing more effective therapy strategies for cancer, known as chronotherapy. The models and the frameworks proposed are considered as useful tools for mathematically exploring and understanding cell fate decision.

Keywords: ATM deficiency, cancer, canonical model, circadian clock, oscillator, p53 network, synchronization, two-phase dynamics, Wip1 overexpression

HASARLI P53 DİNAMİKLERİ İÇİN TEDAVİSEL HEDEFLERİN BELİRLENMESİ AMACIYLA P53 AĞININ OSİLASYON DİNAMİKLERİNİN İNDİRGENMİŞ İKİ BOYUTLU OSİLATÖRLER YARDIMIYLA ANALİZİ

ÖZ

Bu çalışmada, p53 ağının iki-fazlı dinamiğinin içerisinde saklı olan indirgenmiş 2-boyutlu (2-B) bir osilatör modeli sunulmuş, ayrıca p53 ve p53 düzenleyicilerinin hücre kaderine nasıl etki ettiği bu indirgenmiş modele dayalı olarak incelenmiştir. Bu iki boyutlu modelin bir gevşeme osilatörü olduğu ve bu osilatörün modlarının hücre kaderinin belirlenmesinde önemli bir role sahip olduğu gösterilmiştir. p53 inhibitörlerinin, örneğin Mdm2, kanser tedavisi olarak apoptosis yolağını aktive etmek amacıyla kullanılmasının zorluklarının, bu tip bir osilatörün yapısından kaynaklanabileceği gösterilmiştir. Dolayısıyla, alternatif yaklaşımlara ihtiyaç vardır: Hesapsal çalışmaların yardımıyla, Wip1 ve P53DINP1'in hasarlı p53 dinamiklerinin yol açtığı kanserin tedavisi için hedef proteinler olabileceği gösterilmiş ve biyolojik veriler ile de teyit edilmiştir. Modelin hassas parametreleri p53 ağı içerisindeki bilinen mutasyonlara denk gelmektedir ve bu bilgi modelin özgün değerini artırmaktadır. Ayrıca, p53 ağı için polinom tipi kanonik bir gevşeme osilatörü geliştirilmiştir. Bu geliştirilen osilatör yardımıyla hücre kaderi çıktılarını belirleyen parametrelerin analitik koşulları belirlenebilmiştir. Geliştirilen etkileşim yapısı yardımıyla, p53 ağının hücreler arası senkronizasyon özelliğinin gürültü ve genetik heterojenlik gibi bozucu etkilere karşı gürbüzlük sağladığı gösterilmiştir. Ayrıca p53 ağı ile sirkadiyen saatin (SS) etkileşimlerinin incelenebilmesi amacıyla bir etkileşim yapısı geliştirilmiştir ve bu sayede SS'in, hücrenin DNA kırığı cevabını destekleyici olduğu gösterilmiştir. Bu iki ağın etkileşimlerinin esaslı bir şekilde anlaşılabilmesi, kronoterapi gibi tedavilerin daha etkili hale getirilmesinde önemlidir. Önerilen modellerin ve yapıların, hücrenin kaderinin nasıl belirlendiğinin matematiksel olarak anlaşılması ve araştırılmasında yararlı araçlar olduğu düşünülmektedir.

Anahtar kelimeler: ATM bozukluğu, iki-fazlı dinamik, kanonik model, kanser, osilatör, p53 ağı, senkronizasyon, sirkadiyen saat, Wip1'in aşırı yüksek ifadesi

CONTENTS

LIST OF FIGURES

LIST OF TABLES

CHAPTER ONE
INTRODUCTION

Cell is a composition of interconnected systems that interact with each other directly or indirectly. Each of these systems processes information from the environment signals and act accordingly to realize its purpose. These systems in cells are called as gene regulatory networks (GRNs) or molecular regulatory networks. Very often, the biological function of these regulatory systems cannot be attributed to an individual gene or a product (Hartwell, Hopfield, Leibler, & Murray, 1999). In other words, the biological function of a GRN is intrinsic to the system, which can only be revealed if the system is investigated as a whole, i.e. via a holistic approach.

To understand GRNs in functioning level, a holistic approach that focuses on the complex interactions among the components of a biological process is needed rather than focusing on individuals in isolation. The difference between the holistic approach and the classical reductionist approach can be explained away by the radio metaphor given by Lazebnik (2002), which we engineers would relate. He suggests that a biologist who takes a reductionist approach would not truly understand how a radio works and would not be able to identify the functional roles of modular parts (such as amplifier, transformer) of a radio, by cataloguing the components (such as capacitors, resistors) according to their shapes, colours, etc. or by removing a certain component at a time. Thus, a quantitative methodology similar to the formalism that engineers use for designing a radio is needed for understanding GRNs in functioning level. Mathematical approaches have been applied to biology to address this issue and to reveal structures that have functioning roles like the modular arrangements in a radio. This new formalism of studying biology using mathematical instruments has been called as systems biology (or computational biology, or mathematical biology) and advances in this area have demonstrated that there are functional modular arrangements in these GRNs, which can be precisely modelled by mathematical models that can make predictions about the system dynamics (Alon, 2006; Tyson, Chen, & Novak, 2003).

One strategy to approach biology in systems level is to develop mathematical models describing the interactions between the components of a biological system. The interactions described very often come from several different wet lab experiments or by deduction (Marino, Hogue, Ray, & Kirschner, 2008). By developing a mathematical model, a computational analogue of a biological process is extracted, so that *in silico* experiments that are hard to realize in wet lab settings can be employed to understand the biological system better. Also, mathematical models reveal insights that cannot be derived from purely intuitive linguistic reasoning from experimental data (Miles MacLeod & Nersessian, 2015). With the analysis of the mathematical models, new emergent behaviors can be examined before going to wet lab and hypotheses to be tested in wet lab settings can be generated.

Mathematical models also provide mechanistic insights revealing how the information in a biological process is managed. Most of the time, complete biological knowledge about how the system functions and the interactions between the components are missing (Chou & Voit, 2009). Thus, the analysis of the mathematical models derived from the currently known interactions of a biological system can predict the missing nodes or point out the essential interactions that underlie the functioning of the process. Essential interactions may guide experimentalists to focus on the right structure, thus avoiding the structures that do not have a profound effect on the system. Since realizing a biological experiment is a time-consuming activity, the clues about essential interactions revealed by mathematical models may speed up the investigation of biological processes. This is especially vital for the diseases that await more efficient and effective cure strategies (e.g. cancer).

Translating from descriptions of biological interactions of a system to a mathematical model is a daunting task. Firstly, most of the time not all of the reactions of a biological process are known. Secondly, even the list of reactions are known, as this list gets longer, the interplay between the reactions become so complex that when an ordinary differential equation model is produced automatically from this list of reactions, the model does not work as expected (Soliman & Heiner, 2010). Thus, in developing a mathematical model, usually there is an expert view on which reactions

to include or on how to add some artificial parameters by approximations that are justified by the structure of the system (Lillacci & Khammash, 2009). In addition, large models include so many variables failing to identify the essential elements and to enhance the qualitative or mechanistic understanding of the system that a human mind can grasp. These large quantitative models with superfluous details are hard to handle, and analyses are usually restricted to simulations. Thus, it is inevitable to trade away detailed explanations by abstractions, approximations, or idealizations for the sake of mechanistic explanations.

Even a simple biological system contains many processes that act together and impossible to de-convolute (Voit & Chou, 2010). Thus, biological systems are overly complex and have redundant components (Nurse, 2008). To understand the biological systems in a qualitative mechanistic manner, sometimes we need to switch to a higher level where we do not need to involve every detail of molecule interactions, but instead think some chains of interactions as a signal that sends information to downstream systems (Bray, 1995) and include only essential parts (Sunnåker, Cedersund, & Jirstrand, 2011). Two approaches can be adopted in this manner. Complicated models can be simplified by making a reduction in model variables and parameters; or canonical models can be developed directly from the known topological structure of the interactions. These reduced models have been found more useful in providing information in comparison to the large models (Voit & Chou, 2010) due to the mechanistic explanations about overall system behaviour that these reduced models can provide (Brigandt, 2013; Craver, 2006). For instance, mathematical models such as Lotka-Volterra models (Lotka, 1910; Volterra, 1927), Goodwin model (Goodwin, 1965), and Fitzhugh-Nagumo model (FitzHugh, 1961) have been found very useful in this context. These approaches reveal valid predictions due the virtue of the modularity in biology, which allows for both investigations in molecular level and functional level.

Several methods have been proposed on how to reduce a higher dimensional mathematical model of a biological process, with the aim of gaining intuitive understanding in the functioning level (Erdrich & Ralf Steuer, 2015; Jonathan R. Karr,

2015; Shodhan Rao, 2013; Soliman & Heiner, 2010). Most common techniques are quasi-steady state approximations and the singular perturbation method (Rao, Schaft, Eunen, Bakker, & Jayawardhana, 2013). Automatic reduction methods are also proposed, mostly depending on the sensitivity of the parameters found by the global and local stability analyses. However, these automatic reduction methods are not reliable as the complexity increases, thus does not guarantee a reliable solution and have no standards.

In that spirit, the aim of this thesis is not to reproduce the exact numerical results of an experimental data or give a model for detailed interactions of a biological system, but rather to describe distinct dynamical behaviors of a biological system in a qualitative manner, namely p53 network, from a systems theory perspective. Besides, experimental studies in p53 network do not allow for such an approach due to the technological constraints in single cell studies. Nevertheless, the experimental studies that have been published so far allow for examining the behaviors in a qualitative (or mechanistic) sense, which one can justify using mathematical instruments by investigating the functional arrangements in the system. Thus, we rather ask the questions of what are the critical structures underlying these complex dynamics of p53 network and why the structure of the system is constructed in this way. The answer to that question is vital, because once an underlying structure for a specific function is understood, it is likely to reveal the design of other systems in which it reappears, even though the constituent elements of these systems are completely different (Alon, 2003; Rosenfeld, Elowitz, & Alon, 2002; Nurse, 2008).

In Chapter 2 of this thesis, we identify the 6-dimensional oscillator subsystem responsible for the three distinct behaviours of p53 network (low state, oscillations, and high state) in 17-dimensional two-phase dynamics model by (Zhang, Liu, & Wang, 2011). We show that this oscillator subsystem controls p53 dynamics and cell fate decision. Thus, a new modularity aspect emerges, in which p53 network is considered as a collective system that consists of an oscillator module and other modules that control this oscillator module to contribute to cell fate decision.

In Chapter 3, we reduce 17-dimensional two-phase dynamics model into a 2-dimensional (2-D) nonlinear oscillator model and interpret the three different behaviors of p53 dynamics from this oscillator perspective. We found that the oscillator is a relaxation type oscillator, which is abundantly found in biological systems, thus increasing the validity of the model.

In Chapter 4, we analyse the introduced 2-D nonlinear oscillator model with the aim of understanding two-phase dynamics better. The analysis on the introduced 2-D nonlinear oscillator model made corrections on the interpretation of the 17-dimensional model and developed a fruitful understanding of the two-phase mechanism. For instance, Mdm2 is known to be a p53 inhibitor. However, we have revealed that abundance of Mdm2 may increase the amplitude of p53 oscillations. The interpretation of this result is in agreement with wet lab results (Manfredi, 2010). Thus, we speculate that this counter-intuitive results may be one of the reasons for the complexity of cancer. We identify P53DINP1 as an accumulating protein that triggers the transition from oscillatory dynamics to a high state. We show that the role of PTEN feedback loop is to drive the concentration of p53 to higher levels in apoptosis.

We also explain the mechanism and the parameters that change characteristics of oscillations without using mathematical terms to a biologist such that he or she will be able to be guided by intuition without having to consult any numerical methods. Thus, he/she can generate his/her own hypothesis about p53 network dynamics regarding the relaxation oscillator perspective.

In Chapter 5, we show that deficient p53 dynamics can be posed as a two dimensional phase space problem using the reduced 2-D oscillator model. The approach of posing deficient p53 dynamics as a phase space problem is a novel mechanistic explanation to those cancer types caused by deficient p53 network dynamics. Using this introduced approach, we demonstrate that deficient p53 dynamics may result from the known mutations such as ATM deficiency, Wip1 overexpression, Mdm2 overexpression and Mdm2 downregulation. We show that these mutations drastically change the phase space of this oscillator and the healthy

state can be regained by some intervention strategies that we propose. Some of the proposed strategies are in agreement with biological findings and some of them need further experimental validations. Moreover, the effectiveness of Wip1 is emphasized regarding intervention strategies, which is consistent with biological findings that recently have proposed Wip1 as a novel target for cancer treatment. The proposed medical strategies for intervention of deficient p53 dynamics could clearly be seen by the analysis using the introduced phase space approach. However, derivation of these strategies from 17-dimensional two-phase model is cumbersome and sometimes intractable. Thus, we emphasize the need for low-dimensional mathematical explanatory models in cancer treatment.

We further discuss that the identified oscillator in p53 network may increase the complexity of cancer since the structure of this oscillator gives results that may seem confusing when studied via classical reductionist approach. Thus, the analysis of the model emphasizes the need for the holistic approach in biology, specifically in cancer. It must be noted that mathematical models in systems biology are never complete. The models are as good as they can provide new predictions and new hypotheses about the working of the system, which can be tested in wet lab settings. As new findings are revealed from p53 network experiments, the proposed 2-D mathematical model can be extended and used modularly.

It might also be noted that abstract explanatory models (e.g. 2-D oscillator model in our case) are accepted to be more useful in terms of control and manipulation (e.g. medical purposes) since the mechanistic explanations of these models provide information about how the system will behave in different circumstances. Due to the large-scale property (the proposed 2-D model is reduced from a 17-dimensional model and preserves its dynamics), the reduced model reduces the risk of neglecting the pathways that control overall dynamics, in comparison with the small connected models that focuses on one aspect of the biological network (Craver, 2006; Miles MacLeod & Nersessian, 2015).

In Chapter 6, we develop a novel 2-dimensional canonical model for two-phase dynamics of p53 network based on the knowledge gained from reducing the two-phase dynamics model and the biological evidence. The proposed canonical model is a relaxation oscillator that is abundantly found in biological systems. The importance of the proposed canonical model is that the analytical conditions underlying each behavior of p53 network are derived, which would be impossible to carry out in 2-D reduced oscillator model from previous chapters. This canonical model, too, is useful in posing those cancer types resulting from deficient p53 network dynamics as a phase space problem, as the previous 2-D model. The canonical model that allows for parametric local stability analysis is very useful in studying it in the context of nonlinear system dynamics, and not only study it via simulation tools. We also derive the role of timescale separation property in construction of relaxation oscillations as a closed form analytical expression. Although timescale separation is known to be vital for relaxation oscillations, to the best of our knowledge in the literature there is no analytical condition on the timescale separation for the existence of oscillations in a relaxation oscillator model without exhaustive assumptions.

In Chapter 7, we introduce a novel coupling framework for the investigation of the synchronization properties of the introduced two 2-D oscillator models. We show that synchronization aids cells in sustaining the p53 oscillations under disruptive conditions, such as noise and genetic heterogeneity. With numerically solving the coupled population of oscillators, we demonstrate that synchronization via coupling confers robustness against noise and genetic heterogeneity. Even, the coupling may help cells that cannot oscillate due to disruptive conditions to oscillate again.

In Chapter 8, we provide a novel framework for interaction between circadian clock and p53 network by integrating the relevant studies in the literature. Circadian clock is known to be an oscillator, which have a positive effect on DNA damage response of p53 network in wet lab experiments. With the provided framework, we show in mathematical terms that circadian clock can increase the amplitude of oscillations and mediate an easier initiation of apoptosis, thus helping p53 network with DNA damage response. This study here can be considered as the first steps of the

systems-level approach to the interaction between circadian clock and p53 network, which, to the best of our knowledge, has not been studied in the literature with mathematical models. A thorough understanding of the interaction between these systems will be helpful in improving the chronotherapy strategy for cancer patients. Also, we show that the interplay between p53 network and circadian clock can be studied as coupling of oscillators using the proposed framework, which would be very intriguing to study in the context of nonlinear systems theory as a future study.

In Chapter 9, we review the studies by highlighting the importance of key findings, proposed frameworks, and proposed models. We also give future directions based on the studies done in this thesis.

CHAPTER TWO

ISOLATION OF CORE OSCILLATOR SUBSYSTEM IN P53 NETWORK USING TWO-PHASE DYNAMICS MODEL

p53 network is a critical system that is studied thoroughly since the majority of human tumors occur due to the defects in this network (IARC TP53 Database, 2017). The gene in the center of this network is called as TP53 or P53, and the product of that gene is the protein p53[1]. p53 network is responsible for the DNA damage response of the cell. DNA damage occurs due to various reasons in the cell, such as hypoxia, telomere erosion, heat shock, ultraviolet (UV) radiation, and ionizing gamma irradiation (Murray-Zmijewski, Slee, & Lu, 2008). The understanding of how p53 network responds to these signals is important since cancer therapies, such as radiotherapy and chemotherapy, use this network to suppress tumour growth via apoptosis (programmed cell death). In this section and throughout this thesis, the primary consideration will be p53 network's response to ionizing gamma irradiation that causes Double Strand Breaks (DSBs) in DNA.

When DSBs occur in DNA, the cell stops growing to avoid passing damaged DNA to daughter cells while it tries to fix DSBs. If the damage is irreparable, then the cell initiate programmed cell death, so called apoptosis. If the damage is repaired, then the cell returns to normal cell cycle progression (i.e. the cell keeps growing until it divides). Thus, with the help of apoptosis, the cells with irreparable DNA damage are continuously removed from the organism.

2.1 Observation of Oscillations in p53 Network

The first evidence of p53 network exhibiting oscillatory dynamics has been shown by giving gamma irradiation to a cell population (Bar-Or, et al., 2000). In this experiment, p53 concentration performed damped oscillations, which was obtained by

---

[1] Usually the code names that start with capital letter represent the genes, whilst the code names that start with lower represent the gene products (i.e. protein). For example, P53 (also known as TP53) is the name of the gene, while p53 is the protein produced as a product of gene P53. Throughout the thesis, we use (P)53 gene with P being capital, but (p)53 dynamics with p being lower case, since the term "dynamics" is associated with concentration levels. Also common use is p53 network, not P53 network.

averaging over cell population. However, single cell studies have shown that it is actually an oscillation, which looks like damped oscillation due to shifts in synchronicity when averaged over a population of cells (Batchelor, Loewer, & Lahav, 2009; Lahav, et al., 2004).

p53 concentration shows a number of pulses, when the cell is exposed to gamma irradiation. As the level of gamma irradiation increases, the number of DSBs in DNA increases, and the time it takes to repair these DSBs also increases. Since p53 concentration oscillates until the repairing process finishes, there is a correlation between the number of pulses and the severity of DNA damage. It has been shown by experimental studies that the number of pulses, but not the amplitude and the period, depends on the level of gamma irradiation (Lahav, et al., 2004). These pulses have been called as "digital pulses."

An Ordinary Differential Equation (ODE) model is suggested by Bar-Or et al. (2000) to replicate damped oscillations, which considers the interaction between p53 and Mdm2 that is a protein which inhibits p53 activity. Even before the confirmation of sustained oscillations by Geva-Zatorsky et al. (2006), a mathematical model have been proposed by Tiana, Jensen, & Sneppen (2002) that replicates sustained oscillations. After the observation of digital pulses in p53 network, there have been a number of approaches that model this phenomenon. Tyson, Chen, & Novak (2003) proposed a mathematical model that shows oscillations, which depends on the p53 and Mdm2 interaction and Monk (2003) proposed a mathematical model that depends on the p53 and Mdm2 interaction together with a stiff time delay. Ciliberto, Novák, & Tyson (2005) suggested a mathematical model in which p53 concentration shows a series of pulses in a limit cycle such that the number of pulses depends on the irradiation level. Ma et al. (2005) proposed a model in which a stochastic DNA repair module activates ATM that evokes p53 oscillations. However, these mentioned models were proposed before Batchelor, Mock, Bhan, Loewer, & Lahav (2008) showed that Wip1 feedback loop is indispensable for the oscillations, but p53-Mdm2 interaction is dispensable. Thus, earlier models that depend on p53-Mdm2 interaction for oscillations are depreciated. However, the idea of modelling digital pulses as the

time spent in a limit cycle depending on the level of DNA damage, as Ciliberto et al. (2005) and Ma, et al., (2005) use in their models, is a practical method used by several modelers later (Sun & Cui, 2015). This practical method is also adopted by Zhang et al. (2011) in modeling two-phase dynamics of p53 network as will be detailed.

2.2 Control of Cell Fate via Two-phase Dynamics

The studies showed that oscillations of p53 concentration and sustained steady state of high p53 level[2] cause different cell fate decisions (Batchelor, Loewer, & Lahav, 2009; Batchelor, Loewer, Mock, & Lahav, 2011; Batchelor, Mock et al., 2008; Lahav, 2004; Lahav et al., 2004; Geva-Zatorsky et al., 2006; Purvis et al., 2012). Basal (low) p53 level indicates the normal growing conditions. Oscillation of p53 concentration is associated with cell cycle arrest (i.e. cell stops growing), whilst sustained high p53 level is associated with apoptosis, thus p53 dynamics directly influences cell fate. (Zhang et al., 2011) proposed a 17-dimensional mathematical model that is able to replicate p53 dynamics controlling cell fate. In their model, they describe the cell fate decision as a two-phase dynamics under DNA damage caused by gamma irradiation. The model by Zhang et al. (2011) is numerically solved to demonstrate two-phase dynamics as in Figure 2.1 (The ordinary differential equations defining the models are solved by ode45 solver available in MATLAB[3] numerical software environment). In the first phase, (active) p53 level oscillates giving a well-timed quanta of p53 until the damage is repaired. If the damage is not fixed in a certain amount of time (around in 1500 minutes), then the cell enters the second phase initiating apoptosis. In this second phase, p53 level rises to a steady state value higher enough to trigger caspase mechanism that is responsible for initiating apoptosis (Figure 2.1a). If the damage is fixed in a certain amount of time, then p53 level goes back to a basal steady state value without entering the second phase (Figure 2.1b). One hypothesis about the advantage of oscillations is that the oscillations in the first phase reduces the risk of having too much p53 and leading to premature cell death (Lahav, et al., 2004). The two-phase model by (Zhang et al., 2011) determines the cell fate depending on the duration -

---

[2] Sometimes the term "level" is used in place of "concentration" to emphasize the association with a qualitative distinct behavior.
[3] www.mathworks.com

accordingly severity- of DNA damage. The model successfully shows the oscillations of p53 level and the high p53 level in two distinct phases, so called two-phase dynamics.
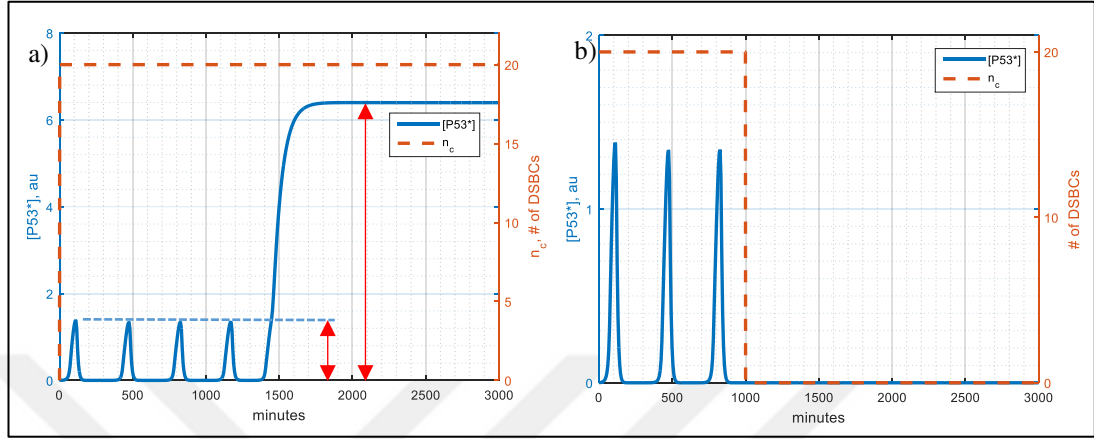
Figure 2.1 p53* (active p53) level exhibiting two-phase dynamics according to the model by (Zhang, Liu, & Wang, 2011). a) Two-phase dynamics is observed if n_c is kept as 20 for a long time (i.e. 1500 minutes). b) The second phase (apoptosis) is not observed, only the first phase is observed if n_c falls to zero before 1500 minutes

The model proposed by (Zhang et al., 2011) is interesting from the systems theory perspective, since it is capable of showing an equilibrium at a low level, oscillations, and an equilibrium at a high level. In addition, the high level of p53* (active p53) in the second phase, which indicates apoptosis, is higher than the maximum peaks of oscillations (Figure 2.1a). This fine distinction between the peaks of p53* oscillations in the first phase and constant high level of p53* in the second phase is thought to guarantee a more reliable decision of cell fate. Although model simulations are provided in the publication by (Zhang et al., 2011), the analytical explanations of how the model performs these three distinct behaviors, what are the determinants that are responsible for transient oscillatory regime, and how p53* goes to a level higher than the peaks of oscillations are missing due to the simple fact that the model they propose is a multidimensional model with several variables. Thus, the analysis of the model is restricted to only simulations, which can only give answers to limited questions. For example, showing a few pulses of p53* via a numerical simulation is not enough to show that there is actually an oscillation. It may be an oscillation with a very slow damping that may be unnoticed. In the coming sections, we extract the oscillator

subsystem and reduce it to two dimensions to show that it actually oscillates by using Poincaré -Bendixson Theorem.

2.3 Investigation of Two-phase Dynamics Model by Zhang et al. (2011)

In this section, the two-phase dynamics model by Zhang et al. (2011) is investigated to identify the subsystems in p53 network. Identifying subsystems will help the reduction process, and the extraction of essential modules. For this purpose, we illustrate the 17-dimensional two-phase model as a block diagram in MATLAB/Simulink environment, providing a systems-theoretical framework based on the differential equations as in Figure 2.2 (See Appendix-1 for two-phase model equations).

The block diagram of the 17-dimensional two-phase model is shown in Figure 2.2a. With the aid of the arrows, the state variables that subsystems share can easily be seen. Normally in biological areas, a model is sketched as a directed graph, where arrows indicate the activation of the process (See Figure 2.2b). However, in our illustration in Figure 2.2a, the arrows indicate the transfer of a state variable from one subsystem to the other.

To review the two-phase dynamics model by Zhang et al. (2011) in a concise way, we divide it into meaningful modular subsystems as in Figure 2.2a by inspection. Each subsystem numbered from 2 to 9 corresponds to a set of differential equations whilst repair subsystem numbered as 1 is a stochastic system. The subsystems we identify are 1) Repair subsystem, 2) ATM sensor subsystem (Equations A.1-A.3 in Appendix-1), 3) p53 subsystem (Equations A.4-A.7), 4) Wip1 subsystem (Equation A.17), 5) P53DINP1 subsystem (Equations A.15 and A.18), 6) PTEN subsystem (Equations A.11-A.14 and A.19), 7) Mdm2 subsystem (Equations A.8-A.10), 8) p21 subsystem (Equation A.20), 9-) Caspase subsystem (Equations A.21-A.23).

Moreover, three feedback loops can be identified by investigating the sharing of variables in the system in Figure 2.2a, which are also identified by Zhang et al. (2011): 1) ATM-p53-Wip1 feedback loop (Wip1 feedback loop) with the name of feedback

variable and as constituted by ATM sensor subsystem, p53 subsystem and Wip1 subsystem, 2) p53-PTEN-Akt-Mdm2 feedback loop (PTEN feedback loop) as constituted by P53DINP1 subsystem, PTEN subsystem and Mdm2 subsystem, and 3) the feedback loop between p53 subsystem and Mdm2 subsystem (p53-Mdm2 feedback loop). Differently from the paper by Zhang et al. (2011), the full two-phase model will be reviewed in light of these subsystems that we identified with modular perspective by emphasizing the key points that will be helpful for discussions in the next chapters.
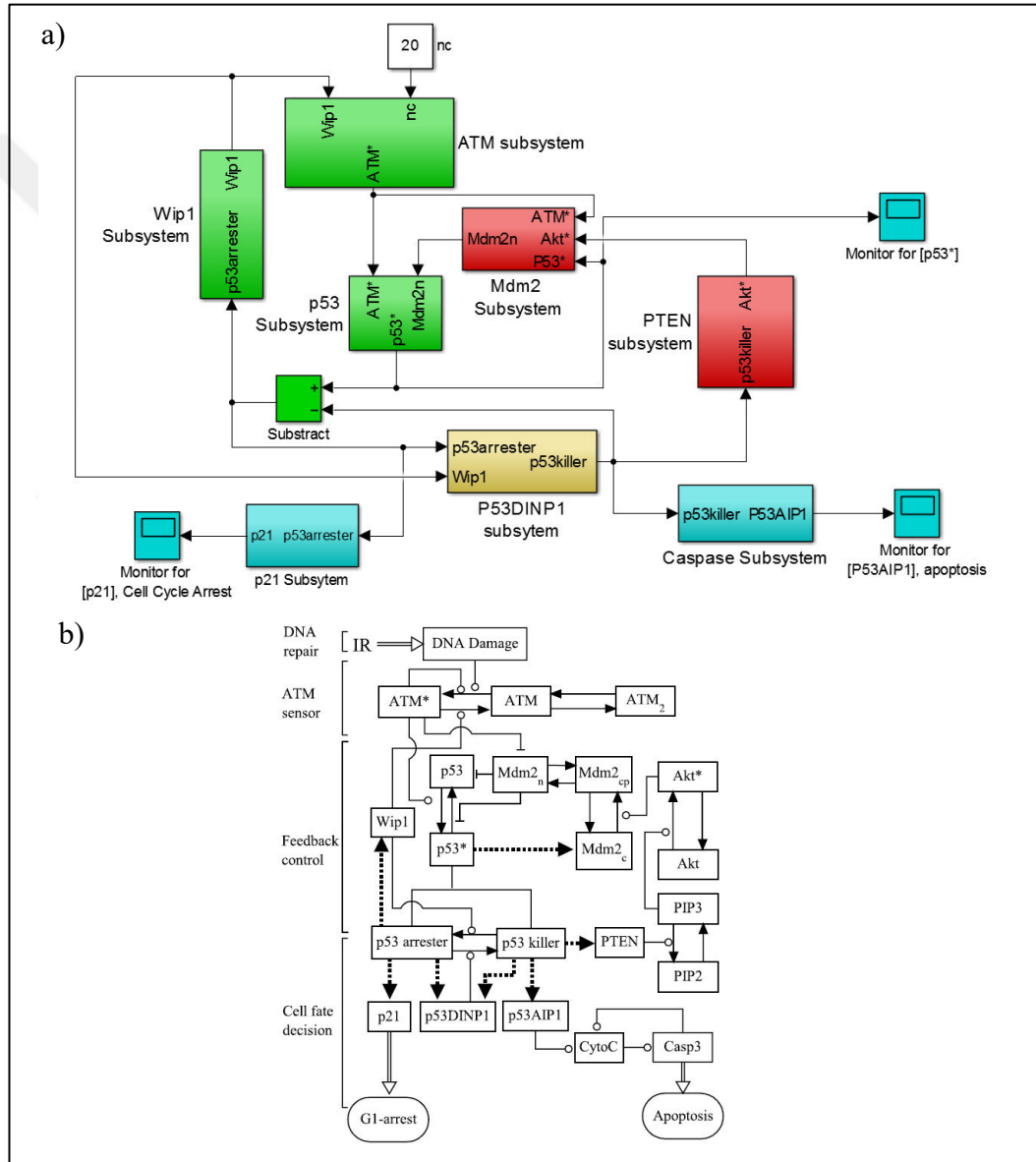
Figure 2.2 Representations of 17-dimensional two-phase model by Zhang et al. (2011). a) Our representation with subsystems in Matlab/Simulink. b) Schematic representation by Zhang et al. (2011)

1) Repair subsystem: Given the gamma radiation to the p53 network, random number of double-strand breaks (DSBs) is formed based on the radiation dose (Stewart, 2001; Ma et al., 2005). Initial number of DSBs obeys a Poisson distribution whose average is proportional to the radiation dose. After the DSBs occur in DNA, repair molecules try to fix them by forming a DSB-repair protein complex (DSBCs). Repair mechanism in the paper by Zhang et al. (2011) is based on the 2-lesion kinetic model by Ma et al. (2005). In 2-lesion kinetic model, damage in DNA is repaired by as low as 20 repair molecules, and the the number of DSBs is reduced as they are repaired by repair molecules by a stochastic simulation (as shown in Figure 2.3a,b) while the model equations (A.1-A.23 in Appendix 1) are solved numerically at the same time. The parameter n_c indicates the number of (DSBCs) DSB-repair protein complexes. Since the number of repair proteins are 20, the number of DSBCs (i.e. n_c) at any time cannot exceed 20 (Figure 2.3a). Thus, in a full repair activity, i.e. all repair molecules are assigned to a DSB, maximum of 20 DSBCs may exist. When a repair molecule finishes repairing a DSB, it is assigned to another DSB so that all DSBs can be repaired. For analytical purposes, in the next sessions we avoid n_c taking random values. Instead, we assume two values of n_c for simplicity: 20 DSBCs ($n_c = 20$) for damage, zero DSBC ($n_c = 0$) for no damage. Figure 2.3a shows our approximation to a simulated stochastic repair system. Although (Zhang, Liu, & Wang, 2011) shares a pseudocode based on a Monte Carlo simulation for the stochastic repair system, we replicate the simulations based on Gillespie Algorithm that is a type of Monte Carlo simulation, which is known to provide an exact stochastic simulation of biochemical processes (Gillespie, 1977). The Matlab code employing Gillespie Algorithm for the stochastic simulation of 2-lesion kinetic model is provided in Appendix-2.
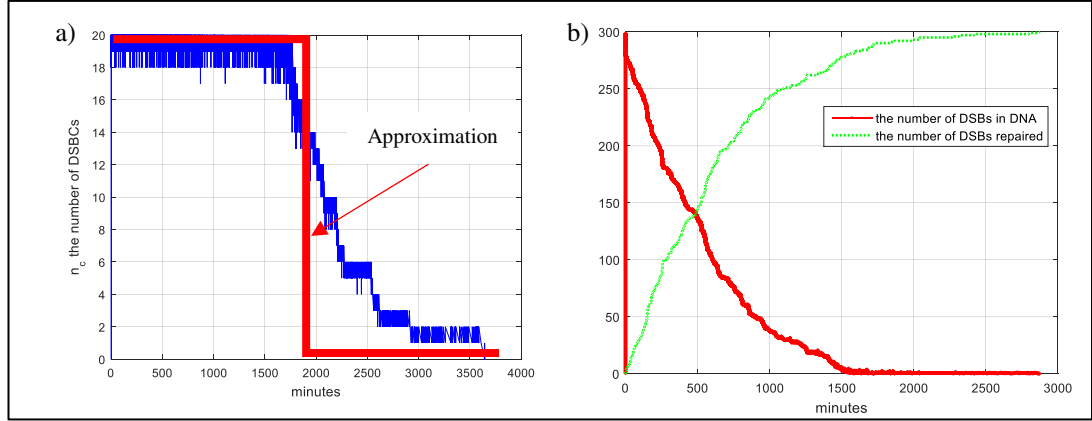
Figure 2.3 Stochastic repair subsystem is simulated by employing Gillespie Algorithm. The initial number of 300 DSBs in DNA is assumed. a) The change of n_c (the number of DSBCs) is illustrated, which can be approximated by a step-like change b) The change of remaining DSBs and the repaired DSBs are illustrated

2)   ATM sensor subsystem: ATM sensor subsystem consists of phosphorylated monomer (active) ATM*, inactive monomer ATM and inactive dimer ATM_2. ATM is activated by n_c, the number of DSBCs.   The activation of ATM by DSBCs is characterized by n_c-dependent ATM activation rate, and inhibition of ATM by Wip1 is represented in the deactivation rate of ATM (See Equations A.1-A.3 in Appendix 1).

3)   p53 subsystem: p53 subsystem consists of inactive p53 and active (phosphorylated) p53*. ATM* (active (phosphorylated) ATM) activates P53 by two ways: (i) Phosphorylating p53 to disassociate it from its inhibitor, Mdm2, and (ii) Degrading Mdm2 by phosphorylating Mdm2. As shown in Figure 2.2a, ATM* enters both p53 subsystem and Mdm2 subsystem. In two-phase model, p53* is categorized into p53arrester and p53killer. p53arrester is a form of p53* which are phosphorylated on ser15/20 by ATM*, while p53killer is a form of p53* which is phosphorylated on ser46 in addition to ser15/20. Phosphorylation on the region ser15/20 of p53 induces cell cycle arrest while phosphorylation on the region ser46 in addition to ser15/20 induces apoptosis. Phosphorylation on the region ser15/20 is mediated by ATM*, whilst phosphorylation on ser46 is mediated by P53DINP1. Total concentration of p53* is the sum of the concentrations of p53arrester and p53killer in the environment. In the 17-dimensional two-phase model, concentration of p53killer and p53* are

determined by Equations A.15 and A.6 respectively, whilst concentration of p53arrester is simply the difference between p53* and p53killer as indicated by Equation A.16.

4) **p21 subsystem:** Concentration of p21 level is in direct correlation with p53arrester level. The oscillation of p53arrester level reflects on p21 level and cell cycle is arrested to avoid passing of damaged DNA to daughter cells. Oscillations of p21 level is assumed as the indicator of cell cycle arrest.

5) **Wip1 subsystem:** Wip1 is the target of p53arrester. Wip1 level increases by p53arrester, but not p53killer. Elevated Wip1 level greatly inhibits ATM* activity, even in the presence of DNA damage. Wip1 also enhances the P53DINP1 level.

6) **P53DINP1 subsystem:** P53DINP1 module is activated by p53arrester, Wip1, and p53killer. p53arresters are turned into p53killers by P53DINP1 via phosphorylation on ser46. The oscillation in the network promotes the accumulation of P53DINP1. After P53DINP1 passes an intrinsic threshold value, its activity greatly effects the network: Concentration of p53arrester drops to such a low value that ATM-p53-Wip1 feedback loop shuts off and oscillations stop. We will show that P53DINP1 is an oscillation accumulation triggered protein and its role in triggering the second phase has not referred in the paper by Zhang et al. (2011).

7) **PTEN subsystem:** PTEN subsystem becomes dominant in the second phase. In the second phase, p53killer level increases PTEN level. Enhanced PTEN level then deactivates Akt*, and decreasing of Akt* level also decreases $Mdm2_n$ level which in turn increases the constant high level of p53* in the second phase. PTEN feedback is important for elevating sustained p53* level to a higher value than the peaks of p53* level oscillation. There is a sequential predominance of Wip1 feedback and PTEN feedback loops. In the first phase, Wip1 feedback loop is dominant; in the second phase, Wip1 feedback loop shuts off and PTEN feedback loop becomes dominant.

8) **Mdm2 subsystem:** In the second phase, PTEN subsystem decreases $Mdm2_n$ level to drive p53* level to a higher steady state value than the peaks of p53* oscillation. The central role of Mdm2 subsystem is in the second phase, so in the first phase, Mdm2 subsystem dynamics can be ignored. It has been shown by Zhang et al. (2011) in their model and by Batchelor, Mock et al. (2008) in wet lab experiment that p53-Mdm2 feedback loop is not responsible for oscillations. It is thought to be for fine-tuning the oscillations.

9) **Caspase subsystem:** Caspase subsystem is activated by a high steady state level of p53killers. The peaks of p53killer oscillation in the first phase are not sufficient to activate caspase subsystem. The high steady state of Casp3 level is assumed to trigger apoptosis.

2.4 Recognition of the Core Oscillator Subsystem in 17-dimensional Two-phase Model

This section is devoted to the recognition of the core oscillator subsystem of 6-dimensional via segregation of the subsystems, which underpins the oscillatory dynamics of 17-dimensional two-phase model . It should be first noted that ATM-p53-Wip1 feedback loop (ATM sensor subsystem, p53 subsystem and Wip1 subsystem in Figure 2.2a) is responsible for the oscillations in the first phase, while p53-PTEN-Mdm2 (p53 subsystem, PTEN subsystem and Mdm2 subsystem in Figure 2.2a) feedback loop becomes dominant in the second phase. Since there is a sequential predominance of feedback loops, to analyze the oscillations in the first phase, PTEN feedback loop can be ignored for the sake of simplicity as also suggested by Zhang et al. (2011).

Focusing on the first phase, core oscillator subsystem of p53 network can be extracted by isolating Wip1 feedback loop from PTEN feedback loop. To do so, we keep the state variables, [p53killer][4] and [$Mdm2_n$], that are passed from red blocks as constant (Figure 2.2a). The roles of [p53killer] and [$Mdm2_n$] become important in the

---

[4] Square brackets [ ] refers to the concentration of a protein. Sometimes, instead of using the term "concentration", the term "level" is used. For example, p53 level or [p53].

second phase. We set [Mdm2$_n$] as constant at its prescribed initial value of 0.26 and [p53killer] at its prescribed initial value of zero. It is observed from our simulations that the small deviations in these two parameters do not change the qualitative behavior of the first phase dynamics (i.e. oscillations). It can be seen from Figure 2.2a that p21 subsystem and caspase subsystem do not provide any feedback signal to the p53 network, having no effect on qualitative p53 dynamics, so they can be ignored too. Table 2.1 presents the resulting isolated subsystem that is the core oscillator subsystem of 17-dimensional two-phase model.

Table 2.1 Isolated oscillator subsystem in 17-dimensional model of two-phase dynamics (See (Zhang, Liu, & Wang, 2011) for parameter definitions and values)

Equation number	Equations
1	$\frac{d[ATM_2]}{dt} = 0.5 * k_{dim}[ATM]^2 - k_{undim}[ATM_2]$
2	$\frac{d[ATM^*]}{dt} = k_{acatm}\frac{n_c}{n_c+j_{nc}}[ATM^*]\frac{[ATM]}{([ATM]+j_{acatm})} - k_{deatm}(1+[Wip1])\frac{[ATM^*]}{([ATM^*]+j_{deatm})}$
3	$\frac{d[p53^*]}{dt} = k_{acp531}\frac{[ATM^*]}{([ATM^*]+j_{atm})}[p53] - k_{dep53}[p53^*] - k_{dp53s}[Mdm2_n]\frac{[p53^*]}{j_{1p53n}+[p53^*]}$
4	$\frac{d[p53]}{dt} = k_{sp53} - k_{dp53n}[p53] - k_{dp53}[Mdm2_n]\frac{[p53]}{j_{1p53n}+[p53]} - k_{acp53}[p53] + k_{dep53}[p53^*]$
5	$\frac{d[Wip1]}{dt} = k_{swip10} + k_{swip1}\frac{[p53arrester]^3}{(j_{swip1}{}^3+[p53arrester]^3)} - k_{dpwip1}[Wip1]$
6	$\frac{d[Mdm2_n]}{dt} = k_i[Mdm2_{cp}] - k_0[Mdm2_n] - k_{dmdm2n}[Mdm2_n]$
7	$[ATM] = ATM_{tot} - 2[ATM_2] - [ATM^*]$
8	$k_{dmdm2n} = k_{dmdm2n0} + k_{dmdm2n1}\frac{[ATM^*]}{([ATM^*]+j_{atm})}$
9	$[p53^*] = [p53arrester] + [p53killer]$

Table 2.2 Parameters underlying the three modes of isolated core oscillator subsystem

	p53* dynamics	n_c	Equation 9 in Table 1
1.	Low steady state of [p53*]	0	[p53*] = [p53arrester] + [p53killer]
2.	Oscillations of [p53*]	20	[p53*] = [p53arrester] + [p53killer]
3.	High steady state of [p53*]	20	[p53*] = [p53killer]; [p53arrester]=0;

As depicted in Figure 2.4, the obtained 6-dimensional oscillator subsystem is able to show all of the three modes, namely the equilibrium at the low level of [p53*], the oscillation and the equilibrium at the high level of [p53*], depending on the value of n_c and the [p53killer] and [p53arrester] as summarized in Table 2.2. It should be

noticed that, in 17-dimensional two-phase model, the value of n_c, [p53arrester], and [p53killer] are controlled by other subsystems. Thus, we provide a modular perspective to the two-phase dynamics of p53 network. In this modular perspective, an oscillator is at the center of the p53 network and other subsystems influence this oscillator by various parameters as illustrated in Figure 2.5.

In the high equilibrium case of 6-dimensional model (See Figure 2.4b), the high level is not as high as in Figure 2.1a, where we numerically solved the whole 17-dimensional model. The reason is discarding of PTEN feedback loop whose function is to shift the high equilibrium to higher levels in two-phase model. However, we demonstrated that 6-dimensional model exhibits the same qualitative behaviors as 17-dimensional two-phase model.
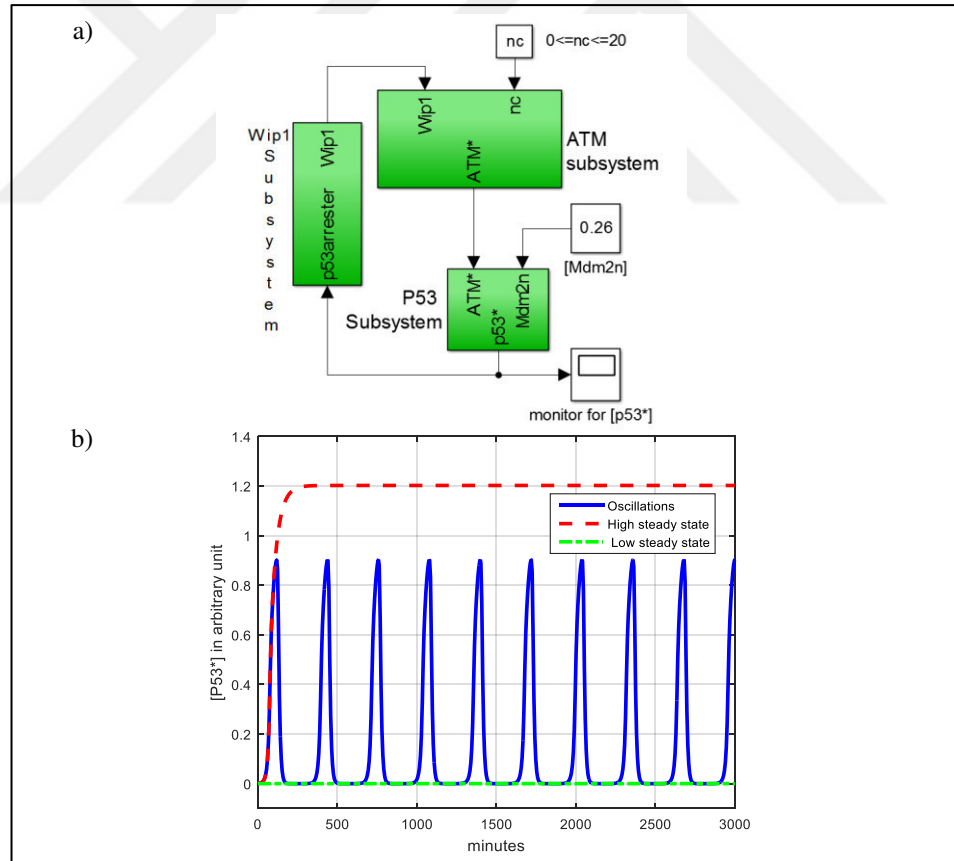
Figure 2.4 The core oscillator subsystem in Table 2.1. a) The oscillator subsystem in 17-dimensional two-phase model is identified, isolated and illustrated in Matlab/Simulink. b) The identified oscillator subsystem is numerically solved for three different set of parameters indicated in Table 2.2, to demonstrate three modes of p53 dynamics
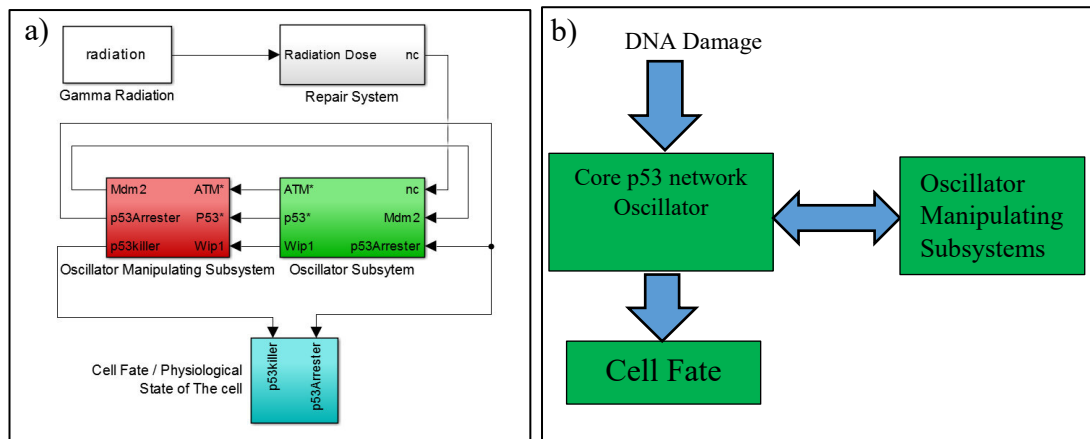
Figure 2.5 Representing p53 network from the modular perspective such that there is a core oscillator subsystem in the centre of the network and other subsystems manipulate the oscillator to control cell fate. a) Modular representation via Matlab/Simulink. b) Modular schematic representation

CHAPTER THREE
DIMENSIONALITY REDUCTION AND ANALYSIS

In 17-dimensional two-phase model of p53 network, different p53 dynamics result in different consequences: Oscillation of p53arrester level results in cell cycle arrest via stimulating p21 (Batchelor, Mock et al., 2008; Gartel & Radhakrishnan, 2005), high steady state of p53killer level results in apoptosis via stimulating caspase mechanism (Essmann, Engels, Totzke, Schulze-Osthoff, & Jänicke, 2004; Marchenko, Zaika, & Moll, 2000; Mihara, et al., 2003), and low level of p53 is the indicator of normal cell cycle progression (Michael & Oren, 2003). These consequences of the two-phase dynamics can be correlated to the p53 levels and a few other variables such as [ATM*] and [Wip1] only rather than a variety of highly possibly superfluous variables by getting rid of downstream elements, which is consistent with biological findings (Purvis et al., 2012). One of the main aims of this thesis is to introduce a 2-dimensional (2-D) model that solely describes these modes of p53 dynamics in a compact and efficient way ignoring non-essential components. The idea behind this observation of the possibility of reducing 17-dimensional model into 2-D model relies on the fact that any continuous time integer dimensional dynamical system is, in some sense, qualitatively equivalent to an oscillatory 2-D dynamical system.

3.1 Reduction to 2-dimensional Model

Reduction of high order systems into low order ones is done to simplify complex systems for the purpose of easy analysis and understanding essential components of the systems. In a successful reduction, the simplified system displays the same qualitative behavior with a smaller number of state variables and parameters. This subsection introduces a reduced 2-D differential equations model of ATM and Wip1 variables, which possesses the same qualitative behavior with that of 6-dimensional isolated oscillator subsystem described in Section 2.4. The obtained 2-D model is given in Table 3.1 and details of the reduction process are given in Appendix-3. In our 2-D model, ATM directly signals to Wip1 via algebraic [p53*] equation (i.e. Equation 3 of Table 3.1). With appropriate settings of parameters given in Table 2.2, this simple model of ATM and Wip1 successfully elucidates the three modes of p53 dynamics,

namely the modes of low [p53*] level, [p53*] oscillations, and high [p53*] level. (See Figure 3.1c-d for the time evolutions of [p53*], [ATM*] and [Wip1] in the three modes of the introduced 2-D model, and Figure 3.1a-b for those of the 6-dimensional model.) The reduced 2-D model successfully inherits the qualitative behavior of the two-phase dynamics of the Zhang's model (Zhang et al., 2011) with an expense of the changes in the amplitude and frequency of the signals. It should be noted that the original amplitude and frequency might be reconstructed by scaling the time and range of the variables. However, this is not our concern here.

The proposed simplification of the Zhang's model down to the network of ATM and Wip1 variables is in agreement with the experimental work by (Shreeram et al., 2006) in which they show that the mutual relationship between ATM and Wip1 plays an important role in tumorigenesis. In the 2-D model, we characterize [p53*] as with an algebraic equation in a way that it has a few but operationally well-defined parameters (See Equation 3 of Table 3.1). While [p53*] is inversely correlated with [Mdm2$_n$], it is directly proportional to [ATM*] (i.e. phosphorylated ATM). Therefore, the ATM dynamics reflects on [p53*]. [p53*] oscillates whenever [ATM*] oscillates. When [ATM*] is in high or low steady state, [p53*] is at a high or low level, respectively. This is also consistent with the experimental observation that ATM is the main upstream signal of p53 dynamics and p53 pulses originate from recurrent initiation of ATM (Batchelor, Mock et al., 2008). The number of DSBCs (i.e. n$_c$) is an external stimulus that starts the oscillations.

Table 3.1 The introduced 2-dimensional oscillator model of two-phase dynamics

Equation number	Equations
1	$\frac{d[ATM^*]}{dt} = k_{acatm}\ \frac{n_c}{(n_c + jn_c)}[ATM^*]\ \frac{\sqrt{0.1(ATM_{tot}-[ATM^*])}}{(\sqrt{0.1(ATM_{tot}-[ATM^*])}\ + jacatm)} - k_{deatm}\ \frac{(1+[Wip1])[ATM^*]}{([ATM^*]+j_{deatm})}$
2	$\frac{d[Wip1]}{dt} = k_{swip10} + k_{swip1}\frac{[p53Arrester]^3}{(j_{swip1}{}^3+[p53Arrester]^3)} - k_{dwip1}[Wip1]$
3	$[p53^*] = [p53arrester] + [p53killer] = [ATM^*](1.5 - 3.947[Mdm2_n])$

Both models (the identified 6-dimensional oscillator subsystem and the introduced 2-D oscillator) is able to show three qualitative behaviors: 1) low steady state of [p53*]

when there is no DSBC activity, 2) oscillations of [p53*] in case of DSBCs, 3) high steady state of [p53*] when p53arrester is zero and there is DSBC activity. In case of 3), [p53*] consists of p53killers only, since p53arrester is zero. The models are compared in Figure 3.1. In Figure 3.1a, 6-dimensional oscillator model is numerically solved for the cases of $n_c = 20$ and $n_c = 0$. When n_c is 20 indicating a high DSBC activity, [p53*] starts to oscillate. When n_c is 0, [p53*] stays at a low steady state. In Figure 3.1b, 6-dimensional model is numerically simulated to demonstrate the case of apoptosis as a two-phase dynamics. When n_c is 20, [p53*] starts to oscillate. After 750 minutes passed, [p53arrester] is made zero in the solver algorithm to indicate that all p53* consists of p53killer. In this case, [p53*] value goes to a high steady state. It must be noted that the ratio of p53arrester and p53killer is controlled by P53DINP1 subsystem in the 17-dimensional two-phase model. Here, these effects of P53DINP1 subsystem is simulated by changing the ratio of p53arrester and p53killer at appropriate times by the algorithm. Also, in apoptosis it must be noted that there is not a fine distinction between the high steady state of [p53*] and the peaks of oscillations (See Figure 3.1b,d) . This is due to the fact that, highest level of [p53*] in the second phase is determined by [$Mdm2_n$] via PTEN feedback loop. In this simulation, since we keep [$Mdm2_n$] as constant, its effect on the highest level of p53* is not seen.

In Figure 3.1c, the introduced 2-D oscillator model is numerically solved for the cases of $n_c = 20$ and $n_c = 0$. [p53*] oscillates when $n_c = 20$. It must be noted that there are negligible inaccuracies in the amplitude and frequency of the signals because of the approximations done in the reduction process. The period of oscillations and the amplitudes can be fine-tuned by changing appropriate parameters. However, this is not the concern here. The reduced model successfully inherits the qualitative behaviour of the 17-dimensional model by Zhang et al. (2011). In Figure 3.1d, 2-D model is numerically solved to demonstrate the case of apoptosis. It successfully shows the high equilibrium behaviour of [p53*] for appropriate parameter settings that would be set by other modules in p53 network, but here we set them by the algorithm (See Table 2.2).
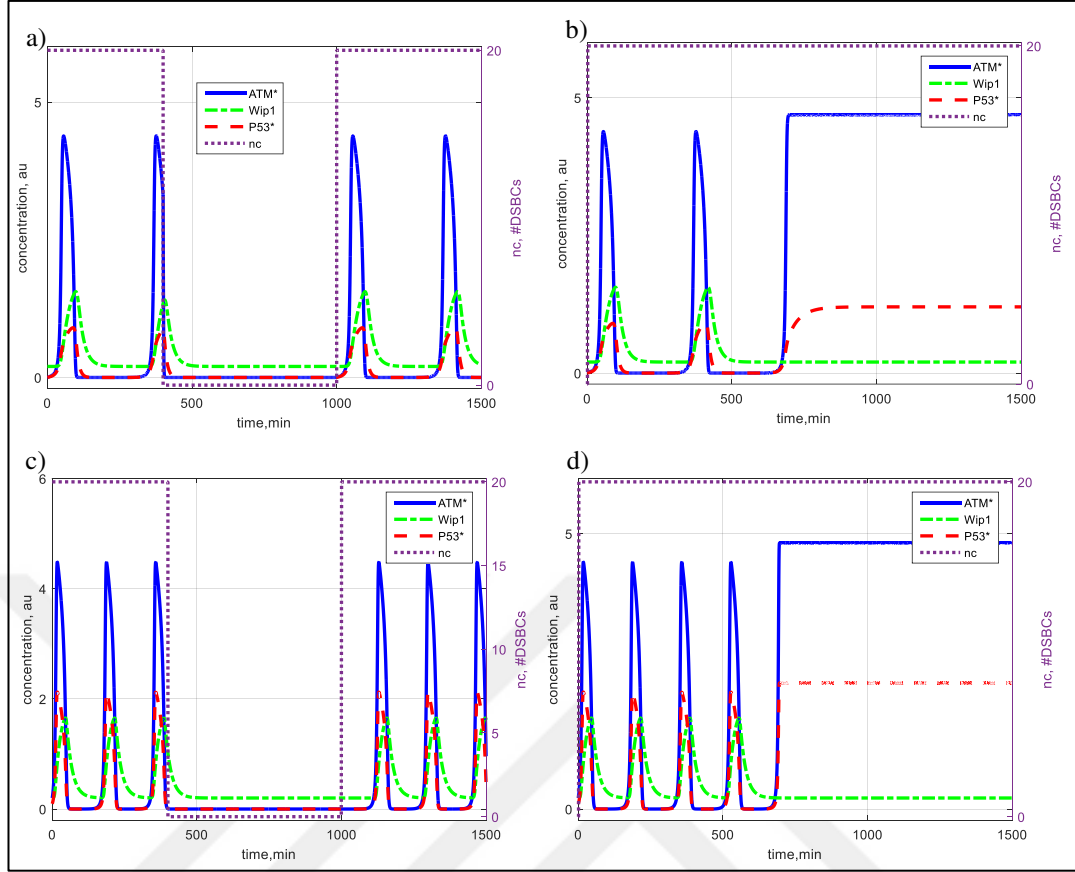
Figure 3.1 Comparison of reduced 2-D ATM-Wip1 oscillator and 6-dimensional identified oscillator subsystem for various n_c values. a) 6-dimensional oscillator subsystem showing oscillations as well as recovery of low level [p53*] mode after DNA damage is repaired. b) 6-dimensional oscillator subsystem showing two-phase dynamics. c) 2-dimensional reduced oscillator model showing oscillations as well as recovery of low level [p53*] mode after DNA damage is repaired. d) 2-D reduced oscillator model showing two-phase dynamics

3.2 Analysis of Oscillations by Dynamic Route Approach

In this subsection, firstly bistable dynamics of [ATM*] is analyzed by employing dynamic route approach to Equation 1 of Table 3 by quasi steady-state assumption for Wip1 variable and then oscillatory ATM-Wip1 interaction is demonstrated by using 2-D phase portraits.

As depicted in Figure 3.2, [ATM*] dynamics has one or two stable equilibrium points in a physiologically meaningful range (i.e. the set of nonnegative [ATM*] values) depending on the values of n_c and [Wip1]. Characteristics of [ATM*] dynamics change as with the combined effect of Wip1 and n_c (See Figure 3.2b). As n_c

phosphorylates ATM and drives its concentration to a high steady state; Wip1 dephosphorylates ATM* and drives its concentration to a low steady state even in the presence of DNA damage (i.e. the case of high n_c value) (See Figure 3.2b).

Dynamic route approach applied to [ATM*] dynamics for typical Wip1 values leading to different sets of equilibrium dynamics for [ATM*] can assist to show how oscillations are produced (See Figure 3.2a). Basal level of Wip1 is chosen as 0.2 and n_c is 0 representing the situation before the damage. In this initial condition, [ATM*] has only one equilibrium point at zero which is asymptotically stable (See the bottom curve of the upper red dotted bunch of [ATM*] graphs in Figure 3.2b).

When setting n_c to 20 to represent the damage, [ATM*] characteristics change as: Equilibrium at zero becomes unstable and, under arbitrary small perturbation, [ATM*] goes up to the asymptotically stable equilibrium at the high steady state value (Figure 3.2a.1). As [ATM*] goes into this high steady state, at the same time, in accordance with Equation 2 and 3 of Table 3, Wip1 increases. So, it pulls the curve of ATM* rate (i.e. d[ATM*]/dt) downward first creating a saddle point at an intermediate ATM* value (See Figure 3.2a.3) and then leading the zero equilibrium point of [ATM*] to become asymptotically stable (See Figure 3.2a.4). Zero value of [ATM*] relaxes [Wip1] to its rest state of $k_{swip10}/k_{dwip1} = 0.2$, and this ATM-Wip1 interaction repeats itself over again causing oscillations.

There are discontinuous jumps of [ATM*] level when the characteristics change from (Figure 3.2a-3) to (Figure 3.2a-4) and (Figure 3.2a-2) to (Figure 3.2a-1). The discontinuous jump as transition from (Figure 3.2a-3) to (Figure 3.2a-4) occurs from the saddle node to stable steady state at zero, while from (Figure 3.2a-2) to (Figure 3.2a-1) occurs from unstable steady state at zero to a high stable steady state located around 4.9.
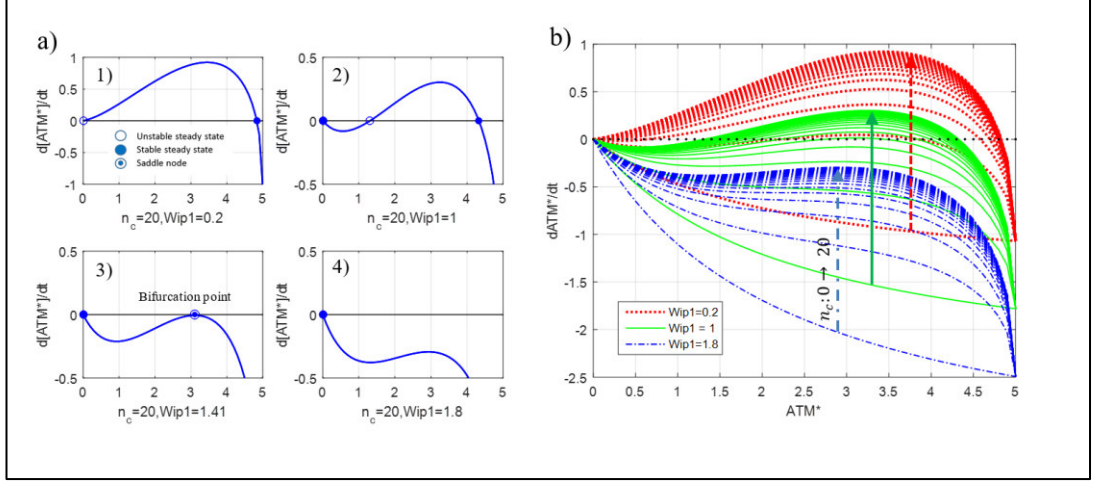
Figure 3.2 Dynamic route approach is employed for explaining the oscillations of the introduced 2-dimensional oscillator model

3.3 Phase Space Analysis of the Introduced 2-dimensional Model

In this subsection, we analyze the phase space of the 2-D model and show how different behaviors are determined by the organization of the nullclines in the phase space. Since these behaviors are directly related to the cell fate outcomes, providing a mechanistic insight to the interplay between ATM and Wip1 may contribute to the systems-level understanding of the damage response of the cell. The damage response of the cell is also used by intervention strategies of cancer. Thus, a better understanding of this mechanism will help developing better strategies.

In the analysis of a system, equilibrium points are of great importance, however due to the complexity of the 2-D oscillator model, finding equilibrium points analytically is impossible (The degree of resulting polynomial describing the location of equilibrium points is more than 5, which is known to have no explicit solution). However, nullclines can be sketched and numerical approximated values for equilibrium points can be calculated and shown in a graph.

The nullclines of a differential equation system are the set of points that make the equations zero. In this case, we have 2 differential equations and we need to look for

the curves that make these differential equations zero. By arranging 2-D oscillator model as in Equations (3.1) and (3.2).

$$\frac{d[ATM^*]}{dt} = k_{deatm} \frac{[ATM^*]}{([ATM^*] + j_{deatm})} \ (F([ATM^*], n_c) - [Wip1]) \tag{3.1}$$

$$\frac{d[Wip1]}{dt} = k_{dwip1} \ (G([p53arrester], [ATM^*]) - [Wip1]) \tag{3.2}$$

where the functions F and G are expressed as:

$F([ATM^*], n_c)$

$$= \frac{1}{k_{deatm} \frac{[ATM^*]}{([ATM^*] + j_{deatm})}} \left(k_{acatm} \frac{n_c}{(n_c + jn_c)} [ATM^*] \frac{\sqrt{0.1(ATM_{tot} - [ATM^*])}}{(\sqrt{0.1(ATM_{tot} - [ATM^*])} + jacatm)} \right.$$
$$\left. - kdeatm \frac{[ATM^*]}{([ATM^*] + j_{deatm})} \right) \tag{3.3}$$

$G([p53arrester], [ATM^*])$

$$= \frac{1}{k_{dwip1}} (k_{swip10} + k_{swip1} \frac{[p53Arrester]^3}{(j_{swip1}{}^3 + [p53Arrester]^3)}) \tag{3.4}$$

The reduced one-dimensional ATM equation expressed in (3.1) has one more nullcline, which is the separatrix, [ATM*] = 0. When [ATM*] is zero, it is clear that Equation (3.1) becomes zero.

To show how the nullclines are organized in these three different behaviors, we sketch the nullclines in the phase space in case of (i) low stable equilibrium state of [p53*], (ii) oscillations of [p53*] and (iii) high stable equilibrium state of [p53*]. Next, we investigate the phase space.

(i) Low stable equilibrium state of [p53*]: When n_c is zero, indicating no DNA damage, the organization of nullclines in the phase space is shown in Figure 3.3. In this case, in the positive region, there is only one equilibrium point which is located at the intersection of nullclines [ATM*] = 0 and G-nullcline. The equilibrium point is stable. The stability of the equilibrium point is investigated by locally linearizing the 2-D model at that point. Calculating the Jacobian matrix at that point, it is found that the eigenvalues are -0.05 and -0.6783, which indicates the equilibrium is stable. Thus, any initial condition in the positive quadrant goes to this point where [ATM*] is zero

and Wip1 is at basal level of around 0.2. There is also another equilibrium point that could be seen in Figure 3.3 when the figure is extended to the negative regions. However, we are only interested in the positive regions of the system. The nullcline [ATM*] = 0, which is an attracting separatrix for [Wip1] > 0, does not allow to transfer of the positive trajectories to the negative region as can be understood from the directional field. Since any initial condition that starts in the positive quadrant would end up in the steady state which is located at around ([ATM*], [Wip1]) = (0,0.2), we do not have to bother to investigate the equilibrium points in the negative regions.
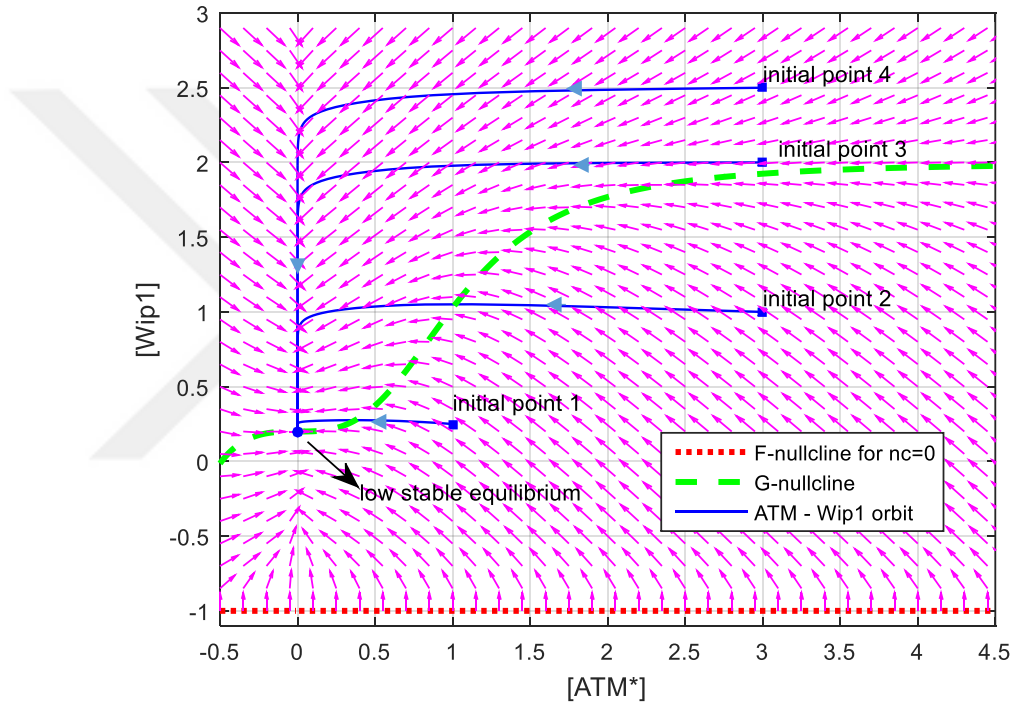
Figure 3.3 Representation of phase space of the introduced 2-D oscillator model, when $n_c = 0$. In this case, the point ([Wip1],[ATM*])= (0.2,0) is the only stable steady state in the positive quadrant

(ii) Oscillations of [p53*]: When there is high DSBC activity, (i.e. $n_c = 20$), the organization of nullclines are shown in Figure 3.4. The F-nullcline goes upward and intersects with G-nullcline in the positive quadrant. The stability of the equilibrium point located at the intersection of the nullclines in the positive quadrant can be determined by calculating eigenvalues via Jacobian matrix at that point. The eigenvalues are found to be 0.0578 - 0.1110i and 0.0578 + 0.1110i, which indicates that the equilibrium point is unstable.

For 2-dimensional systems, the existence of oscillations can be proven by applying Poincare-Bendixson theorem. It is not easy to show that a system actually oscillates via simulation since the oscillations may contain a small damping property that cannot be spotted by eye. However, using Poincaré-Bendixson theorem, we can show that there is actually an oscillation. The theorem states that for 2-dimensional systems, if there is a bounded trapping region and if that region does not contain any stable fixed point, there is a limit cycle oscillation.

To apply Poincaré-Bendixson theorem, first we have to show that there is a trapping region. The existence of trapping region can be inferred by looking at the directional field in the positive region. The arrows indicate that the trajectories that start in the positive region cannot across to negative region due to the nullcline [ATM*] = 0. Also, when [ATM*] and [Wip1] values are large, the directional field again indicates that trajectories cannot escape to infinity since the arrows point towards inward. Thus, we conclude that there is a trapping region in the positive quadrant when n_c is 20. Since, the equilibrium point in this trapping region is unstable, applying Poincaré-Bendixson theorem, we conclude that there is indeed a limit cycle oscillation.

By examining a trajectory, one period of oscillation can be explained with the help of Figure 3.5. The starting point is chosen as (ATM*, Wip1) = (3,1). At the starting point, Wip1 is under F-nullcline and G-nullcline. So, both $\frac{d[Wip1]}{dt}$ and $\frac{d[ATM^*]}{dt}$ will be positive, as a result, [Wip1] and [ATM*] will increase. Also, the velocity vectors indicate the direction of the trace. When the point crosses F-nullcline at the Point 1, [ATM*] value will decrease since $\frac{d[ATM^*]}{dt}$ will be negative. But, [Wip1] will increase since [Wip1] is above F-nullcline. Also, another notification here is that F-nullcline will behave like a wall till the knee, Point 2. This property is important for characterization of relaxation oscillations, where jumping behavior occurs. Point 2 corresponds to Figure 3.2a-3 where dynamic route approach is applied. After Point 3, both $\frac{d[Wip1]}{dt}$ and $\frac{d[ATM^*]}{dt}$ will be negative. Both of them will increase. When Point 4 is crossed, dWip1/dt will go on being negative and $\frac{d[ATM^*]}{dt}$ will be changed to from

negative to positive. When Point 5 is crossed, both $\frac{d[Wip1]}{dt}$ and $\frac{d[ATM^*]}{dt}$ will be positive. A new jump phenomenon too occurs, as trajectory goes from Point 5 to Point 1 starting the next period of oscillations. Note that, these explanations of oscillations via dynamic route approach or a phase space analysis does not give the proof for the oscillations, however just confirms it. The existence of oscillations are inferred by applying Poincaré-Bendixson theorem. The explanations are to give the mechanistic insights to the oscillations.
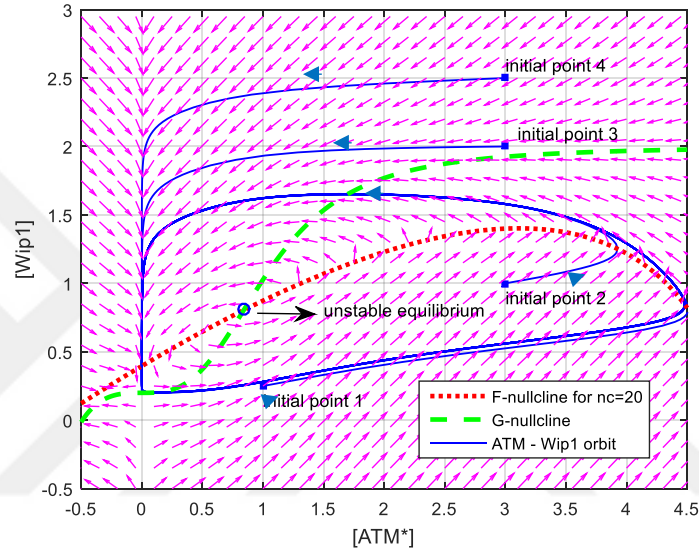
Figure 3.4 Representation of phase space of the introduced 2-D oscillator model when $n_c = 20$. In this case, F-nullcline shifts upward and intersect G-nullcline at an unstable steady state steady state
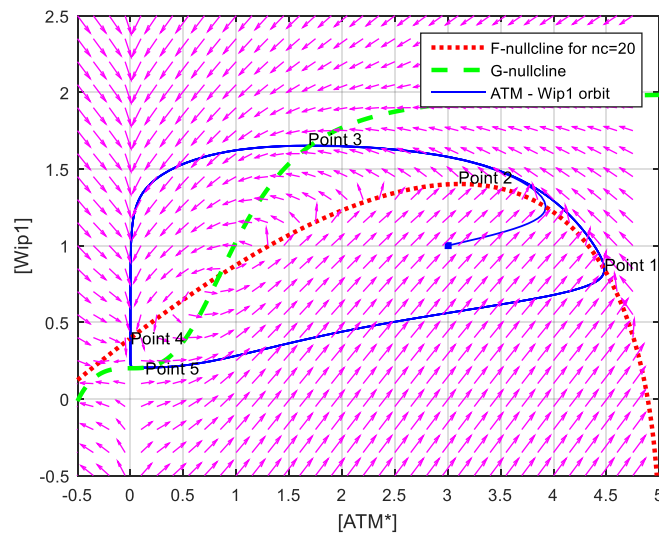
Figure 3.5 Representation of critical transitions in oscillations in phase space of the introduced 2-D oscillator model

31

The jumps of [ATM*] value in the oscillations contribute to the fast dynamics of [ATM*], while [Wip1] variable constitutes the slow part of the system. The jumps and the characterization of oscillations by fast and slow parts are the indicator that the oscillations are of relaxation type.

(iii) High steady state of [p53*]: When n_c is 20 and all p53arresters are zero, the G-nullcline moves downward as shown in Figure 3.6. This time the equilibrium point in the positive region is stable, since the eigenvalues are -0.05 and -0.4654. Thus, all trajectories that start in the positive quadrant goes towards this stable point, which has a stable steady state at a high [ATM*] value. This high [ATM*] value also indicate that [p53*] will be in a high level indicating apoptosis.

The introduced 2-D oscillator model is able to exhibit not only the digital pulses but also low and high equilibrium states of [p53*] which is required for normal cell growth and for apoptosis, respectively. When [p53arrester] = 0, Wip1 feedback loop shuts off, the model dynamics is governed only by [ATM*] equation that has bistable characteristics. In this case, the value of n_c determines whether [ATM*] will have a high or low stable equilibrium state value. If $n_c = 20$ when Wip1 feedback loop shuts off, F- and G-nullclines intersect at the high stable equilibrium state of [ATM*] (Figure 3.6). [ATM*] goes to high equilibrium state, so does [p53*] in accordance with the algebraic relation in Equation (3) of Table 3.1. Since p53arrester is forced to be zero, all [p53*] become [p53killer] ready to trigger apoptosis.
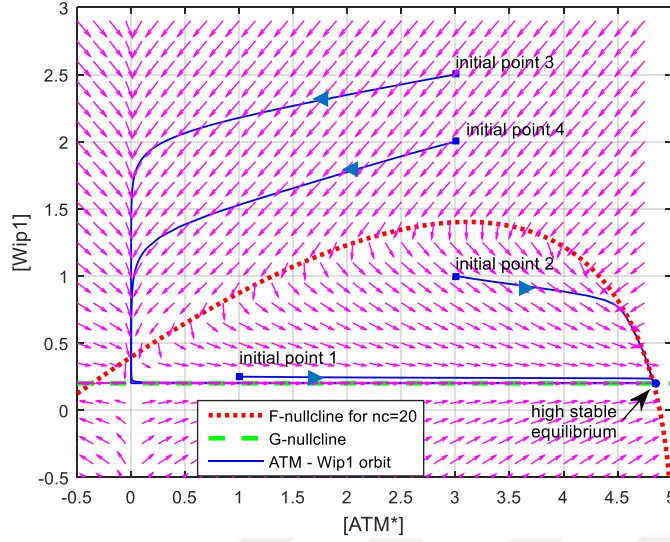
Figure 3.6 Organization of nullclines in the case of apoptosis due to $n_c = 20$ and [p53arrester] = 0

3.4 2-D Model Exhibits Relaxation Type Oscillations

Relaxation type oscillations are frequently seen in biology and known to give the organism robust oscillatory property. Examples include and not restricted to pacemaker cells in heart (Grudziński & Żebrowski, 2004), MAPK signaling (Kochańczyk et al., 2017), MPF activity in frog egg extracts (Tyson & Novak, 2015), and regulation of autophagy (Szymańska, Martin, MacKeigan, Hlavacek, & Lipniacki, 2015). Relaxation oscillations are characterized by jump phenomenon and fast and slow parts in the periodic trajectory.

Since Wip1 equation indicated in (3.2) has a slower dynamics providing a proper intrinsic time delay, [ATM*] is able to switch between these high and low steady states forming repeated pulses. Therefore, p53 network model owes its oscillations to the interaction between the bistable characteristic of fast ATM dynamics and intrinsic time delay of slow Wip1 negative feedback loop. Indeed, this topological structure of ATM-Wip1 resembles a bistable frustrated unit model that is able to exhibit relaxation oscillations (Kaluza & Meyer-Ortmanns, 2010; Krishna, Semsey, & Jensen, 2009). The proposed model equations have considerable robustness since parametric uncertainty is allowed as long as [ATM] equation has bistability and Wip1 feedback

loop offers a proper time delay such that ATM has enough time to switch between stable nodes. A sufficient amount of relaxation time (i.e. time delay) is necessary for [ATM*] to reach its steady state on every pulse, therefore to exhibit higher oscillations. If the relaxation time is not sufficient, [ATM*] will switch back to zero value before reaching the high steady state, resulting in weaker oscillations. That is, the relaxation time determines the strength of the oscillations, which is a property of relaxation oscillators.

Since the oscillatory response happens due to the transition from stable (See Figure 3.3) to unstable (See Figure 3.4) intersection point of nullclines, the system gives a complete oscillatory response or no response at all and the external stimulus, n_c, does not appreciably influence the amplitude of this relaxation oscillation (Figure 3.7). This is known as all-or-none phenomenon that is biologically an intriguing property of relaxation oscillators (FitzHugh, 1961; Van der Pol & Mark, 1928;). In fact, observations in wet lab experiments support the existence of a relaxation oscillator in p53 network. For example, (Lahav et al., 2004) states that "The fixed mean height and duration of p53 pulses do not depend on the amount of DNA damage" and (Geva-Zatorsky et al., 2006) states that "The peak amplitude and timing did not depend on the dose of irradiation."
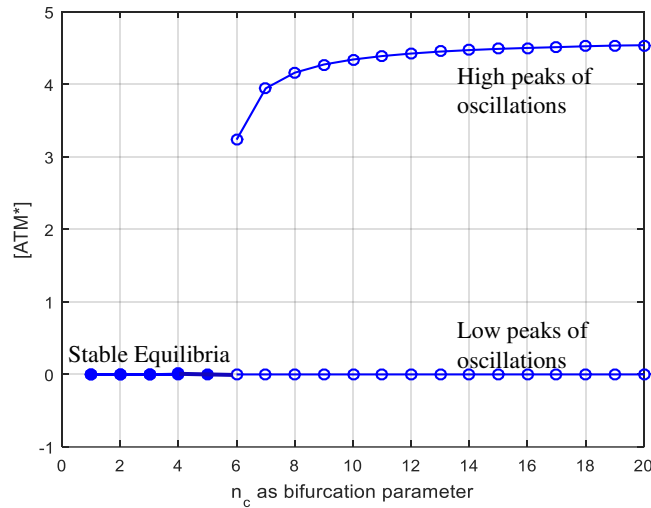
Figure 3.7 Dynamics of [ATM*] taking n_c as bifurcation parameter. If n_c is smaller than 6, [ATM*] stays at zero. If n_c is greater than 6, [ATM*] level oscillates

3.5 1-dimensional State Dependent Delay Differential Equation Model for ATM-Wip1 Interaction in p53 Network

One of the characteristics of relaxation oscillators is that the relaxation time determines the frequency and amplitudes of oscillations. In ATM-Wip1 oscillator, Wip1 dynamics and $[Mdm2_n]$ both contribute to the relaxation time (See Equation 2 and 3 of Table 3.1). $[Mdm2_n]$ contributes to relaxation time via Wip1 equation defined by (3.2). To investigate separately the contribution of these two determinants to the relaxation time and oscillations, we reduce the 2-D ATM-Wip1 oscillator model into 1-dimensional (1-D) state-dependent delay (SDD) differential equation of $[ATM^*]$ by indicating the time delay contribution of Wip1 explicitly as τ and keeping $[Mdm2_n]$ as a parameter as shown in Table 3.2 (See (Kozyreff & Erneux, 2014) for general SDD differential equations). Taking τ as bifurcation parameter for different $[Mdm2_n]$ values, Figure 3.8a shows that $[Mdm2_n]$ has positive effect on the amplitudes of $[ATM^*]$ oscillations regardless of τ. $[ATM^*]$ is known to have positive effect on cell cycle arrest after ionizing radiation (Samuel, Weber, & Funk, 2002). Thus, according to the proposed 2-D model, $[Mdm2_n]$ has positive effect on cell cycle arrest due to its enhancement on $[ATM^*]$ level oscillations.

In Figure 3.8a τ (time delay by Wip1 equation) is taken as bifurcation parameter for $[ATM^*]$ variable. Oscillation starts at $\tau = 2$ and $\tau = 3$ for $[Mdm2_n] = 0.26$ and 0.1, respectively. As time delay by Wip1 increases, the amplitude of oscillations increases and eventually saturates at the high stable equilibrium state of $[ATM^*]$ equation. Low $Mdm2_n$ level of 0.1 in the first phase has a potential to decrease amplitudes of oscillations in case of small time delay of Wip1 feedback loop. Therefore, enhanced level of $[Mdm2_n]$ is good for oscillations indicating it may have an antitumor activity. In Figure 3.8b, the same procedure in Figure 3.8a is applied for $[p53^*]$ variable (Equation 3 in Table 3.1). Low level of $[Mdm2_n]$ increases the amplitudes of $[p53^*]$ oscillations, only if intrinsic time delay provided by Wip1 exceeds 8 minutes.

Table 3.2 1-dimensional state dependent delay differential equation model of 2-dimensional oscillator

Equation number	Equations
1	$$\frac{d[ATM^*]}{dt} = k_{acatm} \; \frac{n_c}{(n_c + jn_c)} [ATM^*] \frac{\sqrt{0.1*(ATM_{tot}-[ATM^*])}}{(\sqrt{0.1*(ATM_{tot}-[ATM^*])} \; + jacatm)} - k_{deatm} \frac{(1 + [Wip1])[ATM^*]}{([ATM^*] + j_{deatm})}$$
2	$$[p53arrester] = [ATM^*](t-\tau)(1.5 - 3.947[Mdm2_n])$$
3	$$[Wip1] = \frac{1}{k_{dwip1}}(k_{swip10} + k_{swip1}\frac{[p53arrester]^3}{(j_{swip1}{}^3+[p53arrester]^3)})$$

Since Figure 3.8a and Figure 3.8b lack the frequency information, time evaluation for [ATM*] is sketched as in Figure 3.8c,d. 1-D SDD model (Table 3.2) is solved until 4000 minutes to give time for transient effects to disappear. At $\tau = 3$, the proposed 2-D model exhibits oscillation only for $[Mdm2_n] = 0.26$, not $[Mdm2_n] = 0.1$. At $\tau = 5$, the amplitude of oscillations at $[Mdm2_n] = 0.26$ is bigger. At $\tau = 18$, the amplitude of oscillation is at its maximum value of high steady state of [ATM*]. Since τ is relatively high, at both values of $[Mdm2_n]$, ATM dynamics (3.1) have enough time to reach its high steady state. As the time delay of Wip1 increases, the period of oscillations increases too. Also, it can be seen that $[Mdm2_n]$ has similar effect as τ. At $\tau = 5$, for $[Mdm2_n] = 0.26$, the period is around 28 minutes, and for $[Mdm2_n] = 0.1$, the period is about 36 minutes. This increase in the period of oscillations are due to $[Mdm2_n]$'s contribution to the relaxation time. Since after the relaxation regime finishes, the next pulse begins, the amount of relaxation time also is a determinant for the period of oscillations. This is one of the property of relaxation oscillations. We can generalize this finding to any p53 inhibitor. Thus, the complex effect of $[Mdm2_n]$ on the amplitudes and periods are due to the relaxation type of p53 network oscillator.
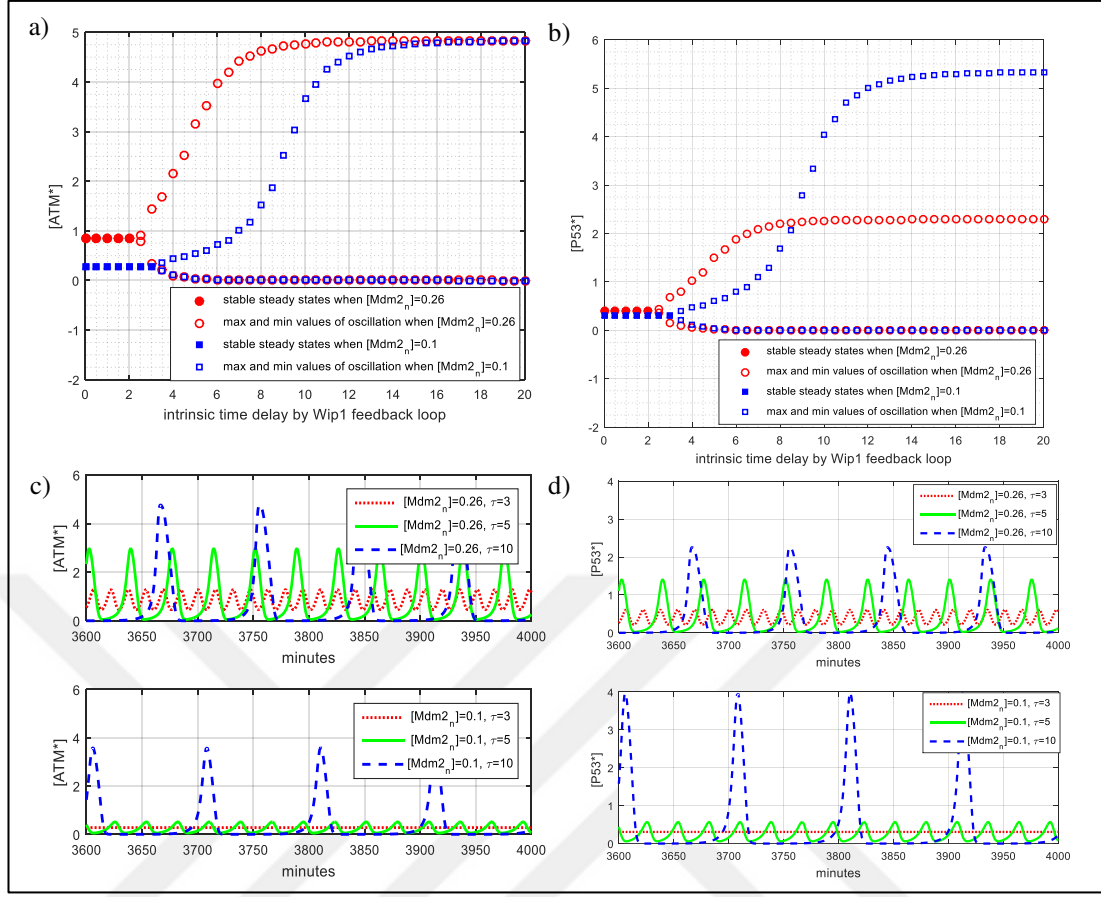
Figure 3.8 Numerical simulations of the introduced 1-D SDD Oscillator model in Table 3.2 to examine the effects of $Mdm2_n$ on amplitudes and frequencies via relaxation time

As shown in Figure 3.8d, for [p53*], when $[Mdm2_n] = 0.1$ and τ is 5, the oscillations are weak; however, when τ is 10, amplitude of [p53*] oscillations are enhanced. There is possibility that $Mdm2_n$ has enhancing effect on [p53*] oscillations when Wip1 delay is properly tuned. So, the intrinsic time delay of Wip1 and the level of $[Mdm2_n]$ must be well adjusted as a trade-off between decreasing [ATM*], increasing [p53*], and period of oscillations. Thus, the effect of $[Mdm2_n]$ on [p53*] oscillations is rather complex. Depending on the value of τ, $[Mdm2_n]$ may enhance or weaken [p53*] oscillations due to the nonlinear algebraic Equation 3 in Table 3.1, although it seems to always have a amplification/saturation effect on [ATM*] that [p53*] depends on (Figure 3.8b). For τ between 3 and 8, [p53*] oscillations are enhanced, for τ greater than 8, the oscillations are weakened by $[Mdm2_n]$. For the parameters of the reduced ATM-Wip1 oscillator equations in Table 3.1, the intrinsic time delay of Wip1 is

37

around 4 minutes, so abundance of [$Mdm2_n$] increases the amplitudes of [p53*] oscillations. Although [$Mdm2_n$] is a negative regulator of p53, it has a positive effect on [p53*] oscillations thus on cell cycle arrest. Then, we conclude that Mdm2 is good for enhancing DNA damage response and hence considered as a tumor suppressor.

After finding these counter-intuitive results mathematically, we look for the biological relevance of these results and find that these results correlate with the biological findings. In wet lab experiments, it has been shown that Mdm2 may exert effects that suppress cell proliferation (Manfredi, 2010) and mitotic progression (Manfredi, 2010; Brown, Thomas, & Deb, 1998; Dang et al., 2002). In addition, Manfredi (2010) showed that loss of Mdm2 enhanced tumor formation. This counter-intuitive finding could be explained away by 2-D oscillator model that we proposed here. Our explanation is as this: Loss of Mdm2 results in weaker oscillations of p53* level which may enhance tumor formation due to the deficient cell cycle arrest. However, it must be noted that these referenced works did not aim to study p53 oscillations, but study the cell cycle arrest. However, it is known that cell cycle arrest occurs due to p53 oscillations (Batchelor, Loewer, & Lahav, 2009; Batchelor, Mock et al., 2008; Lahav, et al., 2004).

CHAPTER FOUR

DETERMINANTS OF TWO-PHASE DYNAMICS OF P53 NETWORK AS REVEALED BY THE INTRODUCED 2-D OSCILLATOR MODEL

Zhang et al. (2011) argues that the first and second phase of the two-phase dynamics of 17-dimensional p53 network model becomes active depending on the relative strengths of Wip1 and PTEN feedback loops. In contrast to the study by Zhang et al. (2011), this chapter describes the phases based on a 2-D oscillator model excited by DSBCs as its two different qualitative modes in the following way. 1) Wip1 feedback loop, which feedbacks ATM to itself, is the source of oscillation, which appears in the first phase, as also explained in Zhang et al. (2011). 2) The second phase appears after the oscillation stops due to the extinction of p53arrester by the accumulated activity of P53DINP1 no matter what the relative strength of PTEN feedback loop over Wip1 feedback loop is, opposing to the argument by Zhang et al. (2011). 3) The role of PTEN feedback loop is twofold: The activation of PTEN feedback loop in the first phase decreases the amplitudes of the oscillation but does not stop the oscillation while, in the second phase, it boosts up the level of equilibrium state of p53 to initiate apoptosis.

4.1 P53DINP1 Acts as an Oscillation Accumulation Triggered Genetic Switch

Since apoptosis is a decision, there must be a switching action, which requires an interaction with a switch. Here, we reveal functional importance of P53DINP1 as a switch, more specifically as an oscillation accumulation triggered genetic switch (OATGS) (He & Liu, 2014) in two-phase dynamics. To demonstrate the switching action of P53DINP1, we add the dynamics of P53DINP1 and p53killer to the isolated core oscillator subsystem defined in Table 2.1 (See Figure 4.1a). The resulting model is solved numerically as in Figure 4.1b,c. It can be seen that P53DINP1 activity increases as it accumulates over oscillations. When its activity becomes so high that it turns all p53arresters in the environment into p53killers, Wip1 feedback loop shuts off to stop oscillation due to the extinction of p53arresters. In this case, oscillator stops in the same conditions as in Figure 3.6, thus [ATM*] goes to the high steady state elevating [p53*] ([p53killers]) to high state, too. This analysis supports a potential cancer therapeutic approach by elevating [P53DINP1] to drive cell to apoptosis. The

apoptotic importance of P53DINP1 is stated in experimental findings (Okamura et al., 2001) and is patented for the use of cancer therapeutic strategy (U.S. Patent No. 7,371,835, 2008). From the modular perspective, P53DINP1 can be seen as a tool that stops the oscillator in the core of p53 network by accumulating over pulses.

When P53DINP1 activity is included into core oscillator subsystem, effect of Mdm2 can be automatically seen in the first phase and the second phase of p53 dynamics as in Figure 4.1c. Low $[Mdm2_n]$ value of 0.1 decreases the amplitude of oscillations but increases the $[p53^*]$ (i.e. p53killer) at apoptosis. When $[Mdm2_n]$ is 0.26, the amplitude of oscillations is bigger but $[p53^*]$ level in apoptosis is smaller. So, to maintain a strong oscillation in the first phase and higher sustained value at apoptosis, $[Mdm2_n]$ value must be degraded just after the oscillator stops by the extinction of p53arrester, which is maintained by P53DINP1 activity in 17-dimensional two-phase model. This indicates that the ultimate function of PTEN feedback loop activated by P53DINP1 in the second phase is to drop $[Mdm2_n]$ value to a very low value in order to drive $[p53^*]$ level to a higher value than the peaks of $[p53^*]$ oscillation. Large distinction between the peaks of $[p53^*]$ oscillations in the first phase and constant high level of $[p53^*]$ in the second phase guarantees a more reliable decision of cell fate.

When P53DINP1 stops the oscillator such that $[p53^*]$ level is in high state (Figure 4.1b,c), the level of p53killer is not sufficient to trigger caspase mechanism for initiating apoptosis. Therefore, $[Mdm2_n]$ must be decreased in the second phase to elevate [p53killer] to the higher steady state. We emphasize the finding that switching to apoptosis and maintaining a proper high level to trigger apoptosis are two different things. The new finding here is very important in pointing out that stopping the oscillator to trigger apoptosis and providing sufficient $[p53^*]$ levels after the oscillator stops require two different actions and both are necessary and important. Thus, stopping the oscillator is the first critical step in initiating apoptosis.
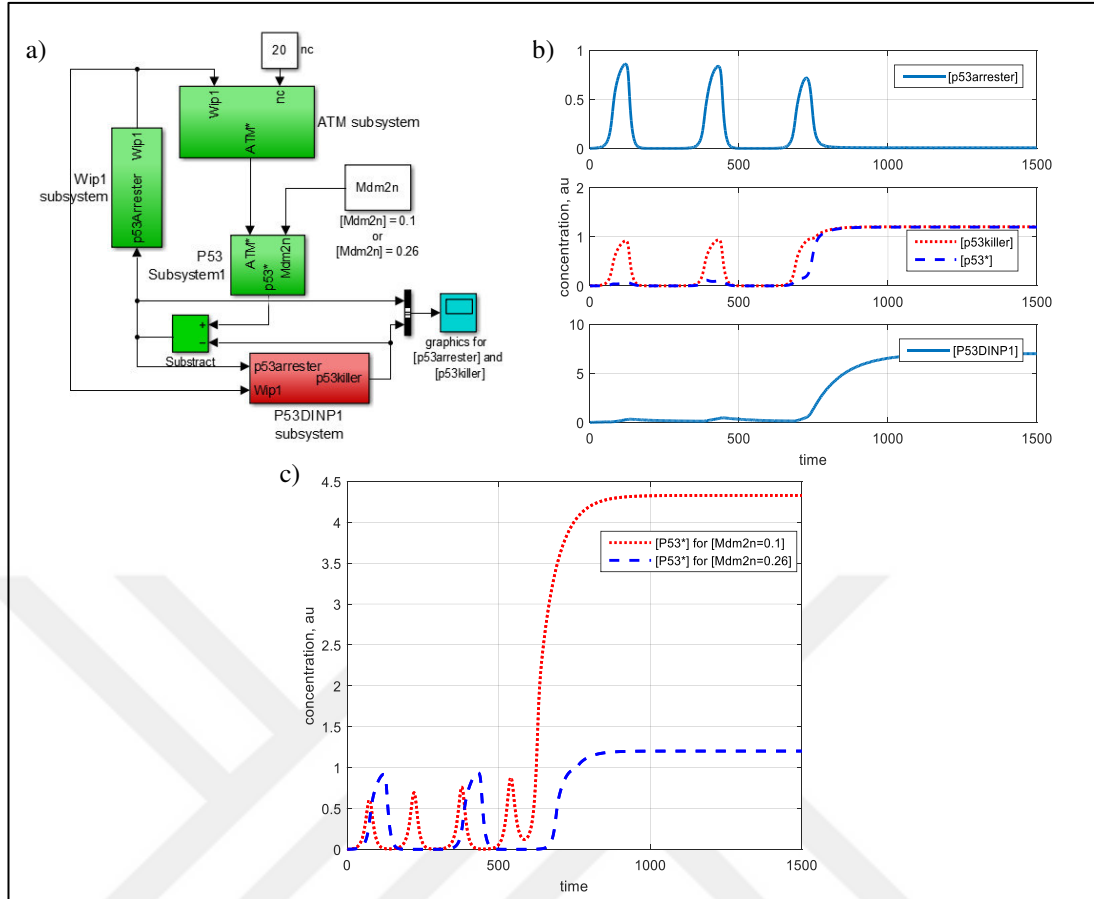
Figure 4.1 P53DINP1 acts as an OATGS and the ultimate function of PTEN is to downgrade [Mdm2$_n$] to low values in second phase

4.2 Function of PTEN Feedback Loop in Two-phase Dynamics

In 17-dimensional two-phase model by Zhang et al. (2011), decreasing of [Mdm2$_n$] is done by activation of PTEN feedback loop in the second phase. A clear distinction to be done here: The activation of PTEN feedback loop does not make the switching action from the first phase to the second phase, but it maintains a higher level of [p53*] by reducing [Mdm2$_n$] in the second phase (See Figure 4.1c for the effects of decreasing of [Mdm2$_n$]). In fact, as we revealed in Section 3.5, the strength of PTEN feedback has a negative effect on the first phase by weakening the oscillations, due to the relaxation time effect of Mdm2. Therefore, PTEN feedback must be activated just after the switching action is done by P53DINP1 in contrast to the claim of Zhang et al. (2011)

41

in which the level of PTEN (accordingly $Mdm2_n$) determines whether p53 acts as a pulse generator or a switch in the second phase.

CHAPTER FIVE
ANALYSIS OF VARIATIONS IN P53 NETWORK BY THE PROPOSED 2-DIMENSIONAL OSCILLATOR MODEL AND REVEALING POSSIBLE THERAPEUTIC STRATEGIES FOR DEFICIENT P53 DYNAMICS

It has been shown that sensitive parameters that change bifurcation points usually correspond to high frequency oncogenic mutations in reality (Chen, Yue, & Ouyang, 2014). These parameters are sensitive parameters that change the phase space of the system. In our case, the intersection type of nullclines determines the characteristics of the phase space and any parameter that significantly changes the location of nullclines may correspond to an oncogenic mutation. Here we show that mutations, such as Wip1 overexpression, ATM deficiency, Mdm2 overexpression and Mdm2 downregulation can be modelled by changing corresponding parameters in the 2-D system resulting in change of phase space and evaluate the 2-D model's predictive power. In order to understand the mechanism of how Wip1 overexpression and ATM deficiency cause cancer, we use different parameter selections that characterizes these mutations in phase space of the model. The phase space analysis of mutations reveal cancer therapy strategies for these types of cancer.

5.1 Wip1 Overexpression and Downregulation

Wip1 overexpression is a mutation that is found in several types of cancers and has an oncogenic function (Bulavin et al., 2002; Castellino, et al., 2008; Fuku, Semba, Yutori, & Yokozaki, 2007; Fumiko et al., 2003; Lowe et al., 2012; Rauta, et al., 2006) which is characterized by the high levels of Wip1 in cell. This situation can be embedded into the proposed 2-D model by modifying Equation (3.2) via increasing the Wip1 production rate by a constant, K_{wip1} as shown in (5.1). As K_{wip1} increases, the G-nullcline moves upward, changing the phase space of the system. The system loses its ability to oscillate (Figure 5.1a). Since oscillations are important for arresting cell cycle (Purvis et al., 2012), and defects in cell cycle arrest is the prerequisite of cancer (Green & Evan, 2002; Lowe et al., 2012; Xu & D., 1996), we speculate that Wip1 overexpression may cause cancer by removing cell's ability to arrest cell cycle. This analysis also supports the biological experiments (Bulavin et al., 2002) (Lambros

et al., 2010) which confirm that Wip1 overexpression may cause tumorigenesis even if cell has normal functioning p53 (i.e. no mutation in p53). To recover healthy phase space, G-nullcline must be moved downward, which can be possible by degradation of Wip1. This suggestion is in agreement with (Richter et al., 2015) that shows Wip1 overexpression can be recovered by Wip1 degradation.

$$\frac{d[\text{Wip1}]}{dt} = \mathbf{K_{Wip1}} * (k_{swip10} + k_{swip1} \frac{[\text{p53arrester}]^3}{(j_{swip1}{}^3 + [\text{p53arrester}]^3)}) \tag{5.1}$$
$$- k_{dwip1}[\text{Wip1}]$$
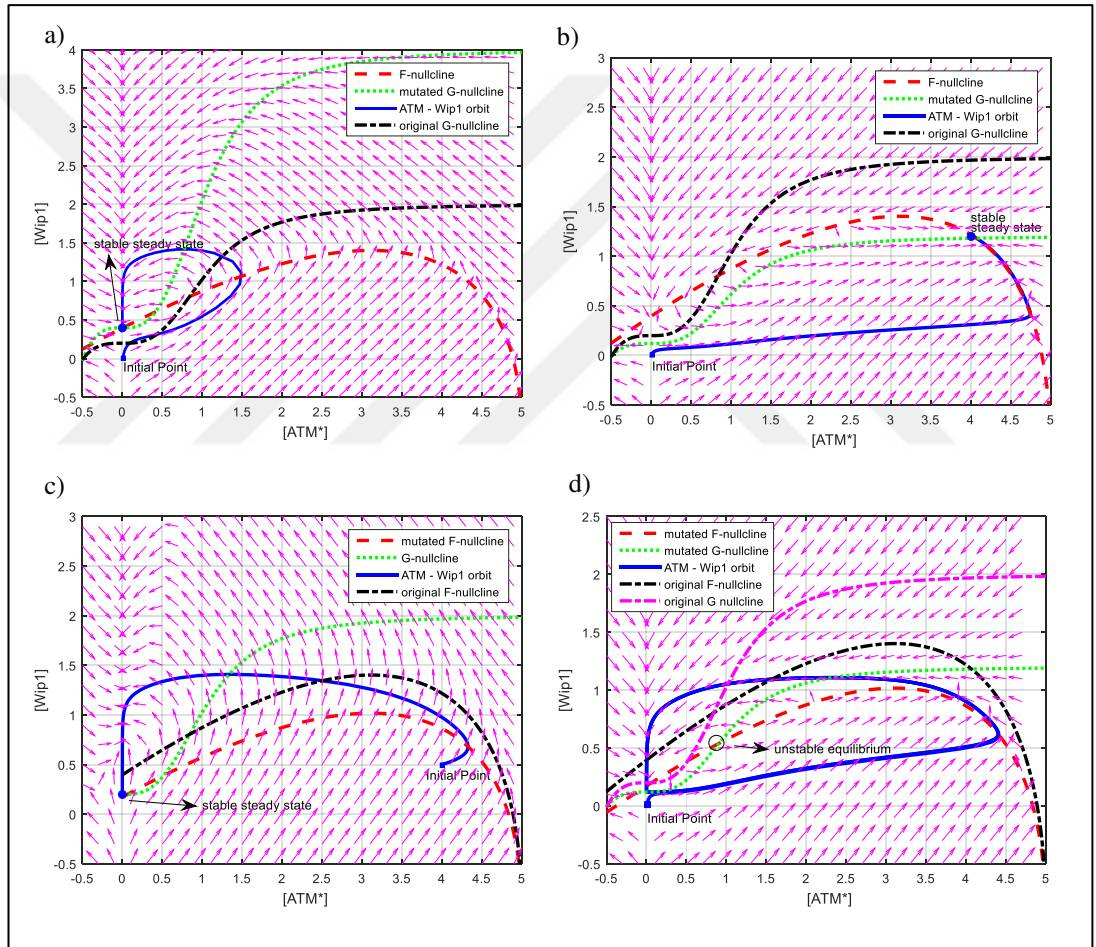
Figure 5.1 The effect of mutations to the phase space of 2-dimensional oscillator. a) Wip1-overexpression, K_{wip1} in Equation (5.1) is 2. b) Wip1 nullity, K_{wip1} in Equation (5.1) is 0.6, i.e. less than 1. c) ATM deficiency, K_{ATM} in Equation (5.2) is 5. d) Degradation of Wip1 compensates ATM deficiency. Oscillatory response is recovered. K_{wip1} in Equation (5.1) is 5 and K_{ATM} in Equation (5.2) is 0.6

44

It has been shown that loss of Wip1 function sensitizes cells to DNA-damage induced apoptosis (Kong, Jiang, & Mercer, 2009; Xia, Ongusaha, Lee, & Liou, 2009). By decreasing Wip1 activity via decreasing K_{wip1} in (5.1), G-nullcline moves downward and intersects F-nullcline at a stable high steady state Figure 5.1b. Since the oscillator stops at a high steady state, cell may now trigger apoptosis. The ability to go apoptosis easily, makes cell resistant to tumor formation (Shreeram, et al., 2006a) (Wang, et al., 2015; Yi et al., 2015). The analysis here demonstrates mathematically that Wip1 is an attractive therapeutic target and agrees with biological findings (Belova, Demidov, Fornace, & Bulavin, 2005; Rayter et al., 2008; Saito-Ohara et al., 2003; Tan et al., 2009; Yamaguchi et al., 2006; Yoda et al., 2008). This analysis partly explains the finding that depletion of Wip1 sensitizes cells to apoptosis in (Goloudina et al., 2012).

5.2 ATM Deficiency

ATM deficiency is an ATM mutation and characterized by insensitiveness to the damage. This mutation can be embedded into our 2-D model, by decreasing sensitiveness of ATM to n_c, with a constant K_{ATM} as shown in Equation (5.5). By increasing K_{ATM}, the sensitiveness of ATM for the parameter n_c can be decreased. As a result, F-nullcline moves downward changing the phase space and removing the system's ability to oscillate and to arrest cell cycle (Figure 5.1c). In the literature, some studies demonstrate that mutation in ATM causes defective cell cycle checkpoint activation (Delia, Fontanella, Ferrario, Chessa, & Mizutani, 2003; Lavin & Kozlov, 2007; Xu & Baltimore, 1996).

$$\frac{d[ATM^*]}{dt} = k_{acatm} \frac{n_c}{(n_c + K_{ATM} * jn_c)}[ATM^*]\frac{\sqrt{0.1*(ATM_{tot} - [ATM^*])}}{\left(\sqrt{0.1*(ATM_{tot} - [ATM^*])} + jacatm\right)} - kdeatm\,(\,1 + [\,Wip1\,]\,)\frac{[ATM^*]}{([ATM^*] + j_{deatm})} \quad (5.5)$$

5.3 Degradation of Wip1 Rescues ATM Deficiency

Another prediction can be obtained from the phase space perspective: the moving of G-nullcline downward can be compensated by moving F-nullcline downward too and can keep the qualitative property of the phase space. To move F-nullcline

downward, Wip1 activity must be reduced by increasing K_{wip1} value in (5.1). As a result, the ability to oscillate is re-gained. In fact, (Darlington et al., 2012) showed in wet lab experiment that absence of Wip1 rescues ATM deficiency phenotypes in mice. Although, our 2-D model is not detailed to account for wet lab experiments, it is capable of pointing out mathematically that degradation of Wip1 may rescue ATM mutation, since nullclines are moved in the appropriate directions to recover the phase space.

5.4 Effect of Mdm2 Overexpression and Mdm2 Downregulation on Cell Fate

Overexpression of Mdm2 exist in some tumors (Reifenberger, Liu, Ichimura, Schmidt, & Collins, 2003). We speculate that, the consequence of overexpression of Mdm2 does not originate from straightforward suppressor-effector relationship resulting in p53 downregulation. The effect of the overexpression of Mdm2 is modelled via the introduced 2-D oscillator as: Increasing of $[Mdm2_n]$ stops the oscillations and driving the trajectories towards a relatively high steady state as shown in Figure 5.2a. Since the oscillation stops due to a dysfunction of $[Mdm2_n]$, $Mdm2_n$ cannot be utilized further in the second phase of the p53 dynamics to elevate $[p53*]$ to a higher level, resulting in a failed apoptosis.
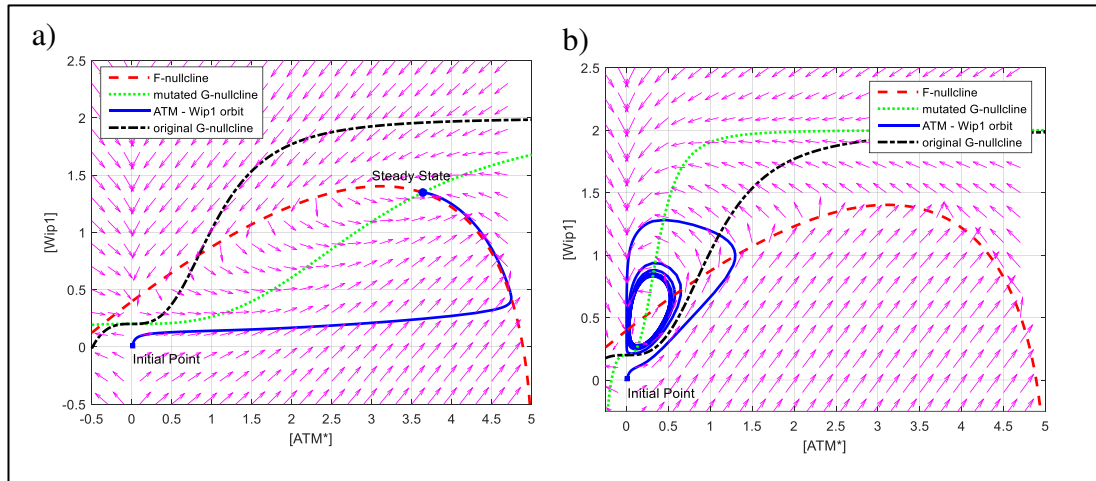
Figure 5.2 Downregulation and upregulation of $Mdm2_n$ changes the location of G-nullcline and affects the phase space of oscillator

In our 2-D oscillator model, downregulation of $Mdm2_n$ results in smaller amplitude oscillations (Figure 5.2b). According to our model, decreasing p53 inhibitor (e.g. $Mdm2_n$) levels does not cause a sustained high level of [p53*] for triggering apoptosis. This feature of 2-D oscillator model implies that p53-Mdm2 interaction, although it is structurally and biologically well-understood (El-Deiry, 1998), would affect p53 network in an unexpected way causing an additional level of complexity. The relaxation oscillator nature of the 2-D oscillator may be a source of confounding characteristics in p53 network that must be taken into account by experimentalists and it may be one of the reasons for why p53 network is becoming controversial, obsolete, and more confusing as new experiments are done (Bensussen & Díaz, 2012; Braithwaite & Prives., 2006).

5.5 A New Concept: Cancer Therapy Strategies That Obey Two-phase Dynamics

As we described previously, decreasing p53 inhibitors (e.g. $Mdm2_n$) as a cancer therapeutic approach may have counter-intuitive consequences hard to predict in the absence of a deep understanding of the p53 network. Without the knowledge of the current phase of the oscillator, degrading p53 inhibitors may harm the cell. So, a better drug to drive a cell to apoptosis would be a combination of drugs, which first stops the oscillator and then try to degrade p53 inhibitors (There are available tools, for example (Hünten, Siemens, Kaller, & Hermeking, 2013)). It means that the drug development process should take two-phase dynamics into consideration. Therefore, a drug that targets the oscillator to regain its healthy phase space would be invaluable. Such a drug development approach proposed in this paper requires a systems-level understanding of p53 network, which employs computational studies.

It must be noted that the model here is a framework since it is developed from several experiments which generates a conceptual understanding of p53 dynamics. The use of the model is for understanding the complexity of p53 dynamics, and for now its actual use in realistic conditions would be impractical. In this regard, the author emphasizes that the models in systems biology are as good as they can provide new predictions and new hypotheses about the working of the system, which can be tested

in wet lab settings. Thus, the model serves in that direction. As new findings are revealed from p53 network experiments, the proposed 2-D mathematical model can be used as a guide for more realistic complex models.

It is known that a weak cell cycle arrest signal is the prerequisite of cancer (Xu & Baltimore, 1996). So, strengthening the [p53*] oscillations may be an effective way of preventing cancer. A possible way to strengthen the oscillations may be to synchronize p53 network oscillator by another oscillator that has effect on the high steady state of [ATM*]. A candidate for this may be the circadian clock rhythm. Circadian clock and the DNA damage response is coupled through ATM (Sancar et al., 2010) and it has been shown that cancer therapies work better if circadian rhythm is taken into account (Kang & Sancar, 2009). Since circadian rhythm is produced by an oscillator and DNA damage response model involves an oscillator model (as we have shown in this chapter), mathematically investigating the coupling of these two oscillators in therapies would be valuable and it may support the current wet lab experiments as well as making testable predictions for further experiments. In Chapter 8, we propose a mathematical coupling framework in this direction.

5.6 Discussion

Wip1, which is one of the oscillating variable in the proposed model, is reported to exhibit non-oscillatory dynamics in U2OS cell line after IR exposure (Lu, et al., 2007) (Jonak, et al., 2016). In contrast, oscillatory dynamics of Wip1 is observed upon exposure of IR in some cell line studies (Batchelor, Mock, Bhan, Loewer, & Lahav, 2008) (Lu, et al., 2007). In this regard, the model can be considered as a theoretical model for some particular cell lines that possess oscillatory Wip1 dynamics. Nevertheless, it should be noted that the models that have the ability to oscillate are likely to exhibit non-oscillatory behaviour by tuning certain parameters. However, the models that lack the ability to oscillate needs substantial changes to transform its dynamics into oscillations. So, considering the fact that both oscillatory and non-oscillatory dynamics of Wip1 exist, oscillator models are more likely to point out also the mechanisms in non-oscillatory dynamics of Wip1. The search for parameter space

and mechanisms underlying the non-oscillatory dynamics of Wip1 can be studied as future studies.

Hat, Kochańczyk, Bogdał, & Lipniacki (2016) shows that if Wip1 synthesis rate is too high, oscillations are ceased. In agreement with (Hat, Kochańczyk, Bogdał, & Lipniacki, 2016), we showed in Figure 3.8 that if Wip1 feedback loop is too fast (i.e. intrinsic time delay is too small), which can be the result of the increased synthesis rate of Wip1, the oscillations are ceased. Also, the studies done for Wip1 overexpression in Figure 5.1a shows that high synthesis rate of Wip1 causes oscillations to stop.

Wip1 feedback is shown to be indispensable for the oscillations, however Mdm2 feedback is not sufficient to explain the oscillations, so questionable (Batchelor, Mock, Bhan, Loewer, & Lahav, 2008) (Sun & Cui, 2015). We just isolate the system from Mdm2 dynamics to show a resulting complex dynamics implying that Wip1 is indispensable, whereas Mdm2 is dispensable for the existence of oscillations, as with proposing a model under the isolation of Mdm2 dynamics. However, it should be noted that there are models that relies on p53-Mdm2 feedback loop and are capable of showing qualitative behaviours of p53 network (Leenders & Tuszynski, 2013) (Hunziker, Jensen, & Krishna, 2010).

CHAPTER SIX

A NOVEL 2-DIMENSIONAL POLYNOMIAL TYPE CANONICAL RELAXATION OSCILLATOR MODEL FOR P53 NETWORK

Although mathematical models are helpful in understanding how the system functions, most of the time comprehensive models to describe every detail of chemical processes is infeasible since biological processes in the cell is too complex and there are highly connected components whose interactions are not revealed yet or only known in the form of "repressing" and "enhancing". Therefore, inevitably most of the time, mathematical models proposed in systems biology focuses on the motifs arising from the main topological structure of the network omitting some of the chemical reaction details. Nevertheless, this does not diminish the importance of mathematical models, since the topological structure determines the dynamics of a biological process. Moreover, models focusing on topology is more likely to find missing nodes or to reveal essential nodes of the system.

As a biological process contains many components, so does the mathematical model of that biological process, which makes it hard to manage and understand. That's why sometimes we need to further simplify the model just to grasp how the system functions, and analyze it easily (Hartwell, Hopfield, Leibler, & Murray, 1999). Besides, studying the simpler system helps to understand the more comprehensive model of that system. Especially, if there are experimental studies revealing the structure of the system, canonical models derived from this structure can provide an abstraction of the mechanism of the whole system.

In this thesis, following a minimalist approach, we propose a 2-dimensional canonical relaxation oscillator model with polynomial terms only to describe the qualitative behavior of p53 dynamics. The model is based on the interaction between ATM and Wip1 variables which have been observed as the most essential elements of the p53 network in a series of works (Batchelor, Loewer et al., 2011; Batchelor, Mock et al., 2008; Purvis, et al., 2012; Zhang et al., 2011).The simplicity of the proposed 2-dimensional polynomial type canonical model also allows for mechanistic

50

understanding of p53 dynamics and of the qualitative changes caused by the model parameters together with their biological meanings. The model could provide researchers with an intuitive guidance without a need to consult any numerical method. Thus, in the perspective of relaxation oscillations, one can generate hypotheses about controlling p53 dynamics with the aim of developing therapeutic interventions.

2-D canonical relaxation oscillator model could be more useful in comparison to the large scale models. Canonical models provide information about the overall system behaviors due to the mechanistic explanations that they provide (Voit & Chou, 2010). A few to mention, Lotka-Volterra (Lotka, 1910; Volterra, 1927), Goodwin (Goodwin, 1965), and Fitzhugh-Nagumo (FitzHugh, 1961) canonical models have been found very useful in the contexts of ecology, biochemistry, and neurophysiology, respectively. The canonical approach reveals valid predictions by virtue of the modularity in biology, which allows for investigations both in molecular level and in functional level.

The proposed canonical oscillator model is a relaxation type oscillator, which is abundantly found in biological systems, thus increasing the validity of the model. It may serve as a suitable model for describing relaxation oscillatory dynamics of p53 network in particular and gene regulatory networks in general as does Fitzhugh-Nagumo model for neurons. As with the other relaxation oscillators, such as pacemaker cells in heart (Grudziński & Żebrowski, 2004), MAPK signaling (Kochańczyk, et al., 2017), MPF activity in frog egg extracts (Tyson & Novak, 2015), regulation of autophagy (Szymańska et al. 2015), and van der Pol model in electronics (Van der Pol, 1926), the developed canonical relaxation oscillator is characterized by jump phenomenon and fast and slow dynamical parts in the periodic trajectory, yielding constant amplitude robust oscillatory property. The importance of the proposed canonical model from the mathematical perspective is that it allows for derivation of the analytical conditions underlying each qualitative behavior of p53 network dynamics. The model allows deriving the role of timescale separation property in construction of relaxation oscillations by means of a closed form analytical expression. The model is especially useful in posing the mutation types caused by

deficient p53 network dynamics, e.g. ATM deficiency and Wip1 overexpression, as a phase space problem, thus providing a way of developing intervention strategies for these types of mutations causing cancer.

6.1 Indispensability of ATM and Wip1 for Three Modes of p53 Dynamics

It is known that p53 network regulates the DNA damage response of the cell (Murray-Zmijewski, Slee, & Lu, 2008). Studies show that p53 level is at low values under normal unstressed conditions (Michael & Oren, 2003). However, upon the exposure of gamma irradiation, double strand breaks (DSBs) in DNA occur and p53 level starts to oscillate as pulses (Lahav et al., 2004). With the onset of p53 oscillation, cell cycle is arrested to avoid the proliferation of the damaged cell, and at the same time DNA damage is being repaired by repair molecules (Toettcher et al., 2009). After a few pulses if DNA damage is not repaired, then p53 level goes to the fixed high level and maintained at that level until apoptosis is triggered (Purvis, et al., 2012; Purvis & Lahav, 2013; Vousden & Lane, 2007). If the damage is repaired, then p53 level goes back to the low level and normal cell cycle progression is continued (Branzei & Foiani, 2008). This mechanism of response give cell some flexibility such that only if attempts to repair fail, then the decision of apoptosis is given (Batchelor, Mock et al., 2008; Lahav et al., 2004; Purvis et al., 2012; Zhang, Brazhnik, & Tyson., 2007). A 17-dimensional mathematical model is proposed in (Zhang et al., 2011) for describing the aforementioned flexibility of p53 dynamics showing three qualitative modes: low level (unstressed conditions), oscillations (cell cycle arrest) and a sustained high level (apoptosis).

In p53 network, DSBs upon the exposure of gamma radiation are detected by Ataxia Telangiectasia Mutated (ATM) (Kurz & Lees-Miller, 2004; Pandita et al., 2000). When there are DSBs in DNA, repair molecules form a complex with DSBs (DSBCs) (Ma et al., 2005; Rothkamm, Krüger, Thompson, & Löbrich, 2003). The produced DSBCs activates ATM by phosphorylation. Experimental studies show that even at low IR doses, i.e. a few DSBs, ATM is rapidly activated and transformed to active ATM (ATM*), suggesting that ATM is highly sensitive to DSBs (Bakkenist & Kastan, 2003). A positive feedback loop of ATM* allows for this rapid activation and gives

the property of switch-like behaviors of ATM. Mathematical models suggest that ATM has bistability property due to this auto-activation (i.e. positive feedback loop) (Ma et al., 2005; Mouri, Nacher, & Akutsu, 2009). According to this suggestion, ATM* level stays at a low steady state in the absence of DSBCs and switches to a high steady state in case of DSBCs. Activation of ATM is regarded as the first step of DNA damage response (Bakkenist & Kastan, 2003).

One of the important roles of ATM is signaling the DNA damage to p53 (Batchelor, Loewer, Mock, & Lahav, 2011). After IR exposure, p53 activity is elevated due to the phosphorylation by ATM. p53 activation increases the expression of Wip1 (Wild-type p53-Induced Phosphatase 1), which is known to be an inhibitor of ATM*. Thus, this sequence of interactions form a negative feedback loop between ATM and Wip1 (Shreeram, et al., 2006) (Figure 6.1a). Although other interactions exist, such as Wip1 inhibition of p53, ATM inhibition of p53 inhibitor Mdm2 (Lahav et al., 2004) (Batchelor, Loewer, Mock, & Lahav, 2011), only feedback loop interaction between ATM and Wip1 dynamics has been reported to be indispensable for p53 oscillations (Batchelor, Loewer, Mock, & Lahav, 2011). In addition, there are experimental studies demonstrating that interplay between ATM and Wip1 is the key in regulation of cell cycle checkpoints and apoptosis (Darlington, et al., 2012; Shreeram, et al., 2006a, 2006b; Xia, Ongusaha, Lee, & Liou, 2009). Also in mathematical models, the importance of ATM and Wip1 negative feedback loop in describing p53 network dynamics has been demonstrated (Batchelor, Mock, Bhan, Loewer, & Lahav, 2008; Zhang et al., 2011) and in Chapter 2 and 3 of this thesis. Thus, in this chapter we only focus on the construction of p53 network dynamics by the topological structure of ATM and Wip1 interaction.

The ATM and Wip1 proteins separately or together have been included in the models that attempt to simulate p53 oscillations. For example, Mouri, Nacher, & Akutsu (2009) suggested a model which shows the activation of ATM by DSBs. They mathematically reveal that ATM dynamics must possess the bistability property to account for the switch-like behaviours. Ma et al. (2005) proposed a model in which a bistable ATM sensor module switches p53-Mdm2 oscillator on or off. However, this

model does not include Wip1 feedback loop which is now known indispensable for oscillations (Batchelor, Mock et al., 2008). The studies show via wet lab experiments also that Mdm2 and p53 interaction is not responsible for oscillations (Batchelor, Mock et al., 2008). On the other hand, Zhang et al. (2011) proposed a comprehensive mathematical model, in which ATM switches p53 oscillations on or off. In their model, feedback loop interaction between ATM and Wip1 is indispensable for oscillations. Also via mathematical model, Zhang et al. (2011) describes the two-phase dynamics of p53, in which p53 is driven into high levels only after the oscillation phase when the DNA damage is unrepairable. In their model, distraction of Wip1 feedback loop is the key to change of dynamics of p53 network, i.e. the transition from oscillatory to fixed high level state. There are several other models that try to replicate the oscillatory dynamics of p53 (Sun & Cui, 2015). However, the models that keep ATM and Wip1 interaction on the forefront and study the high and low states as well as oscillations are rare (Sun & Cui, 2015; Zhang et al., 2011).

Focusing on the interaction between the bistable ATM characteristics and Wip1 feedback loop, in this thesis, we propose a 2-dimensional canonical relaxation oscillator model that is able to replicate the three distinct qualitative behaviour of p53 network: 1) rest state, 2) oscillations and 3) high steady state. For the sake of obtaining lower dimensional models, p53 may simply be hidden, so ATM* is directly linked to Wip1 activity (See Figure 6.1b). In the proposed model, ATM has been chosen as the representative variable of p53 dynamics, due to the direct proportional relation between p53 and ATM.

Three qualitative modes of p53 dynamics can be represented by the constructed canonical model as follows. Low state of p53* is observed when there is no DSBC activity. In this case, ATM* stays at low level, so is p53* indicating normal cell cycle progression (Michael & Oren, 2003). Oscillations of p53* is observed when there is DSBC activity. In this case, ATM* level switches to a high steady state rapidly. ATM* increases the activity of Wip1 which in turn deactivates ATM* even in the presence of DSBC. As ATM* level falls, Wip1 activity (level) decreases also. With the decrease of inhibitory Wip1 activity, ATM is again activated by DSBCs if DSBCs still persist

in the environment. Thus, ATM repeatedly checks for the existence of DSBs (Batchelor, Mock et al., 2008). If ATM is activated by the existent DSBCs, Wip1 level is re-activated. As this sequence is repeated, ATM* and Wip1 oscillations are formed. Since p53 is on the feedback loop between ATM* and Wip1, we can further assume that p53* level oscillates too indicating cell cycle arrest. Indeed, this is in agreement with biological findings where it has been shown that p53 oscillations result from the recurrent initiation of ATM activity (Batchelor, Mock et al., 2008). High steady state of p53* indicating apoptosis is observed when there are DSBCs in the environment and at the same time Wip1 feedback loop is distracted (see Figure 6.1c). In this case, DSBCs activates ATM* and the increased ATM* level is stuck at a high level due to the absence of inhibitory Wip1 activity. With the increased ATM* level, p53* level also stays at a high level indicating the initiation of apoptosis.
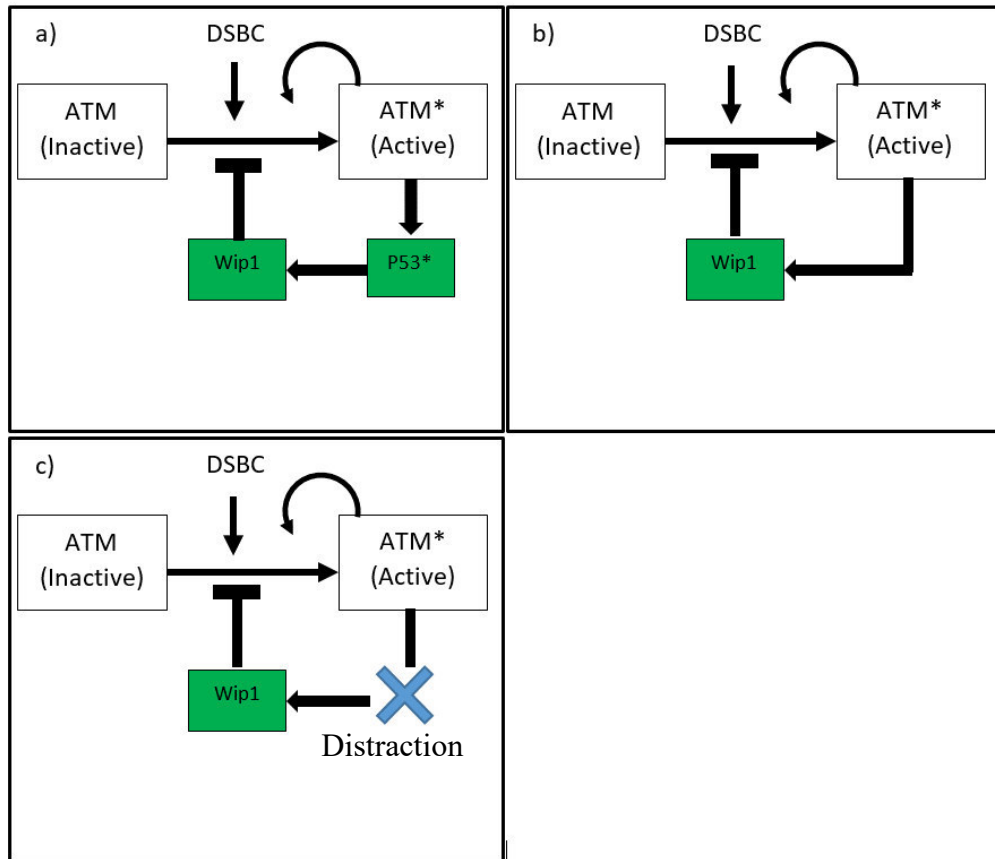
Figure 6.1 Simple interaction diagram of ATM and Wip1 that shows three different behaviors. a) ATM-p53-Wip1 interaction. b) p53 is hidden by considering ATM directly influences Wip1. c) When there is DSBC activity (i.e. high n_c), distraction of Wip1 feedback loop is the indicator of apoptosis (a sustained high level of ATM*, accordingly a sustained high level of p53*)

6.2 2-dimensional Polynomial Type Canonical Relaxation Oscillator Model of p53 Network

We propose a canonical relaxation oscillator model with polynomial terms only for p53 network as defined by the ordinary differential equations of two state variables in (6.1) and (6.2), under the constraint given in (6.3) which is able to replicate the three qualitative behaviors of p53 network. When relevant parameters of the model are adjusted properly, the model is able to show: 1) low equilibrium state 2) oscillations 3) high equilibrium state. Although, the proposed model shows these behaviors distinctively, the model can be extended to higher dimensions with the introduction of new variables that manipulate those relevant parameters automatically. For example, an oscillation accumulation term (e.g. P53DINP1) can be added to the model, to make the switching from oscillations to high steady state if DSBs are not repaired after a few pulses. However, it is not the concern here. We focus on the emergence of these three distinct behaviors from the topological structure between the bistable ATM and Wip1 feedback loop by proposing the following canonical model with polynomial terms that have the interpretability of known interactions between ATM and Wip1.

$$\dot{x} = \frac{1}{\tau_1}(-x[r\,(x^2 - (a+b)x) + ab + cy - rd]) \tag{6.1}$$

$$\dot{y} = \frac{1}{\tau_2}(z + mx - ny) \tag{6.2}$$

$$ab - d + \frac{cz}{n} < 0 \tag{6.3}$$

Above, x and y stand for ATM* and Wip1 levels, respectively, $\dot{x} \overset{\text{def}}{=} \frac{dx}{dt}$ and $\dot{y} \overset{\text{def}}{=} \frac{dy}{dt}$. The parameters a, b, c, d, n, z, τ_1 and τ_2 are positive constants whilst m is nonnegative. The parameter r is an external signal modelled as a constant whose value may change between 0 and 1 indicating the severity of the DNA damage.

The right side of (6.1) is set as a third order polynomial, since bistability dynamics can be obtained by having at least 3 equilibrium points, two of which are asymptotically stable and the third is a repeller (Avcu et al., 2015, 2016). In this way, bistable dynamics of ATM is constructed by the minimalist approach followed in this thesis. Negative feedback loop to be provided by Wip1 can be obtained by introducing

the term $-x(cy)$ in (6.1) and the term mx in (6.2). The parameter m is used for modelling the cut off of Wip1 negative feedback loop as with setting it to zero (see Figure 6.1c). The positive values of m are for modelling the link between ATM and Wip1. To possess the desired p53 dynamics, the values of the model parameters must be chosen such that the constraint in (6.3) is satisfied. Throughout the analyses in the thesis, $b > a$ is assumed with no loss of generality.

Since the bistable ATM dynamics and Wip1 negative feedback loop constitute the backbone of p53 network dynamics as we show in Chapters 2 and 3, a biologically meaningful mathematical model must have these properties. Equation (6.1) provides the bistable property of ATM, whilst (6.2) provides the feedback loop property of Wip1. Due to the direct relation between ATM* and p53 dynamics, x can be considered as the representative variable of p53 dynamics as well. Figure 6.2 gives time evolution of x level demonstrating the aforementioned three distinct modes of p53 dynamics for the constant parameters $P^* \stackrel{\text{def}}{=} \{a = 5, b = 10, c = 15, d = 70, n = 0.8, z = 0.5, \tau_1 = 1, \tau_2 = 1\}$, and adjustable (mode design) parameters $m \in \{0, 1.25\}$ and $r \in \{0,1\}$. Herein, the low equilibrium state mode is obtained when $r = 0$ and $m = 1.25$, the oscillation when $r = 1$ and $m = 1.25$, and high equilibrium state when $r = 1$ and $m = 0$. These selected values of the parameters will be used throughout the analyses, unless stated otherwise.

The parameter r in (6.1) models the input $N_c/(1 + N_c)$, having a saturation property, where N_c is the number of DSBCs. As N_c increases, the term r goes to 1 asymptotically. This assumption is fitted to the consideration of (Zhang, Liu, & Wang, 2011) in modelling the activation of ATM by DSBCs. If there is no DSBC activity (N_c = 0), indicating no DNA damage, then the parameter r becomes zero.

In the introduced model, the variable x (ATM) is regulated negatively by y (Wip1), whilst y is regulated positively by x. In addition, x has a self-activation property with the term "rdx", which stands for the auto-activation property of ATM. The term "$-xab$" stands for degradation of ATM. Wip1 is known to reset ATM activity even in the presence of DNA damage (Shreeram, et al., 2006a). Thus, the term "$-xcy$" is

included in (6.1) for the strong inhibition property of Wip1 on ATM. On the other hand, the term "$cy - rd$" changes the location of the critical points of the parabola defined by factor $Q(x) \overset{\text{def}}{=} r\left(x^2 - (a+b)x\right) + ab + cy - rd$ in (6.1), so does dynamical properties of the model which is crucial in forming of oscillations as will be detailed in the following sections.
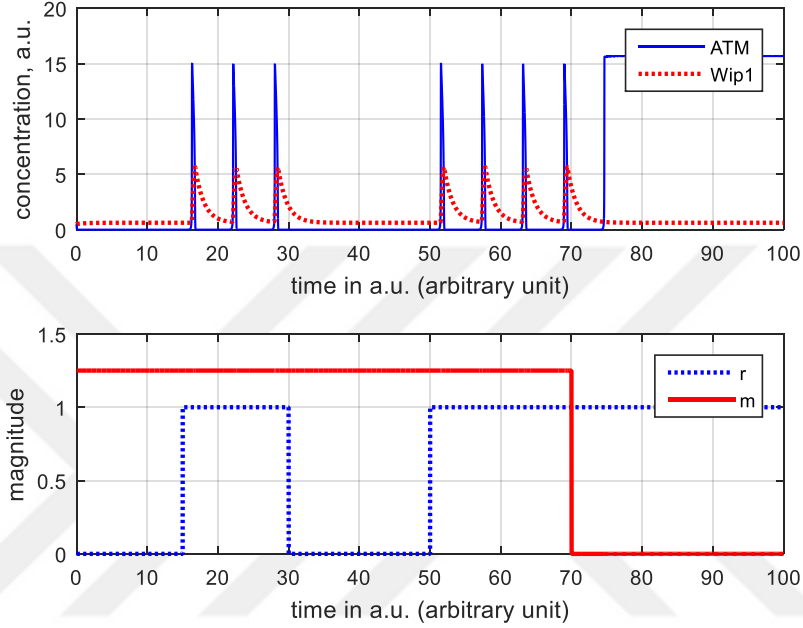
Figure 6.2 The proposed canonical 2-D oscillator model defined by Equations (6.1) and (6.2) is able to replicate three qualitative behaviours of p53 network, namely low state, oscillations and a (sustained) high state

Equation (6.2) has a constant production rate of z. The term "mx" stands for the activation of y by x and the term "$-ny$" stands for the degradation of y. Since y feeds back negatively to x, this means x suppresses itself after a time delay by a feedback loop.

Figure 6.2 gives time evolution of x level demonstrating the aforementioned three distinct behaviours of p53 dynamics. The parameters are chosen as $a = 5, b = 10, c = 15, d = 70, m = 1.25, n = 0.8, z = 0.5, \tau_1 = \tau_2 = 1$. In the time intervals [0, 20] and [30, 50], there are no DSBs in DNA. Thus, the representative variable ATM is at rest state. In the time intervals [15, 30] and [50, 70] there is a high DSBC activity and Wip1 feedback loop is on as indicated by the parameters r = 1 and

m = 1.25, respectively. In this case, ATM level oscillates. When time is greater than 70 a.u., r is still 1 but the parameter m is made zero to cut off y (Wip1) feedback loop. In this case, ATM level stops oscillating and goes to a fixed high level indicating the initiation of apoptosis.

Since ATM* (x) dynamics is known to be fast and Wip1 (y) feedback is relatively slow, the proposed model must account for this time scale separation property. Indeed, the mechanism of the proposed model is suitable to be split into fast and slow dynamics for this timescale separation since the dynamics of x naturally tends to be faster than the dynamics of y, due to the jumps in x dynamics as will be detailed in the following sections. We provide also time scaling parameters τ_1 and τ_2, for further tuning the periods of the oscillations.

6.3 Analysis of Three Modes of the Model

To demonstrate the three modes of the model, namely low and high equilibrium states, and oscillation, we employ a parametric local stability analysis in this section. We show which parameters are critical for the existence of any of these three dynamical behaviours and which ranges of these parameters ensure these behaviours. Since the proposed model is of 2-dimensional, graphical methods, namely the dynamic route and phase portrait, can be employed as the analysis and design tools. As will be seen, the analysis of the model is tractable due to the polynomial nature of the nonlinearities.

In the analysis of a model, the location and the Lyapunov stability of equilibrium points are of great importance. The location of equilibriums of a 2-dimensional system given with Ordinary Differential Equations (ODEs) can be found by the intersection of nullclines that are defined as $\dot{x} = 0$ and $\dot{y} = 0$ in $x - y$ space. Stability information of these equilibria can be obtained from the local stability analysis that involves computation of eigenvalues of Jacobian matrix evaluated at those equilibria. There are three nullclines of the system. Equation (6.1) has two nullclines each of which makes $\dot{x}$ zero. One of the nullclines of (6.1) is the vertical axis given in (6.4), and the other

nullcline is the set of points defined by (6.5). Equation (6.2) has one nullcline defined by (6.6).

$$x_{nullcline1}: x = 0 \tag{6.4}$$

$$x_{nullcline2}: y_x = -\frac{rx^2 - r(a + b)x + ab - rd}{c} \tag{6.5}$$

$$y_{nullcline}: y_y = \frac{mx + z}{n} \tag{6.6}$$

As stated, equilibria of the system are the points where $\dot{x}$ and $\dot{y}$ are both zero. Therefore, equilibrium points can be found from the intersection of (6.4) and (6.6) or (6.5) and (6.6). One of the equilibrium points is located at the intersection of (6.4) and (6.6), which is (0,z/n). At the intersection of (6.5) and (6.6), there can be one or two equilibrium points depending on the value of the parameter r. Clearly, if r is zero, (6.5) reduces to a first order polynomial that intersects with (6.6) at only one point. If r is non-zero, then the parabola (6.5) and the line (6.6) intersect at two points. Thus, the system has 2 or 3 equilibria depending on the parameter r under the constraint in (6.3) and the condition $m \neq 0$ whenever $r = 0$.

If r is zero, there is only one more equilibrium point of the system in addition to the equilibrium (0,z/n). In this case, (6.5) reduces to a constant function, $y_x = -\frac{ab}{c}$, and the intersection point of (6.5) and (6.6) becomes $(-\frac{n}{m}\left(\frac{ab}{c} + \frac{z}{n}\right), -\frac{ab}{c})$, which is in the third quadrant.

For a non-zero r, two more equilibrium points in addition to $(0, \frac{z}{n})$ can be found by equating the right hand sides of (6.5) and (6.6) and then solving for x. A quadratic equation whose roots correspond to these equilibrium points is obtained as in (6.7).

$$rx_{eq}^2 - \left(r(a + b) - \frac{cm}{n}\right)x_{eq} + \left(ab - rd + \frac{cz}{n}\right) = 0 \tag{6.7}$$

By using the root formula, two equilibrium points can be expressed as in Table 6.1. Stability of the equilibria can be determined from the Jacobian matrix evaluated at those points. Since the proposed model (6.1)-(6.2) is of 2-dimensional, the Jacobian matrix obtained as (6.8) in terms of model parameters is a 2x2 matrix, having two eigenvalues.

Table 6.1 The equilibrium points of the proposed canonical system model

The parameter, r	Equilibrium points at the intersection of (6.4) and (6.6)	Equilibrium point(s) at the intersection of (6.5) and (6.6)
$0 < r \leq 1$	$(0, z/n)$	x components of the equilibrium points: $$x^*_{1,2} = \frac{\left((a+b) - \frac{cm}{rn}\right) \pm \sqrt{\left((a+b) - \frac{cm}{rn}\right)^2 - \frac{4}{r}\left(ab - rd + \frac{cz}{n}\right)}}{2}$$ y components of the equilibrium points: $$y^*_{1,2} = \frac{mx^*_{1,2} + z}{n}$$
$r = 0$	$(0, z/n)$	$\left(-\frac{n}{m}\left(\frac{ab}{c} + \frac{z}{n}\right), -\frac{ab}{c}\right)$

For the 2-dimensional system, the stability of equilibrium points can be easily determined from the determinant and the trace of the Jacobian matrix without actually finding the eigenvalues. If the determinant $det(J)$ of the Jacobian matrix is negative, then these two eigenvalues are opposite in sign, indicating that the equilibrium is a saddle point. If $det(J) > 0$, then the signs of the eigenvalues are both negative or positive depending on the sign of the trace. If $det(J) > 0$ and the trace is negative, then the eigenvalues are both negative, meaning that the equilibrium point is asymptotically stable, i.e. an attractor. If $det(J) > 0$ and the trace is positive then the eigenvalues are both positive, meaning that the equilibrium point is unstable, i.e. a repeller. Following this discussion, the stability analyses of the equilibrium points given in Table 6.1 will be carried out in Sections 6.3.1-6.3.7.

$$J =$$

$$\begin{bmatrix} 1/\tau_1 & 0 \\ 0 & 1/\tau_2 \end{bmatrix} \begin{bmatrix} \dfrac{-(rx_{eq}^2 - r(a+b)x_{eq} + ab + cy_{eq} - rd) - x_{eq}\left(2rx_{eq} - r(a+b)\right)}{m} & -cx_{eq} \\ & -n \end{bmatrix} \quad (6.8)$$

6.3.1 Normal Cell Cycle Progression: Low Equilibrium State

In this subsection, we show how the proposed 2-dimensional canonical model replicate the low steady state of x. When there is no DSBC activity in DNA, cell is in normal cell cycle progression (i.e. the parameter r is zero). Thus, Equations (6.1) and (6.2) becomes:

$$\dot{x} = \frac{1}{\tau_1}(-x(ab + cy)) \quad (6.9)$$

$$\dot{y} = \frac{1}{\tau_2}(z + mx - ny) \quad (6.10)$$

The nullclines in this case obtained are:

$$x_{nullcline1}:\ x = 0 \quad (6.11)$$

$$x_{nullcline2}:\ y_x = -\frac{ab}{c} \quad (6.12)$$

$$y_{nullcline}:\ y_y = \frac{mx + z}{n} \quad (6.13)$$

The system defined by (6.9) and (6.10) has only two equilibrium points. One of them is located at the intersection of (6.11) and (6.13), whilst the other one is located at the intersection of (6.12) and (6.13). Solving (6.11) and (6.13), the equilibrium point is found as $(x_{eq1}, y_{eq1}) = (0, z/n)$. The location of another equilibrium point, (x_{eq2}, y_{eq2}), is at $\left(-\frac{n}{m}\left(\frac{ab}{c} + \frac{z}{n}\right), -\frac{ab}{c}\right)$ which is not in the positive quadrant. The stability of the equilibrium points can be found from the Jacobian matrix (6.8) evaluated at those equilibrium points. Thus, Jacobian matrix evaluated at $(x_{eq1}, y_{eq1}) = (0, z/n)$ is:

$$J_{(x_{eq1}, y_{eq1})}^{r=0} = \begin{bmatrix} 1/\tau_1 & 0 \\ 0 & 1/\tau_2 \end{bmatrix} \begin{bmatrix} -\left(ab + \dfrac{cz}{n}\right) & 0 \\ m & -n \end{bmatrix} \quad (6.14)$$

whose determinant is:

$$det\left(J^{r=0}_{(x_{eq1},y_{eq1})}\right) = n\left(ab + \frac{cz}{n}\right)\frac{1}{\tau_1\tau_2} \tag{6.15}$$

Determinant in (6.15) is always positive since all parameters are positive. Therefore, we have to check the sign of the trace to determine the stability. The trace of (6.14) is:

$$trace\left(J^{r=0}_{(x_{eq1},y_{eq1})}\right) = -\left(ab + \frac{cz}{n}\right)\frac{1}{\tau_1} - \frac{n}{\tau_2} \tag{6.16}$$

which is always negative. So, it is concluded that the equilibrium point $(x_{eq1}, y_{eq1}) = \left(0, \frac{z}{n}\right)$ always behaves as an attractor when $r = 0$ (i.e. no DSBC activity indicating normal cell cycle progression).

Jacobian matrix evaluated at the second equilibrium point $(x_{eq2}, y_{eq2}) = \left(-\frac{n}{m}\left(\frac{ab}{c} + \frac{z}{n}\right), -\frac{ab}{c}\right)$ is:

$$J^{r=0}_{(x_{eq2},y_{eq2})} = \begin{bmatrix} 1/\tau_1 & 0 \\ 0 & 1/\tau_2 \end{bmatrix}\begin{bmatrix} 0 & c\frac{n}{m}\left(\frac{ab}{c} + \frac{z}{n}\right) \\ m & -n \end{bmatrix} \tag{6.17}$$

whose determinant is obtained as:

$$det\left(J^{r=0}_{(x_{eq,2},y_{eq,2})}\right) = -n\left(ab + \frac{cz}{n}\right)\frac{1}{\tau_1\tau_2} \tag{6.18}$$

The determinant of Jacobian matrix evaluated at (x_{eq2}, y_{eq2}) (6.18) is always negative. No matter what the trace of the Jacobian is, it implies that (x_{eq2}, y_{eq2}) which is always located in the third quadrant is a saddle point.

In conclusion, in the phase space, there is only one stable steady state which is located at $(0, z/n)$ and one saddle equilibrium state located at $\left(-\frac{n}{m}\left(\frac{ab}{c} + \frac{z}{n}\right), -\frac{ab}{c}\right)$. By looking at the organization of equilibrium points and velocity vector field as sketched in Figure 6.3, it is clear that all trajectories that start in the positive quadrant (i.e. biologically meaningful range) goes to the attractor $(0, z/n)$. From biological

63

point of view, when $r = 0$ indicating no DSBC activity, representative variable ATM* goes to zero. Therefore, the proposed model is capable of replicating the rest state of p53 network when there is no damage, as demonstrated by the trajectories of the system in Figure 6.3.
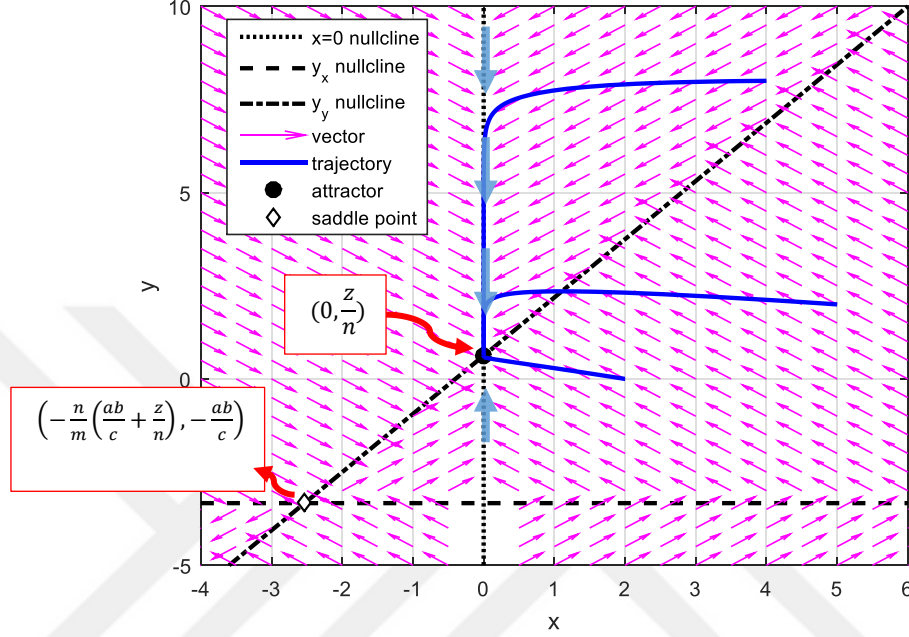
Figure 6.3 When there is no DSBC activity, indicated by $r = 0$, there is only one stable steady state located at $(0, z/n)$

6.3.2 Cell Cycle Arrest: Oscillations

In this subsection, we show how the proposed model is capable of replicating the known oscillations of p53 network. When there are DSBs in DNA, the number N_c of DSBCs raises from zero and the parameter r (i.e. $N_c /(1 + N_c)$) goes asymptotically to 1 as N_c increases. In this case, the oscillatory behaviour of p53 is known to be observed. Replacing the parameter r with its limit value of 1, the system of equations (6.1) and (6.2) become:

$$\frac{dx}{dt} = \frac{1}{\tau_1}(-x[x^2 - (a + b)x + ab + cy - d]) \qquad (6.19)$$

$$\frac{dy}{dt} = \frac{1}{\tau_2}(z + mx - ny) \qquad (6.20)$$

64

In addition to the newly imposed condition $r = 1$ and the constraint in (3), we further assume the following conditions on the model parameters to obtain a limit cycle oscillation in the first quadrant.

$$\frac{m}{n} > \frac{-\frac{1}{c}\left(-\frac{1}{4}(a+b)^2 + ab - d\right) - \frac{z}{n}}{\frac{1}{2}(a+b)} \tag{6.21}$$

$$0 < r_{tr1} < x_{eq2} < r_{tr2} \tag{6.22}$$

x_{eq2} in (6.21) is the equilibrium point defined in (6.31), which is actually the intersection point of the nullcline y_x in (6.27) and the nullcline y_y in (6.28) such that it takes place in the first quadrant when the condition (6.3) is met and it is located on the left of the maximum point $x = \frac{a+b}{2}$ of the nullcline y_x when the condition (6.21) is met. The condition (6.22) together with the parameters r_{tr1} and r_{tr2}, which are defined in (36) is imposed to ensure that the equilibrium point x_{eq2} is an unstable equilibrium point, so keeping the possibility of having oscillation within a trapping region in the first quadrant.

6.3.3 Existence of a Trapping Region in the First Quadrant

We will first show that, for all positive initial conditions and allowable range of parameters, i.e. the positive values of the parameters satisfying the condition in (6.3), the model defined in (6.1)-(6.3) with $r = 1$ has a compact, i.e. closed and bounded, trapping region in the first quadrant. Such a trapping region can be defined as follows.

$$\mathcal{R} \stackrel{\text{def}}{=} \left\{ \begin{pmatrix} x \\ y \end{pmatrix} \in R^2 \,\middle|\, 0 \leq x \leq \bar{b}; \frac{z}{n} \leq y \leq \frac{z}{n} + \frac{m}{n}\bar{b} \right\} \tag{6.23}$$

where, $\bar{b}$ which is defined in (6.24) is the right one of the intersection points of the nullcline y_x in (6.27) and the horizontal line $y = \frac{z}{n}$. A typical $\mathcal{R}$ is illustrated in Figure 6.4.

$$\bar{b} \stackrel{\text{def}}{=} \frac{(a+b) + \sqrt{(a+b)^2 - 4\left(ab - d + \frac{cz}{n}\right)}}{2} \tag{6.24}$$
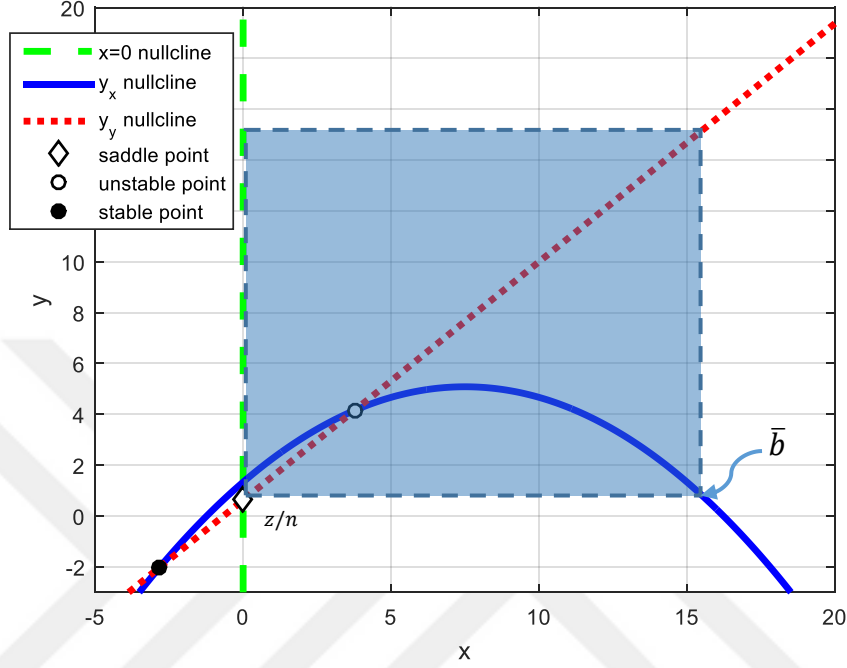
Figure 6.4 Illustration of a possible closed bounded trapping region $\mathcal{R}$ in the positive quadrant for $r=1$

To prove that $\mathcal{R}$ is a trapping region, we will show that i) $\dot{x} \geq 0$ when $x = 0, \frac{z}{n} \leq y \leq \frac{z}{n} + \frac{m}{n}\bar{b}$, ii) $\dot{x} \leq 0$ when $x = \bar{b}$ and $\frac{z}{n} \leq y \leq \frac{z}{n} + \frac{m}{n}\bar{b}$, iii) $\dot{y} \geq 0$ when $0 \leq x \leq \bar{b}$ and $y = \frac{z}{n}$, and iv) $\dot{y} \leq 0$ when $0 \leq x \leq \bar{b}$ and $y = \frac{z}{n} + \frac{m}{n}\bar{b}$. As will be seen from the following analysis, the trajectories not only point inward but also follow a counter-clockwise direction on the boundaries of the trapping region $\mathcal{R}$.

i) When $x = 0$ and $\frac{z}{n} \leq y \leq \frac{z}{n} + \frac{m}{n}\bar{b}$, (6.19) becomes $\dot{x} = 0$. On the other hand, (6.20) yields that $\dot{y} = \frac{1}{\tau_2}(z - ny) = 0$ for $y = \frac{z}{n}$ and $\dot{y} < \frac{1}{\tau_2}\left(z - n\frac{z}{n}\right) = 0$ for $\frac{z}{n} < y \leq \frac{z}{n} + \frac{m}{n}\bar{b}$.

ii) When $x = \bar{b}$ and $\frac{z}{n} \leq y \leq \frac{z}{n} + \frac{m}{n}\bar{b}$,

$$\dot{x} = \frac{1}{\tau_1}\left(-x(x^2 - (a+b)x + ab + cy - d)\right)$$

$$= \frac{1}{\tau_1} \left(-x \left(x^2 - (a+b)x + ab + c\frac{z}{n} - d \right) \right)$$

$$= \frac{1}{\tau_1} \left(-x(x - \bar{a})(x - \bar{b}) \right) = 0 \text{ for } y = \frac{z}{n} \text{ and}$$

$$\dot{x} = \frac{1}{\tau_1} \left(-x(x^2 - (a+b)x + ab + cy - d) \right)$$

$$< \frac{1}{\tau_1} \left(-x \left(x^2 - (a+b)x + ab + c\frac{z}{n} - d \right) \right)$$

$$= \frac{1}{\tau_1} \left(-x(x - \bar{a})(x - \bar{b}) \right) = 0 \text{ for } \frac{z}{n} < y \leq \frac{z}{n} + \frac{m}{n}\bar{b}.$$

The validity of the above derivations follow from that $\bar{a}$ defined in (6.25) and $\bar{b}$ in (6.24) which are the intersection points of the nullcline y_x in (6.27) with the line $y = \frac{z}{n}$ are indeed the real roots of $x^2 - (a+b)x + ab + c\frac{z}{n} - d = 0$ under the constraint of (6.3).

$$\bar{a} \overset{\text{def}}{=} \frac{(a+b) - \sqrt{(a+b)^2 - 4\left(ab - d + \frac{cz}{n}\right)}}{2} \tag{6.25}$$

On the other hand, by (19), we get

$$\dot{y} = \frac{1}{\tau_2}(z + mx - ny) = \frac{1}{\tau_2}(z + m\bar{b} - ny) >$$

$$\frac{1}{\tau_2}\left(z + m\bar{b} - n\left(\frac{z}{n} + \frac{m}{n}\bar{b}\right)\right) = 0$$

.

iii) When $0 \leq x \leq \bar{b}$ and $y = \frac{z}{n}$, we have

$\dot{x} = 0$ for $x = 0$ and

$$\dot{x} = \frac{1}{\tau_1}(-x(x^2 - (a+b)x + ab + cy - d))$$

$$= \frac{1}{\tau_1}\left(-x \left(x^2 - (a+b)x + ab + c\frac{z}{n} - d \right) \right)$$

$$= \frac{1}{\tau_1}(-x(x - \bar{a})(x - \bar{b})) > 0 \text{ for } 0 < x < \bar{b} .$$

This result is seen from that $\bar{a} < 0$ under the constraint in (6.3), $x > 0$ and $x - \bar{b} < 0$.

Furthermore, $\dot{x} = \frac{1}{\tau_1}\left(-x(x-\bar{a})(x-\bar{b}) \right) = 0$ for $x = \bar{b}$. On the other hand,

$\dot{y} = \frac{1}{\tau_2}\left(z + mx - n\frac{z}{n} \right) = \frac{1}{\tau_2}mx = 0$ for $x = 0$ and $\dot{y} = \frac{1}{\tau_2}mx > 0$ for $0 < x \leq$ $\bar{b}$.

iv) When $0 \leq x \leq \bar{b}$ and $y = \frac{z}{n} + \frac{m}{n}\bar{b}$, we have

$\dot{x} = 0$ for $x = 0$ and

$$\dot{x} = \frac{1}{\tau_1}\left(-x(x^2 - (a+b)x + ab + cy - d) \right)$$

$$= \frac{1}{\tau_1}\left(-x\left(x^2 - (a+b)x + ab + c\frac{z}{n} + c\frac{m}{n}\bar{b} - d \right) \right)$$

$$= \frac{1}{\tau_1}\left(-x\left((x-a)(x-b) + c\frac{z}{n} + c\frac{m}{n}\bar{b} - d \right) \right) <$$

$$\frac{1}{\tau_1}\left(-x\left(\left(\frac{a+b}{2} - a\right)\left(\frac{a+b}{2} - b\right) + c\frac{z}{n} + c\frac{m}{n}\bar{b} - d \right) \right) =$$

$$\frac{1}{\tau_1}\left(-x\left(-\frac{1}{4}(b+a)^2 + ab - d + c\frac{z}{n} + c\frac{m}{n}\bar{b} \right) \right) <$$

$$\frac{1}{\tau_1}\left(-x\left(-\frac{1}{4}(b+a)^2 + ab - d + c\frac{z}{n} + c\frac{m}{n}\frac{a+b}{2} \right) \right) < 0$$

for $0 < x \leq \bar{b}$. The first inequality above follows from that $(x-a)(x-b)$ has the minimum at $\frac{a+b}{2}$. The second inequality is seen from the fact that $\bar{b} > \frac{a+b}{2}$ for $\bar{b}$ defined in (6.24). The last inequality is a consequence of the condition in (6.21). On the other hand,

$\dot{y} = \frac{1}{\tau_2}\left(z + mx - n\frac{z}{n} - n\frac{m}{n}\bar{b} \right) = \frac{1}{\tau_2}(-m\bar{b}) < 0$ for $x = 0$ and $\dot{y} = \frac{1}{\tau_2}\left(z + mx - \right.$

$\left. n\frac{z}{n} - n\frac{m}{n}\bar{b} \right) < \frac{1}{\tau_2}(m\bar{b} - m\bar{b}) = 0$ for $0 < x < \bar{b}$ while $\dot{y} = \frac{1}{\tau_2}\left(z + mx - n\frac{z}{n} - \right.$

$\left. n\frac{m}{n}\bar{b} \right) = \frac{1}{\tau_2}(m\bar{b} - m\bar{b}) = 0$ for $x = \bar{b}$.

Thus, it is concluded that there is a closed and bounded trapping region in the first quadrant. It is also seen by the results in i)-iv) that a) $\dot{x} = 0$ and $\dot{y} \leq 0$ for the points lying on the left vertical edge of $\mathcal{R}$, b) $\dot{x} \leq 0$ and $\dot{y} > 0$ for the points on the right

vertical edge, c) $\dot{x} \geq 0$ and $\dot{y} \geq 0$ for the points on the lower horizontal edge, and d) $\dot{x} \leq 0$ and $\dot{y} \leq 0$ for the points lying on the upper horizontal edge.

6.3.4 Determining Locations and Stability Types of Equilibria by Using Nullclines and Jacobian

Now, we will determine all equilibrium points of (6.19)-(6.20) under the constraint in (6.3) and provide their local stability analyses. Then, we will show that, under the parametric conditions in (6.21)-(6.22), the trapping region has indeed two equilibrium points; one of which is a repeller located in the interior of the trapping region such that all nearby trajectories escape away from it and the other equilibrium point is a saddle point $\left(x_{eq1}, y_{eq1}\right) = (0, \frac{z}{n})$ located at the lower left corner of the trapping region $\mathcal{R}$ such that it attracts the trajectories initiated at the vertical axis $x = 0$, and repels all other trajectories started within the trapping region.

We investigate the general characteristics of the nullclines since their organization in the phase space is crucial for the characteristics of the system dynamics such as the location of equilibrium points and the directions of the trajectories. When $r = 1$, the nullclines become:

$$x_{nullcline1}: x = 0 \tag{6.26}$$

$$x_{nullcline2}: y_x = -\frac{x^2 - (a + b)x + ab - d}{c} \tag{6.27}$$

$$y_{nullcline}: y_y = \frac{mx + z}{n} \tag{6.28}$$

Nullcline y_x is a second order polynomial (a parabola) that opens down since the coefficient $-1/c$ of the quadratic term is negative. It has one maximum point at $x = (a + b)/2$. The nullcline y_x cuts the y-axis at $(d - ab)/c$, whilst y_y cuts the y-axis at z/n. As imposed by the constraint of (6.3), we restrict the choice of parameters such that z/n is always smaller than $(d - ab)/c$ to allow just one nontrivial equilibrium point, namely an equilibrium other than the origin, in the first quadrant (see Figure 6.5a,b) for all choices of parameters. y_x cuts x axis at two points as can be found easily by the root formula which is shown in (6.29) and (6.30).
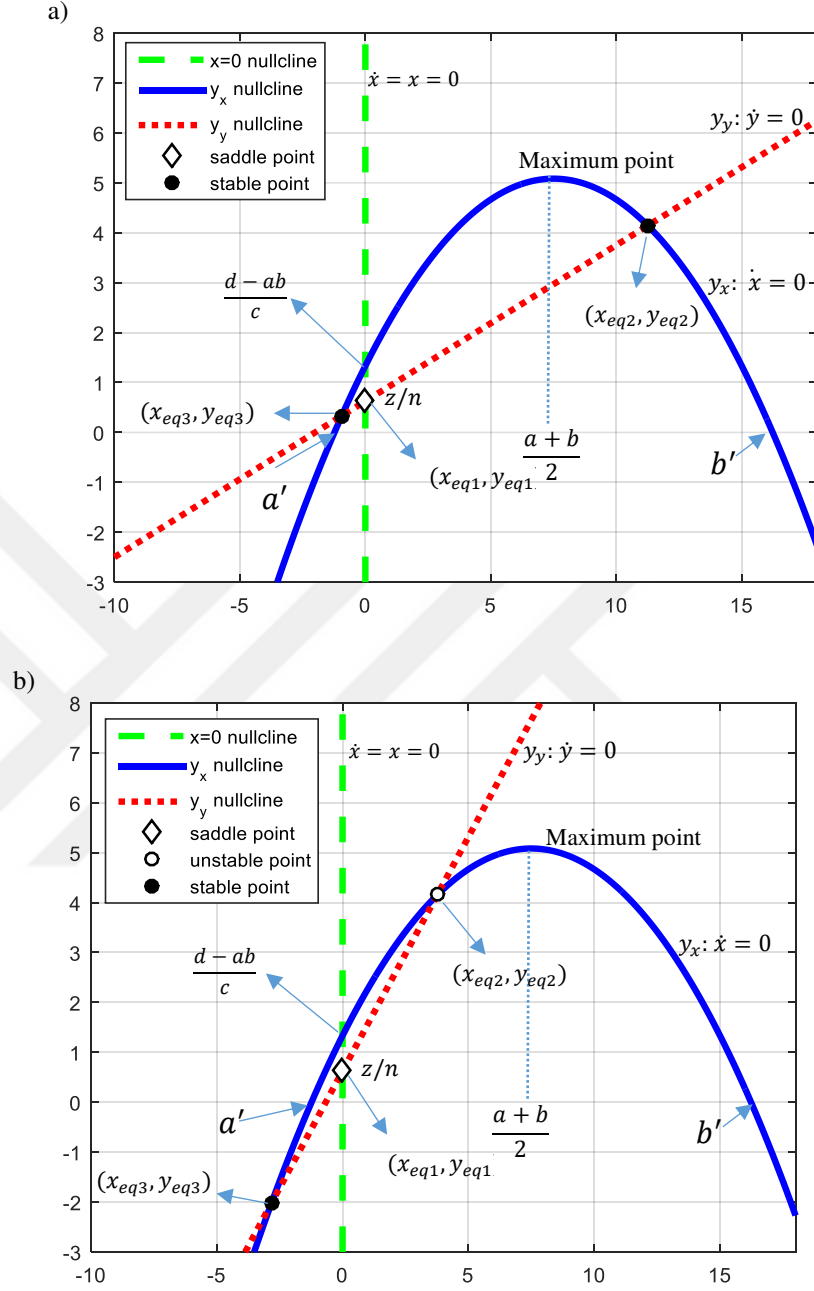
Figure 6.5 Possible nullcline organizations in the phase space. The parameter values are taken as $a = 5, b = 10, c = 15, d = 70, n = 0.8, z = 0.5, \tau_1 = \tau_2 = 1$ whilst m is taken differently in two cases a) The situation of $(x_{eq2}, y_{eq2}) < (a+b)/2$, and m is taken as 0.25. b) The situation of $(x_{eq2}, y_{eq2}) > (a+b)/2$, m is taken as 0.75

$$a' \stackrel{\text{def}}{=} \frac{(a+b) - \sqrt{(a+b)^2 - 4(ab - d)}}{2} \qquad (6.29)$$

$$b' \overset{\text{def}}{=} \frac{(a+b) + \sqrt{(a+b)^2 - 4(ab-d)}}{2} \tag{6.30}$$

b' (6.30) is always positive, whilst a' (6.29) is always negative, since constraint (6.3) also implies that the term "d-ab" must be positive. Figure 6.5 illustrates a possible organization of nullclines in x-y space.

It will be shown in the sequel that, under the constraint in (3), there is always a unique (nontrivial) equilibrium point in the first quadrant such that it is either asymptotically stable, preventing oscillations, or unstable allowing oscillations in the first (biologically meaningful) quadrant.

There are three equilibrium points when r is 1. One of the equilibrium points, (x_{eq1}, y_{eq1}), is $(0, z/n)$ which is at the intersection of (6.26) and (6.28) whilst the other two real equilibrium points, (x_{eq2}, y_{eq2}) and (x_{eq3}, y_{eq3}), are located at the intersections of (6.27) and (6.28), and found as:

$$x_{eq2,3} = \frac{\left((a+b) - \frac{cm}{n}\right) \pm \sqrt{\left((a+b) - \frac{cm}{n}\right)^2 - 4\left(ab - d + \frac{cz}{n}\right)}}{2} \tag{6.31}$$

$$y_{eq2,3} = \frac{mx_{eq2,3} + z}{n} \tag{6.32}$$

Since we limit our model to the constraint in (6.3), $ab - d + \frac{cz}{n} < 0$, there are two nontrivial equilibrium points; one, (x_{eq2}, y_{eq2}), corresponding to the unique intersection point of (6.27) and (6.28) in the positive quadrant, and the other, (x_{eq3}, y_{eq3}), in the third quadrant (see Figure 6.5).

After finding the location of the equilibrium points, now we investigate the stability of the equilibrium points by computing the Jacobian matrix at those points. Since r is 1, Jacobian matrix in (6.8) evaluated at $(x_{eq1}, y_{eq1}) = (0, \frac{z}{n})$ becomes:

$$J^{r=1}_{(x_{eq1}, y_{eq1})} = \begin{bmatrix} \frac{1}{\tau_1} & 0 \\ 0 & \frac{1}{\tau_2} \end{bmatrix} \begin{bmatrix} -\left(ab + \frac{cz}{n} - d\right) & 0 \\ m & -n \end{bmatrix} \tag{6.33}$$

whose determinant is

$$det\left(J_{(x_{eq1},y_{eq1})}^{r=1}\right) = n\left(ab + \frac{cz}{n} - d\right)\frac{1}{\tau_1\tau_2} \tag{6.34}$$

The determinant at the equilibrium point (x_{eq1}, y_{eq1}) is always negative, due to the constraint $ab + \frac{cz}{n} - d < 0$. Thus, we conclude that (x_{eq1}, y_{eq1}) is a saddle point.

It is seen from the velocity vector field depicted in Figure 6.6 that the saddle equilibrium (x_{eq1}, y_{eq1}) attracts all trajectories starting at the vertical axis $x = 0$ while repels all other trajectories starting in the trapping region $\mathcal{R}$, so still saving the possibility of having an oscillation in the resting region $\mathcal{R}\setminus\{(x, y) \in R^2 | x = 0\}$. Herein, there needs a rigorous explanation on why the trajectories starting in the region $\mathcal{R}\setminus\{(x, y) \in R^2 | x = 0\}$ do not reach to the vertical axis $x = 0$, so not to be attracted to the trivial equilibrium point. It is clear that the trajectories originated from or visiting Regions 1 and 4 depicted in Figure 6.6 never hit the vertical axis $x = 0$ since $\dot{x}$ is always nonnegative in Regions 1 and 4. On the other hand, the trajectories originated from or visiting Region 3 tend to the vertical axis $x = 0$ since $\dot{x} \leq 0$ in Region 3. However, these trajectories never reach to the vertical axis due to the following fact: When the trajectories approach to the vertical axis $x = 0$, the velocity $\dot{x}$ in the horizontal direction tends to be linear in x:

$$\dot{x} = \frac{1}{\tau_1}\left(-x(x^2 - (a + b)x + ab + cy - d)\right)$$

$\rightarrow \dot{x} = \frac{1}{\tau_1}\left(-x(ab + cy - d)\right)$. Then, the trajectories converge to exponential functions $x(t_0)exp^{-\frac{ab+cy-d}{\tau_1}(t-t_0)}$ which tend to zero, i.e. $x = 0$, in an asymptotical sense, since $ab + cy - d > 0$ in Region 3 (Observe $y \geq \frac{d-ab}{c}$ in Region 3 from Figure 6.4b and Figure 6.6). Such trajectories cannot settle down to zero in finite time, indeed, they reach to the nullcline $x_{nullcline2}$ defined in (6.27) within a finite elapsed time and then enter Region 4, so change their direction now escaping away from the vertical axis $x = 0$.

To calculate the Jacobian matrix at (x_{eq2}, y_{eq2}) and (x_{eq3}, y_{eq3}), whose x-components are non-zero, Jacobian matrix in (6.8) can be rewritten as:

$$J^{r=1}_{(x_{eq}, y_{eq}) = (x_{eq2,3}, y_{eq2,3})}$$

$$= \begin{bmatrix} \dfrac{1}{\tau_1} & 0 \\ 0 & \dfrac{1}{\tau_2} \end{bmatrix} \begin{bmatrix} \left(\dfrac{1}{x}\dfrac{dx}{dt}\Big|_{x=x_{eq}}\right) - x_{eq}(2x_{eq} - (a + b)) & -cx_{eq} \\ m & -n \end{bmatrix}$$

(6.35)

Since, by definition, $\frac{dx}{dt}\big|_{x=x_{eq}}$ is zero and $x \neq 0$ at (x_{eq2}, y_{eq2}) and (x_{eq3}, y_{eq3}), then the Jacobian matrix in (6.35) reduces to:

$$J^{r=1}_{(x_{eq}, y_{eq}) = (x_{eq2,3}, y_{eq2,3})}$$

$$= \begin{bmatrix} 1/\tau_1 & 0 \\ 0 & 1/\tau_2 \end{bmatrix} \begin{bmatrix} -x_{eq}(2x_{eq} - (a + b)) & -cx_{eq} \\ m & -n \end{bmatrix}$$

(6.36)

The determinant of (6.36) becomes:

$$\det\left(J^{r=1}_{(x_{eq}, y_{eq}) = (x_{eq2,3}, y_{eq2,3})}\right)$$

$$= \frac{2nx_{eq}}{\tau_1 \tau_2}\left(x_{eq} - \frac{(a + b)}{2}\right) + \frac{cmx_{eq}}{\tau_1 \tau_2}$$

(6.37)

$$= \frac{2nx_{eq}}{\tau_1 \tau_2}\left(x_{eq} - \frac{(a + b - cm/n)}{2}\right)$$

If we calculate determinant at (x_{eq2}, y_{eq2}) as in (6.37), it is seen that the determinant is always positive since x_{eq2} is positive and $x_{eq2} > \frac{(a+b-cm/n)}{2}$ as can be deduced from (6.31). If we calculate determinant at (x_{eq3}, y_{eq3}) as in (6.37), again it is seen that the determinant is always positive, since $x_{eq3} < \frac{(a+b-cm/n)}{2}$ and $x_{eq3} < 0$. Thus, both determinants of Jacobian matrix at (x_{eq2}, y_{eq2}) and (x_{eq3}, y_{eq3}) are positive and we need to check the trace to determine their types of stabilities. The trace equation of (6.37) is:

$$trace\left(J^{r=1}_{(x_{eq},\, y_{eq})\, =\, (x_{eq2,3}\, ,\, y_{eq2,3})}\right)$$

$$= -\frac{1}{\tau_1} 2x_{eq}\left(x_{eq} - \frac{(a+b)}{2}\right) - \frac{1}{\tau_2} n \qquad (6.38)$$

It is seen that if $x_{eq,2}$ is greater than $\frac{(a+b)}{2}$ (as illustrated in Figure 6.5a), then the trace (6.38) is always negative. Therefore, we conclude that if the condition $x_{eq2} > \frac{(a+b)}{2}$ holds, then (x_{eq2}, y_{eq2}) is definitely asymptotically stable. However, the reverse is not true. If $x_{eq2} < \frac{(a+b)}{2}$ (as illustrated in Figure 6.5b), then the trace can be negative or positive according to the values of the parameters τ_1, τ_2 and the degradation term of y, i.e. n. It can be seen by employing the following algebraic manipulations that $x_{eq2} < \frac{(a+b)}{2}$ is satisfied whenever the parameters meet the condition in (6.21):

$$\frac{\left((a+b) - \frac{cm}{n}\right) + \sqrt{\left((a+b) - \frac{cm}{n}\right)^2 - 4\left(ab - d + \frac{cz}{n}\right)}}{2}$$

$$= x_{eq2} < \frac{(a+b)}{2} \leftrightarrow$$

$$\frac{cm}{n} > \sqrt{\left((a+b) - \frac{cm}{n}\right)^2 - 4\left(ab - d + \frac{cz}{n}\right)} \leftrightarrow$$

$$\frac{m}{n} > \frac{-\frac{1}{c}\left(-\frac{1}{4}(a+b)^2 + ab - d\right) - \frac{z}{n}}{\frac{1}{2}(a+b)}$$

It is concluded that under condition in (6.21), (x_{eq2}, y_{eq2}) can be either an attractor or a repeller according to the choice of parameter values τ_1, τ_2 , n and the location of the equilibrium.

Since x_{eq3} is negative, the trace (6.38) is always negative. This result together with $\det\left(J^{r=1}_{(x_{eq3},\, y_{eq3})}\right) > 0$ implies that (x_{eq3}, y_{eq3}) is always an attractor (see Figure 6.5).

Now, we will present an additional parametric condition (i.e. the condition in 6.21) to ensure that the trapping region $\mathcal{R}$ found contains a unique (nontrivial) unstable equilibrium point which is indeed a repeller. Since (x_{eq2}, y_{eq2}) is the unique equilibrium in this trapping region, its type of stability will be the determinant for the existence of a periodic solution. If (x_{eq2}, y_{eq2}) is asymptotically stable, then all trajectories that start inside the positive quadrant will be attracted to it; However, if (x_{eq2}, y_{eq2}) is a repeller, then there will be a periodic solution as demonstrated in Figure 6.7.

We had found before that if $x_{eq2} < (a + b)/2$, then there is a range of parameter values that (x_{eq2}, y_{eq2}) is a repeller. We now aim to find this exact interval where (x_{eq2}, y_{eq2}) is definitely a repeller and so enabling to occur oscillations. For this, we re-write (6.38) as a quadratic polynomial:

$$trace\left(J^{r=1}_{(x_{eq},y_{eq})=(x_{eq2,3},y_{eq2,3})}\right) = -\frac{1}{\tau_1}2x_{eq}^2 + \frac{1}{\tau_1}x_{eq}(a + b) - \frac{1}{\tau_2}n$$

The trace equation is parabola that opens down and has a maximum point at $(a + b)/4$. The roots of the trace equation are:

$$r_{tr1,2} = \frac{(a + b) \pm \sqrt{(a + b)^2 - \frac{\tau_1}{\tau_2}8n}}{4}$$

For the real roots, the following inequality is always satisfied:

$$0 < r_{tr1} < r_{tr2} < \frac{a + b}{2}$$

The trace is always positive for the x_{eq} values that satisfy $r_{tr1} < x_{eq} < r_{tr2}$ since it is a parabola that opens down (see Figure 6.7c-d). In the other intervals (i.e. $r_{tr1} > x_{eq}$ and $x_{eq} > r_{tr2}$), the trace is negative. In addition, in case of imaginary roots, the trace is always negative as well (see Figure 6.7 and Figure 6.8). Thus the interval, $r_{tr1} < x_{eq2} < r_{tr2}$, where r_{tr1} and r_{tr2} are real and positive numbers is the exact interval, in which (x_{eq2}, y_{eq2}) is a repeller (see Figure 6.7c). It is concluded

that, together with the conditions in (6.3) and (6.21), the condition in (6.22), which can be given as follows, makes the equilibrium point (x_{eq2}, y_{eq2}) a repeller:

$$0 < \frac{(a+b) - \sqrt{(a+b)^2 - \frac{\tau_1}{\tau_2}8n}}{4}$$

$$< \frac{\left((a+b) - \frac{cm}{n}\right) + \sqrt{\left((a+b) - \frac{cm}{n}\right)^2 - 4\left(ab - d + \frac{cz}{n}\right)}}{2}$$

$$< \frac{(a+b) + \sqrt{(a+b)^2 - \frac{\tau_1}{\tau_2}8n}}{4}$$

As the parameter n or $\frac{\tau_1}{\tau_2}$ gets bigger, the interval $[r_{tr1}, r_{tr2}]$ gets smaller. This finding is crucial since it points out that a fine tuning of the parameter n (i.e. Wip1 degradation term), and the time scale separation between the x and y dynamics specified by the ratio $\frac{\tau_1}{\tau_2}$ are the keys for a larger space of parametric uncertainties that allow oscillations (see Figure 6.8). As $\frac{\tau_1}{\tau_2}$ increases, the distinction between fast and slow dynamics disappear, since as τ_1 gets bigger, fast ATM dynamics become slower. Consequently, the time scale separation and Wip1 degradation term are two important factors for oscillations: A profound difference between time scales is indispensable for robust oscillations and large n values will destroy the oscillations no matter what the other parameters are (see Figure 6.7).

6.3.5 Demonstration of the Existence of a Periodic Solution inside the First Quadrant: An Application of Poincaré–Bendixson Theorem

Poincaré–Bendixson theorem can be stated as "Given a differentiable real dynamical system defined on an open subset of the plane, then every non-empty compact ω-limit set of an orbit, which contains only finitely many equilibrium points, is either i) an equilibrium point, ii) a periodic orbit, or iii) a connected set composed of a finite number of equilibrium points together with homoclinic and heteroclinic orbits connecting these" (Teschl, 2012). Let us first observe that the considered dynamical system given with (6.1) and (6.2) differentiable on any open subset

containing the constructed trapping region $\mathcal{R}$. Under the conditions in (6.3), (6.21) and (6.22), the trapping region $\mathcal{R}$ has two equilibrium points, the one (x_{eq2}, y_{eq2}) placed at the interior of $\mathcal{R}$ is a repeller and the second one $(x_{eq1}, y_{eq1}) = (0, \frac{z}{n})$ is a saddle point attracting the trajectories starting at the vertical axis $x = 0$ while repelling all other trajectories starting in the trapping region $\mathcal{R}$. Thus, we can rule out the existence of homoclinic and/or heteroclinic orbits connecting these two equilibrium points. Let us now consider the trajectories initiated in the region $\mathcal{R} \setminus \left\{ \{(x, y) \in R^2 | x = 0\} \cup (x_{eq2}, y_{eq2}) \right\}$. ω-limit set of such a trajectory is necessarily compact since the trajectory is confined in the compact region $\mathcal{R}$. Then, by applying the Poincaré–Bendixson theorem, we can conclude that there is actually a periodic solution inside the region $\mathcal{R} \setminus \left\{ \{(x, y) \in R^2 | x = 0\} \cup (x_{eq2}, y_{eq2}) \right\}$.

A more intuitive reasoning of the trapping region would be as follows. When $r = 1$, $(x_{eq,1}, y_{eq,1}) = (0, z/n)$ is always a saddle point. The lines $x = 0$ and $y = z/n$ are locally separatrices. Separatrix $x = 0$ is an attracting separatrix, whilst $y = z/n$ is a repelling separatrix as shown by the directional field in Figure 6.6. The nullcline $x = 0$ prevents trajectories from passing to the left half plane. Therefore, we are sure that trajectories that start in the right half plane, will always stay in the right half plane. However, we still have to show that there is a trapping region in the positive quadrant. For this, we divide the right half plane into 4 regions whose boundaries are determined by the nullclines as shown in Figure 6.6. To show that the vector fields in these 4 regions points inward, consider a trajectory with an initial condition in Region-1. The signs of $\dot{x}$ and $\dot{y}$, $\dot{x} > 0$ and $\dot{y} > 0$, imply that this trajectory will eventually cut the nullcline y_x and will cross into Region-2. In Region-2, the signs of system equations are: $\dot{x} < 0$ and $\dot{y} > 0$. In this case, the trajectory will eventually cut the nullcline y_y, and cross into Region-3. In Region-3, the sign combination, $\dot{x} < 0$ and $\dot{y} < 0$, will eventually carry the trajectory to the Region-4. Region-4 is bounded by the saddle point $(0, z/n)$ at the bottom. This property is important, since it states that once a trajectory crosses Region-4 it never goes below the separatrix $y = z/n$. Thus, if there is a periodic solution, limit cycle is bounded by the separatrix $y = z/n$ from the

bottom, preventing limit cycle to cross the negative region, x>0 and y<0, in the phase space and providing a biologically meaningful range of trajectories. At last, once a trajectory is in Region-4, the sign combination, $\dot{x} > 0$ and $\dot{y} < 0$, imply that the direction of field is inward. Thus, the direction of field resulting from the organization of nullclines in the phase space shows that there is a trapping region in the positive quadrant.

To support the idea that trajectories cannot escape to infinity, consider Equations $\dot{x}$ (6.19) and $\dot{y}$ (6.20) in the limit of very large x and y values in the positive quadrant. Then, Equations (6.19) and (6.20) become:

$$\dot{x} = \frac{-x^3}{\tau_1} \tag{6.39}$$

$$\dot{y} = \frac{1}{\tau_2}(z + mx - ny) \tag{6.40}$$

There is one steady state at $(0, z/n)$. Jacobian matrice of the system of (6.39) and (6.40) at $(0, z/n)$ is:

$$J^{r=1}_{(x_{eq1}, y_{eq1}) = \left(0, \frac{z}{n}\right)} = \begin{bmatrix} -(3x^2) & -cx \\ m & -n \end{bmatrix} \begin{bmatrix} 1/\tau_1 & 0 \\ 0 & 1/\tau_2 \end{bmatrix} \tag{6.41}$$

Clearly, determinant of (6.41) is always positive and the trace of (6.41) is always negative indicating that $(0, z/n)$ acts like an attractor for large x and y values. Therefore, x and y values cannot escape to infinity. Consequently, with the local interpretation of the separatrices and investigation of the phase space in the limit of large x and y values, there is a trapping region in the positive quadrant.

The trapping region implies that there is either an attractor or a periodic solution according to the Poincaré-Bendixson theorem. Since (x_{eq2}, y_{eq2}) is the only equilibrium in this trapping region, its type of stability will be the determinant for the existence of a stable steady state or a periodic solution. If (x_{eq2}, y_{eq2}) is stable, then all trajectories that start in the positive quadrant will be attracted to it, if (x_{eq2}, y_{eq2}) is unstable, then there will be a periodic solution as demonstrated in Figure 6.7.
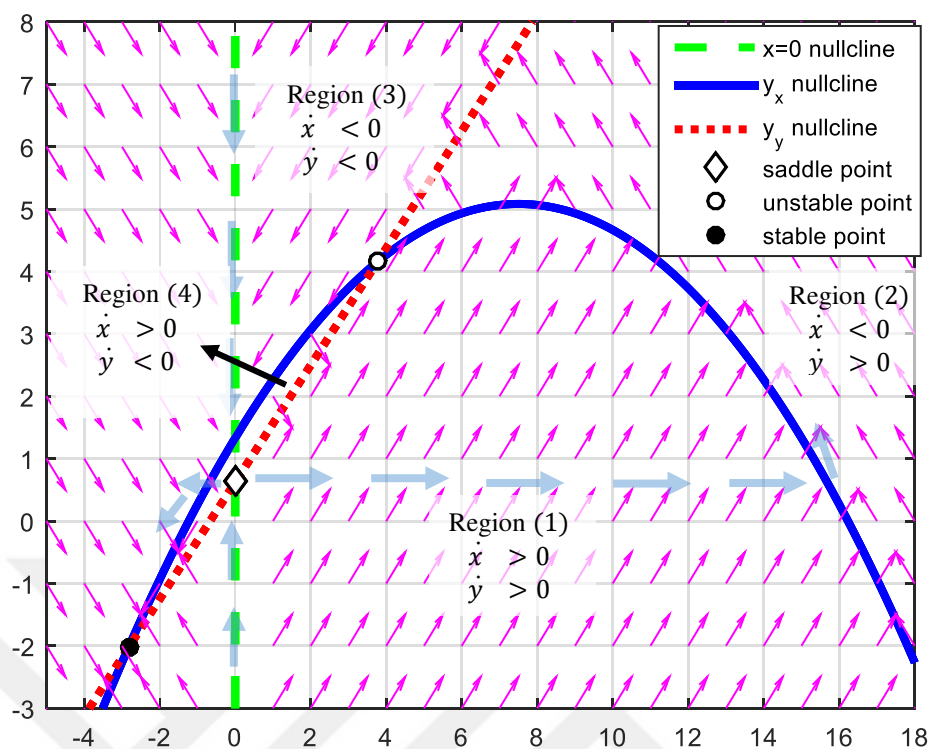
Figure 6.6 Direction field of the phase space of 2-D canonical oscillator model when (x_{eq2}, y_{eq2}) is an unstable equilibrium point
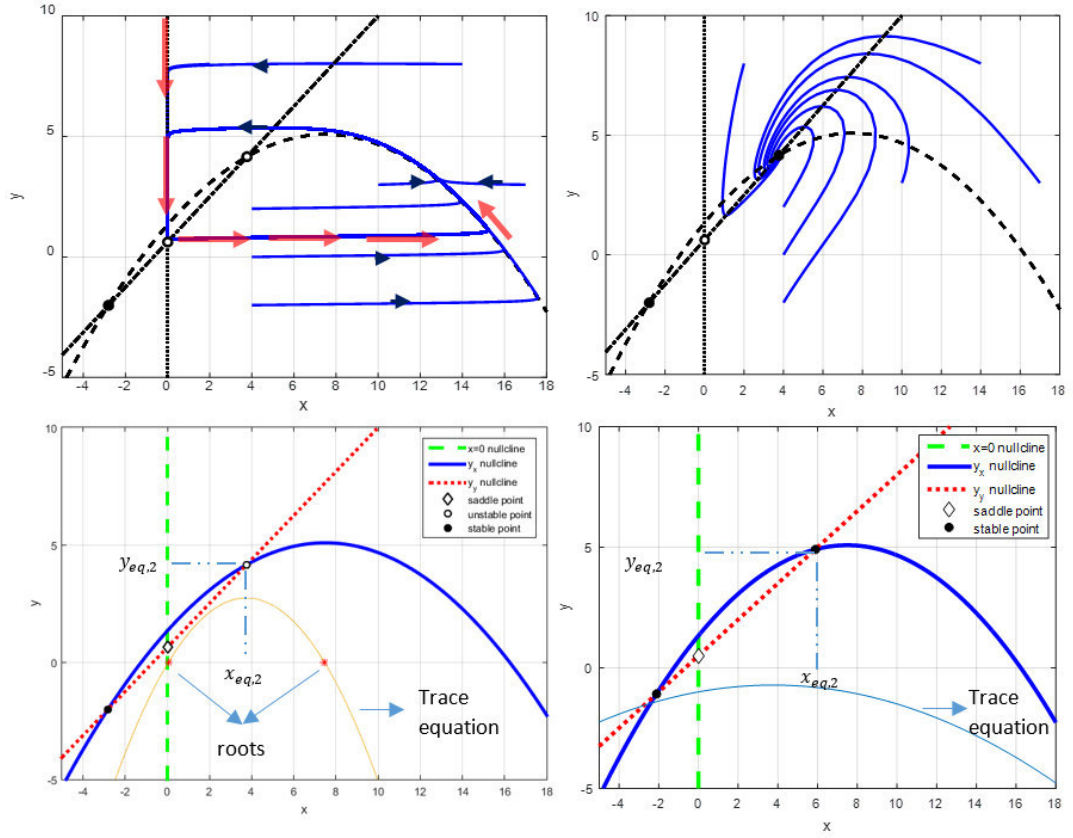
Figure 6.7 Even if the condition $(x_{eq,2}, y_{eq,2}) < $ (a+b)/2 is satisfied, depending on the parameter settings the oscillations may not exist. a) The oscillations exist for parameter settings a = 5, b = 10, c = 15, d = 70, m = 0.75, n = 0.8, z = 0.5, $\tau_1 = \tau_2 = 1$ b) The oscillations does not exist for parameter settings a = 5, b = 10, c = 15, d = 70, m = 75, n = 80, z = 50, $\tau_1 = \tau_2 = 1$. c) The oscillations exist if $x_{eq,2}$ falls between the roots of the trace equation. d) The oscillations do not exist if the trace equation has no real roots

6.3.6 Relaxation Nature of the Oscillations

In this subsection, we show that the proposed model features two main characteristics of relaxation oscillations, namely jump phenomenon and the existence of fast and slow dynamics, thus implying that it is a relaxation oscillator. Assuming there is a fine distinction between the time scales of Equations (6.1) and (6.2), we can analyse (6.1) and (6.2) separately at each time instant and identify the immediate effect of the change in one of the variables on the other for the aim of getting intuitive understanding of the mechanism of the oscillations. We investigate Equations (6.19) and (6.20) and rewrite them as in (6.42) and (6.43). As the variable y changes along the dynamics of the system, the term "cy" in (6.42) changes. However, for the sake of discussion, we investigate the change of the term "$cy - d$" in (6.42) as the variable y

changes. As "$cy - d$" changes, it perturbs the location and changes the types of stability of critical points of (6.42).

$$\dot{x} = P(x) \overset{\text{def}}{=} -\frac{x}{\tau_1} Q(x) \overset{\text{def}}{=}$$

$$\frac{1}{\tau_1}(-x[x^2 - (a+b)x + ab + cy - d])$$

(6.42)

$$\dot{y} = \frac{1}{\tau_2}(z + mx - ny)$$

(6.43)

Clearly x = 0 is one of the critical point of the (6.42), and the other 2 critical points are the roots of the polynomial $Q(x)$ which can be found by the root formula as:

$$a'\text{ and }b' = \frac{a+b}{2} \pm \sqrt{\left(\frac{a+b}{2}\right)^2 - (ab + cy - d)}$$

(6.44)

As it can be seen from (6.44), if "$cy - d$" is zero during any time of the oscillations, then the roots of the polynomial are, a and b. As "$cy - d$" changes during the working of the system, the location of the critical points of (6.44) are perturbed to a' and b'.

Investigating (6.43) separately from (6.42), (6.43) always have a stable equilibrium at $y_{eq} = (mx_{eq} + z)/n$. The location of stable critical point depends on the variable x_{eq}. Thus, the sign of y_{eq} is always positive, if we can show that x_{eq} is always positive once it starts in the positive region.

As the value of the "$cy - d$" changes the location of critical points, the types of the critical points also change. The stability of the critical points can be investigated by locally linearizing (6.42) at critical points. Therefore, by taking the derivative of (6.42) and evaluating it at 3 critical points as in (6.45), (6.46) and (6.47), we get three equations that holds the stability information of those critical points.

$$\frac{d^2x}{dt^2}\Big|_{x=0} = -(ab + cy - d)$$

(6.45)

81

$$\frac{d^2x}{dt^2}\Big|_{x=b'} = -2x\left(x - \frac{(a+b)}{2}\right) \tag{6.46}$$

$$\frac{d^2x}{dt^2}\Big|_{x=a'} = -2x\left(x - \frac{(a+b)}{2}\right) \tag{6.47}$$

Equation (6.44) states that there can be three different situations for roots: 1) one positive and negative root, 2) two positive roots or 3) two imaginary roots with positive real parts, depending on the value of "$cy - d$". However, there cannot be two negative real roots. For situation 1), $ab + cy - d$ must be negative. Thus, it follows from the stability Equation (6.45) that zero is the stable node, b' is the stable node since it is always greater than $(a+b)/2$ (6.46) and a' is unstable node since it is always smaller than $(a+b)/2$ (6.47) (see Figure 6.8a). For the situation 2), $ab + cy - d$ must be positive and the term under square root must be non-negative. In this case, zero is stable node, b' is stable node, and a' is unstable node (see Figure 6.8b). For the situation 3), $ab + cy - d$ must be positive, and the term under square root must be negative. In this case, there is only one real root stably located at zero, and b' and a' are the complex numbers with positive real parts (Figure 6.8d). The location and the stability information of equilibrium points are summarized in Table 6.2.

Table 6.2 The perturbation of the location of the critical points of $\dot{x}$ and stability information as the value of the term "$cy - d$" changes

	a'	b'	x=0
$ab + cy - d < 0$	negative and stable	positive and stable	unstable
$0 < ab + cy - d < \dfrac{a+b}{2}$	Positive and unstable	Positive and stable	stable
$\dfrac{a+b}{2} < ab + cy - d$	Complex	Complex	stable

Under the assumption that there is a fine time scale separation between (6.42) and (6.43) and that the term "$cy - d$" changes such that all 3 possibilities in Table 6.2 occur, the oscillations occur as follows. Starting with low value of Wip1 and high value of ATM as in Figure 6.8a, there is only one stable node. Thus, x values goes to this high value. As x increases y increases too, and "$cy - d$" also increases. As "$cy - $

d" increases, it pulls the $\dot{x}$ curve downward as illustrated in Figure 6.8b, until zero becomes the only attractor as illustrated in Figure 6.8d. A jump phenomenon occurs at $x = (a + b)/2$ as in Figure 6.8c, and x jumps to zero. As the value of x becomes zero, the value of y decreases. Thus "cy-d" term moves $\dot{x}$ curve upward until there is one stable node at a high level as in Figure 6.8a. One more jump phenomenon occurs as zero turns to an unstable node (transition from Figure 6.8d to Figure 6.8a), and x values now jump to that high level. The jumps in trajectory corresponds to the fast parts, whilst moving of the $\dot{x}$ curve downward or upward by Wip1 feedback corresponds to the slow parts in the periodic trajectory.

The proposed model can be characterized by jump phenomenon and time scale separation in dynamics. In fact, we had shown by (6.42) that time scale separation is critical for the oscillations. Thus, the proposed model is an example of a relaxation oscillator.
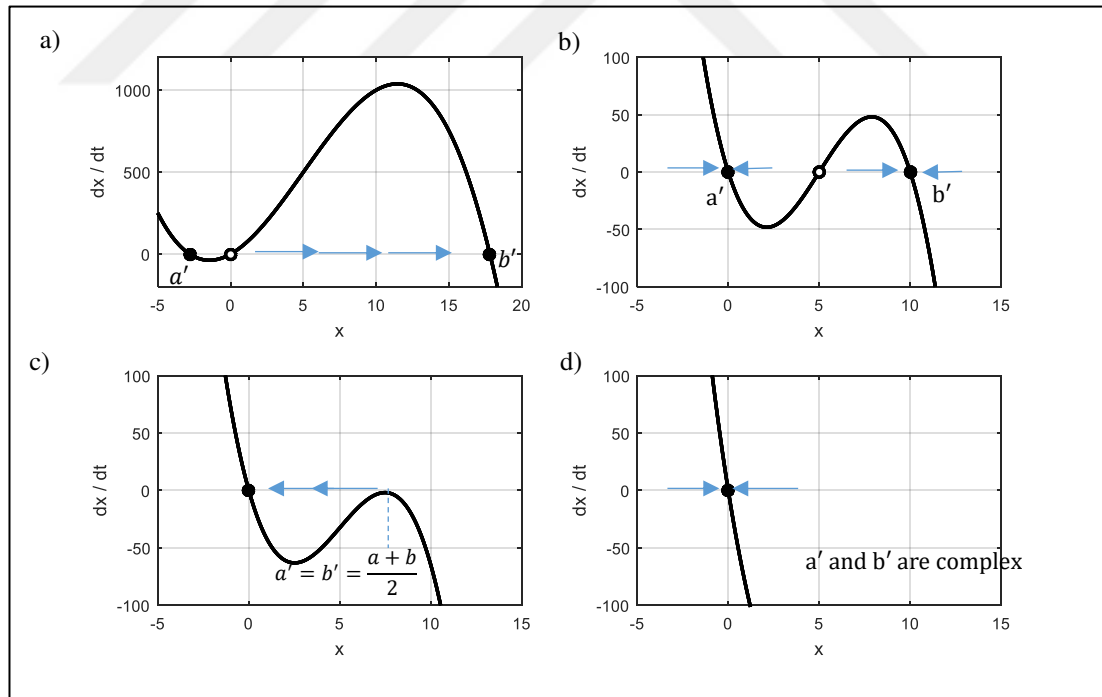
Figure 6.8 Dynamic route approach explaining how the oscillations occur in the canonical 2-D oscillator model

6.3.7 Apoptosis: Stable Steady State Value at a High Level

The high steady state of x value is established when there are DSBCs in DNA and at the same time Wip1 feedback loop is off. In this case, Wip1 is not influenced by ATM (i.e. x) anymore. Therefore, we take the parameter m as zero and system equations turns to (6.48) and (6.49). It should be noted that the case of $m = 0$ makes a similar effect to the one performed by P53DINP1 in Zhang's model (Zhang et al., 2011).

$$\dot{x} = \frac{1}{\tau_1}(-x(x^2 - (a+b)x + ab + cy - d)) \qquad (6.48)$$

$$\dot{y} = \frac{1}{\tau_2}(z + 0 - ny) \qquad (6.49)$$

The nullclines in this case are:

$$x_{nullcline1}: \ x = 0 \qquad (6.50)$$

$$x_{nullcline2}: \ y_x = -\frac{x^2 - (a+b)x + ab - d}{c} \qquad (6.51)$$

$$y_{nullcline}: \ y_y = \frac{z}{n} \qquad (6.52)$$

There are three equilibrium points. One of the equilibrium points is at the intersection between (6.50) and (6.52), which is $(0, z/n)$. The other two is at the intersections of (6.51) and (6.52) and the x-components of these two equilibriums are found as:

$$x_{eq2} = \frac{(a+b) + \sqrt{(a+b)^2 - 4\left(ab - d + \frac{cz}{n}\right)}}{2} > 0 \qquad (6.53)$$

$$x_{eq3} = \frac{(a+b) - \sqrt{(a+b)^2 - 4(ab - d + \frac{cz}{n})}}{2} < 0 \qquad (6.54)$$

The y components are:

$$y_{eq2} = y_{eq3} = z/n \qquad (6.55)$$

Since $ab - d + \frac{cz}{n} < 0$ by the constraint (6.3), then x_{eq2} is always positive and x_{eq3} is always negative.

To find the stability types of these equilibrium points, we again evaluate the Jacobian matrix at those points. Using the Jacobian matrix in (6.8) and evaluating it at $\left(x_{eq1}, y_{eq1}\right) = \left(0, \frac{z}{n}\right)$ when $r = 1$ and $m = 0$, we found Jacobian matrix as:

$$J_{(x_{eq1},y_{eq1})}^{r=1,m=0} = \begin{bmatrix} 1/\tau_1 & 0 \\ 0 & 1/\tau_2 \end{bmatrix} \begin{bmatrix} -\left(ab + \dfrac{cz}{n} - d\right) & 0 \\ 0 & -n \end{bmatrix} \tag{6.56}$$

Since $ab + \frac{cz}{n} - d < 0$ by the constraint (6.3), then determinant of (6.56) is always negative, the point $(0, z/n)$ is a saddle point. Evaluating Jacobian matrix in (6.35) when $r = 1$ and $m = 0$:

$$J_{(x_{eq},y_{eq})=(x_{eq2,3},y_{eq2,3})}^{r=1,m=0} = \begin{bmatrix} 1/\tau_1 & 0 \\ 0 & 1/\tau_2 \end{bmatrix} \begin{bmatrix} -2x_{eq}(x_{eq} - \dfrac{a+b}{2}) & -cx_{eq} \\ 0 & -n \end{bmatrix} \tag{6.57}$$

The determinant of 6.57:

$$\det(J_{x_{eq}=x_{eq2,3},\, y_{eq}=y_{eq2,3}}^{r=1,m=0}) = -\frac{2nx_{eq}}{\tau_1\tau_2}\left(x_{eq} - \frac{a+b}{2}\right) \tag{6.58}$$

If we calculate the determinant (6.58) at $\left(x_{eq2}, y_{eq2}\right)$, it is clear that determinant is always positive since x_{eq2} is positive and $x_{eq2} > \frac{(a+b)}{2}$. Similarly, if we calculate determinant at $\left(x_{eq3}, y_{eq3}\right)$, again determinant is always positive, since $x_{eq3} < \frac{(a+b)}{2}$ and $x_{eq3} < 0$. Thus, both determinants of Jacobian matrix at $\left(x_{eq2}, y_{eq2}\right)$ and $\left(x_{eq3}, y_{eq3}\right)$ are positive and we need to check the trace to determine their types of stabilities. The trace of (6.58) is:

$$trace \left(J^{r=1,m=0}_{(x_{eq}, y_{eq}) = (x_{eq2,3}, y_{eq2,3})} \right)$$

$$= -\frac{1}{\tau_1} 2x_{eq} \left(x_{eq} - \frac{(a+b)}{2} \right) - \frac{1}{\tau_2} n \tag{6.59}$$

which is the same as (6.38), and the trace is always negative for both (x_{eq2}, y_{eq2}) and (x_{eq3}, y_{eq3}) indicating that they are stable attractors (see Figure 6.9). In this case, all the trajectories that start in the region $\mathcal{R} \setminus \{\{(x, y) \in R^2 | x = 0\}\}$ go to (x_{eq2}, y_{eq2}), whose x-component indicates the high level of representative x variable.
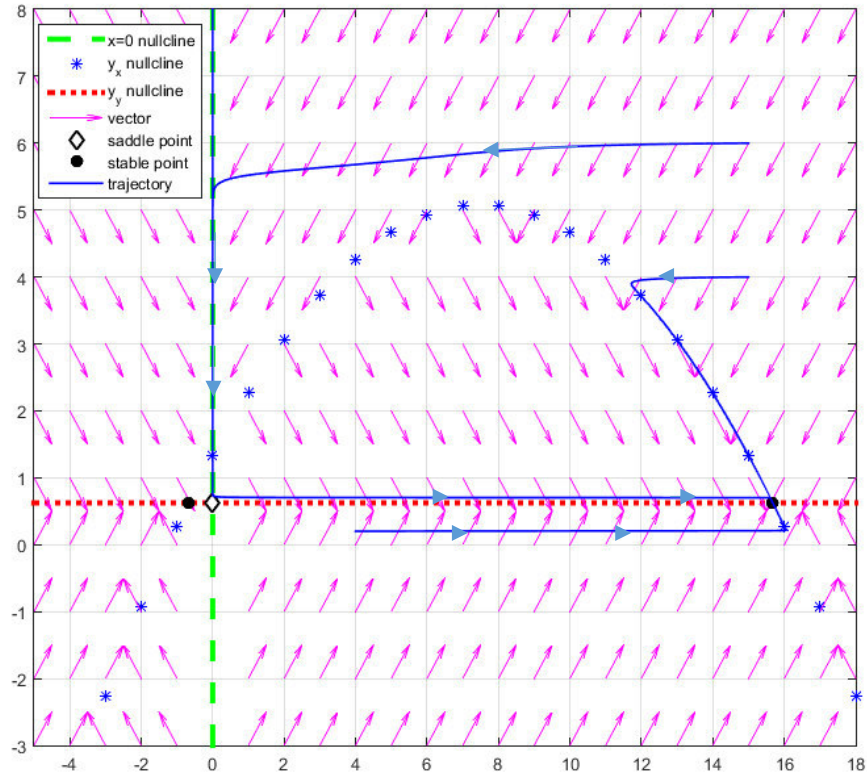
Figure 6.9 Illustration of apoptosis in phase space using 2-D canonical oscillator model for the parameters a = 5, b = 10, c = 15, d = 70, m = 0, n = 0.8, z = 0.5, $\tau_1 = \tau_2 = 1$ and r = 1

6.4 Discussion

The proposed model is based on ATM and Wip1 interaction and now we evaluate our model's predictive ability to characterize the known mutations of ATM and Wip1 from the literature. Wip1 overexpression and ATM deficiency are two mutations that

causes cancer. Wip1 (product of PP1MD gene) overexpression is a type of cancer that is characterized by the high levels of Wip1 in the cell. This situation can be embedded into our model by increasing the Wip1 production rate z in (6.1) such that it violates the constraint (6.3). In this case, the proposed model loses its ability to oscillate. Thus, the cell becomes defective in producing oscillations, so leading to cell cycle arrest (Figure 6.10a).

Since oscillations are important for arresting cell cycle (Purvis et al., 2012), and any defect in cell cycle arrest is the prerequisite of cancer (Green & Evan, 2002; Lowe, et al., 2012; Xu & Baltimore, 1996), we speculate that Wip1 overexpression may cause cancer by removing cell's ability to arrest cell cycle. To recover the oscillations, the parameter n can be increased again so that constraint (6.3) can be satisfied (Figure 6.10b). This is in agreement with findings (Rayter et al., 2008; Richter, et al., 2015) that shows that Wip1 overexpression can be recovered by Wip1 degradation.

ATM deficiency is a mutation and characterized by ATM that loses sensitiveness to the damage. This mutation can be studied by analyzing the parameter r. In our model, parameter r ($r = N_c/(1 + N_c)$) is a measurement of ATM's detection level of DSBCs. We replace r by r/k where $k > 1$ with the aim of decreasing the ATM's sensitiveness. This parametric change moves the y_x nullcline downward. Thus, the nullclines may not intersect at an oscillatory interval and the cell may be defective in oscillations. Indeed, some studies demonstrate that mutation in ATM causes defective cell cycle checkpoint activation (Delia et al., 2003; Lavin & Kozlov, 2007; Xu & Baltimore, 1996).

Darlington et al. (2012) showed in wet lab experiment that absence of Wip1 rescues ATM deficiency phenotypes in mice. We model the absence of Wip1 by increasing the degradation parameter, n. With the increase of n, the slope of y_y decreases and for a sufficiently large n, it may have an intersection at a high level indicating initiation of apoptosis. Thus, we hypothesize that this rescue may be due to the initiation of apoptosis. Because, in ATM deficiency y_x nullcline moves downward, then this could be compensated by moving y_y nullcline downward too and making them cut through

interval of oscillation again. However, further wet lab experiments are needed to be conducted to validate this hypothesis.
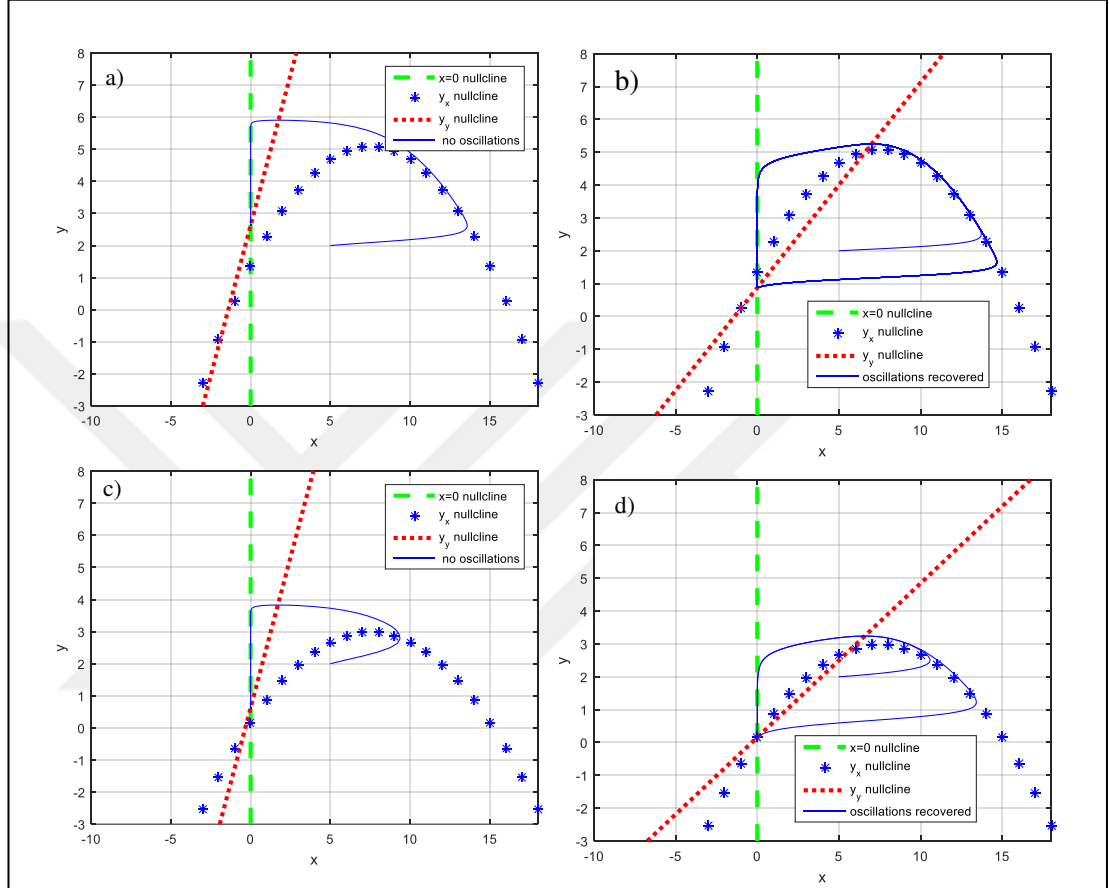
Figure 6.10 Characterization of mutations and recovery from mutations by 2-D canonical oscilllator model. a) Wip1 overexpression is characterized by the parameters $r = 1, a = 5, b = 10, c = 15,$ $d = 70, m = 1.5, n = 0.8, z = 2.1$. The parameter z is increased from 0.5 to 2.1 to model the mutation Wip1 overexpression, in which case the constraint (6.3) is violated. b) Recovering the ability to oscillate in case of Wip1 overexpression by increasing the parameter n from 0.8 to 2.4. c) Characterization of ATM deficiency by the parameters $r = 0.75, a = 5, b = 10, c = 15, d = 70, m = 1.5, n = 0.8, z = 0.5$. d) recovering the ability to oscillate in case of ATM deficiency in c) by increasing the parameter n from 0.8 to 3.2

CHAPTER SEVEN
SYNCHRONIZATION AND ENTRAINMENT PROPERTIES OF THE TWO PROPOSED OSCILLATOR MODELS

Genome integrity, which is critical for proper functioning of cells, is constantly under the risk of damage due to the exposure of various stresses, such as hypoxia, Ionizing Radiation (IR), Ultra Violet light etc. (Murray-Zmijewski et al., 2008). The most deleterious damage is Double Strand Breaks (DSBs) that are caused by Ionizing Radiation (IR). DNA Damage Response (DDR) mechanism that determines the cell fate exists in cells to prevent the risk of DSBs, which is controlled by p53 network. In single cells, studies have shown that cell fate determination upon DSBs caused by IR is controlled by p53 dynamics comprised of three different modes, namely low state, oscillations, and high state as we have discussed in previous chapters. So far, we have focused on the oscillatory dynamics of p53 in a single cell, which causes cell cycle arrest. Cell cycle arrest is important for its role of stopping cellular growth when there is DNA damage, so avoiding the risk of potential tumour formation.

Any deficiency in oscillatory dynamics of p53 leaves cells unprotected towards DNA damage. An unrepaired DNA damage poses a risk of mutations that causes cancer (Lord & Ashworth, 2012). Thus, preservation of oscillations under various disruptive conditions, such as noise and genetic heterogeneity, is crucial in avoiding the risks associated with DNA damage. Thus, p53 network must be robust under such disruptive conditions. In fact, this is a principle of biological systems known as robustness, and not a peculiarity of p53 network only.

Mechanisms that contribute to the robustness of p53 network oscillations have been revealed in various studies. The studies show that additional positive and negative feedback loops in p53 network often contribute to the robustness of the network against parameter perturbations (Kim & Jackson, 2013). Several feedback loops also have been identified in p53 network, such as feedback loops mainly carried out by Mdm2, PTEN, Wip1, Ror-alfa, dapk1, c-Ha-Ras and DDR1 (Deguin-Chambon, Vacher, Jullien, May, & Bourdon, 2000; Doumont et al., 2005; Lahav et al., 2004;

Mayo, Dixon, Durden, Tonks, & Donner, 2002; Ongusaha et al., 2003). However, the negative feedback loop between ATM and Wip1 through p53 is the indispensable one among other feedback loops (Batchelor, Mock et al., 2008). Other feedback loops contribute to the robustness and fine-tuning of period.

Another mechanism that may aid a biological oscillatory system to keep its oscillations under disruptive conditions is the coupling mechanism, which synchronizes the oscillations in a group of individual cells (Kim & Jackson, 2013). Studies in biological oscillatory systems have revealed that synchronization is a form of intercellular communication and implements a relevant biological function (Zhou, Zhang, Yuan, & Chen, 2008) .

Synchronization has been observed in many biological oscillatory systems and, the advantages of the coupling leading to synchronization in sustaining the oscillations under disruptive conditions has been studied in various contexts, which have given fruitful understanding of those systems. For instance, wet lab experiments (Ko et al., 2010; Liu et al., 2007) have shown that circadian rhythm in single cells are not robust to noise or genetic heterogeneity, whereas coupled cells are more robust, so giving a survival advantage. Also in calcium systems noise have been shown to aid oscillations (Li & Wang, 2007). In mathematical terms, it is shown that the synchronization mediated by coupling through a neurotransmitter in SupraChiasmatic Nucleus (SCN) cells play a key role in generating the robust circadian rhythm in mammals (Gonze, Bernard, Waltermann, Kramer, & Herzel, 2005; Marino, Hogue, Ray, & Kirschner, 2008). Pacemaker cells in heart also synchronize to give a coherent rhythm (Krinsky & Kholopov, 1967).

Although, synchronization properties have been investigated in other biological oscillatory systems in several studies, investigation of this property in p53 network is restricted to a few studies (Devi, Alam, & Singh, 2015; Kim & Jackson, 2013), probably due to a lack of low dimensional oscillator models (Note that in the previous chapters, we have provided two 2-dimensional oscillator models for p53 network which may boost such studies). In the study of (Devi, Alam, & Singh, 2015)

oscillations are due to p53-Mdm2 interaction. However, it is known that p53-Mdm2 interaction is not responsible for the oscillations (Batchelor, Mock et al., 2008). Kim & Jackson (2013) studies the synchronization in p53 network using an 11-dimensional model which is modified from the model by (Batchelor, Loewer, Mock, & Lahav, 2011).

Herein, we study the synchronization in p53 network using two proposed 2-dimensional models. First, we propose a novel coupling framework for p53 network for our models based on literature search. After that, we show the advantages of synchronization property in p53 network by employing various numerical simulations.

7.1 A Novel Coupling Framework for Synchronization in p53 Network Using Low Dimensional Oscillator Models

One of the goals of DNA Damage Response (DDR) is to communicate the damage to other cells (Jaiswal & Lindqvist, 2015). This mechanism is known as Radiation Inducer Bystander Effect (RIBE). RIBE can be described as the formation of DDR in non-irradiated cells by the effect of irradiated neighbor cells. Thus, non-irradiated cells exhibit the same responses as irradiated cells (Sedelnikova, et al., 2007). Furthermore, bystander effect is known to alter the dynamics in cells such as proliferation, apoptosis, cell cycle arrest; however there are many unanswered questions about its dynamics (Marín, et al., 2015). Although RIBE is an interaction between irradiated and non-irradiated cells, there are other forms of RIBE between irradiated and irradiated cells as well (Mackonis, et al., 2007). The proteins p53 and ATM are known to be intracellular proteins that mediate the signal for RIBE, while molecules such as Reactive Oxygen Species and Nitric Oxide are known to be intercellular carriers of this signal (Burdak-Rothkamm & Prise, 2009; Ghosh, Ghosh, & Krishna, 2015; Jaiswal & Lindqvist, 2015; Rzeszowska-Wolny, Przybyszewski, & Widel, 2009).

Since the proposed low dimensional oscillator models for p53 network consists of ATM and Wip1, ATM is chosen as the coupling variable. We model the damage signal carried by intercellular molecules as a mean field (see (Gonze et al. 2005) and (Marino et al., 2008) for construction of mean field for synchronization). Thus, the

proposed coupling frameworks for two proposed oscillator models are constructed as follows. The coupling framework for the Polynomial Type Canonical Relaxation Oscillator (PTCRO) model introduced in Chapter 6 is shown by (7.1) and (7.2), whilst the coupling framework for the Reduced Relaxation Oscillator (RRO) model introduced in Chapter 3 is shown by (7.3) and (7.4).

$$\dot{x}_i = \frac{1}{\tau_{1,i}}\left(-x_i\left[r\left(x_i^2 - (a+b)x_i\right) + ab + cy_i - rd\right]\right) + C\frac{1}{N}\sum_{i=1}^{N}x_i \tag{7.1}$$

$$\dot{y}_i = \frac{1}{\tau_{2,i}}(z + mx_i - ny_i) \tag{7.2}$$

$$
\begin{aligned}
\frac{d[ATM_i^*]}{dt} = {}& \mathrm{k_{acatm}}\frac{\mathrm{n_c}}{(\mathrm{n_c} + \mathrm{jn_c})}[ATM_i^*]\frac{\sqrt{0.1(\mathrm{ATM_{tot}} - [ATM_i^*])}}{\left(\sqrt{0.1(\mathrm{ATM_{tot}} - [ATM_i^*])} + \mathrm{jacatm}\right)} \\
& - \mathrm{kdeatm}\,(1 + [Wip1_i])\frac{[ATM_i^*]}{([ATM_i^*] + \mathrm{j_{deatm}})}) + C\frac{1}{N}\sum_{i=1}^{N}[ATM_i^*]
\end{aligned}
\tag{7.3}
$$

$$\frac{d[Wip1_i]}{dt} = \mathrm{k_{swip10}} + \mathrm{k_{swip1}}\frac{[p53Arrester_i]^3}{(\mathrm{j_{swip1}}^3 + [p53Arrester_i]^3)} - \mathrm{k_{dwip1}}[Wip1_i] \tag{7.4}$$

where the term $C\frac{1}{N}\sum_{i=1}^{N}[ATM_i^*]$ is an approximation to the mean field, C is the coupling strength and N is the number of cells in the population. Before diving into more complex cases, we show that the proposed coupling framework is handy for studying the synchronization property of p53 network. For this, we use two identical oscillators with different initial conditions for each oscillator models, i.e. $N = 2$. Figure 7.1 demonstrates the synchronization of two identical PTCRO models (Equations (7.1) and (7.2)) with arbitrary different initial conditions for different coupling strengths. In no coupling case, the oscillators do not synchronize. As the coupling strength increases, the two oscillators synchronize.
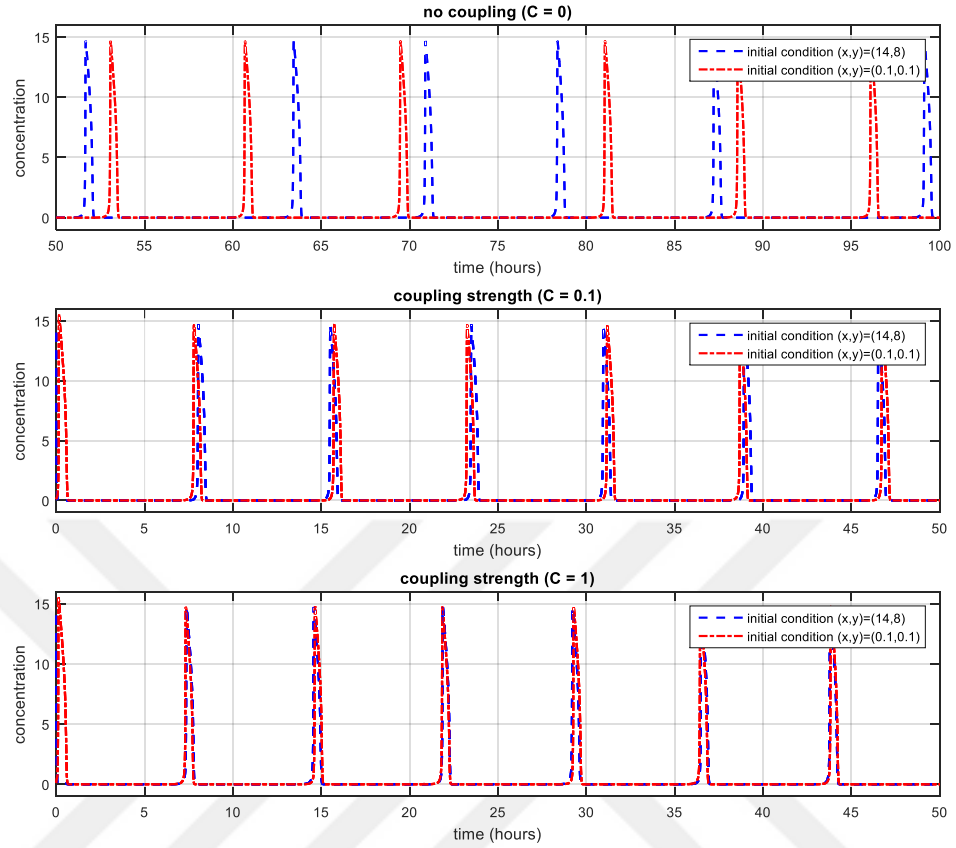
Figure 7.1 The simulation of coupling of the two PTCRO models for different coupling strengths and different initial conditions

Figure 7.2 demonstrates the synchronization of the two identical RRO models with arbitrary different initial conditions via the proposed coupling framework. In no coupling case, the oscillators do not synchronize. However, as the coupling strength increases, the oscillators synchronize. Thus, we conclude the proposed coupling framework is handy for studying the synchronization properties of p53 network as demonstrated by Figure 7.1 and Figure 7.2.
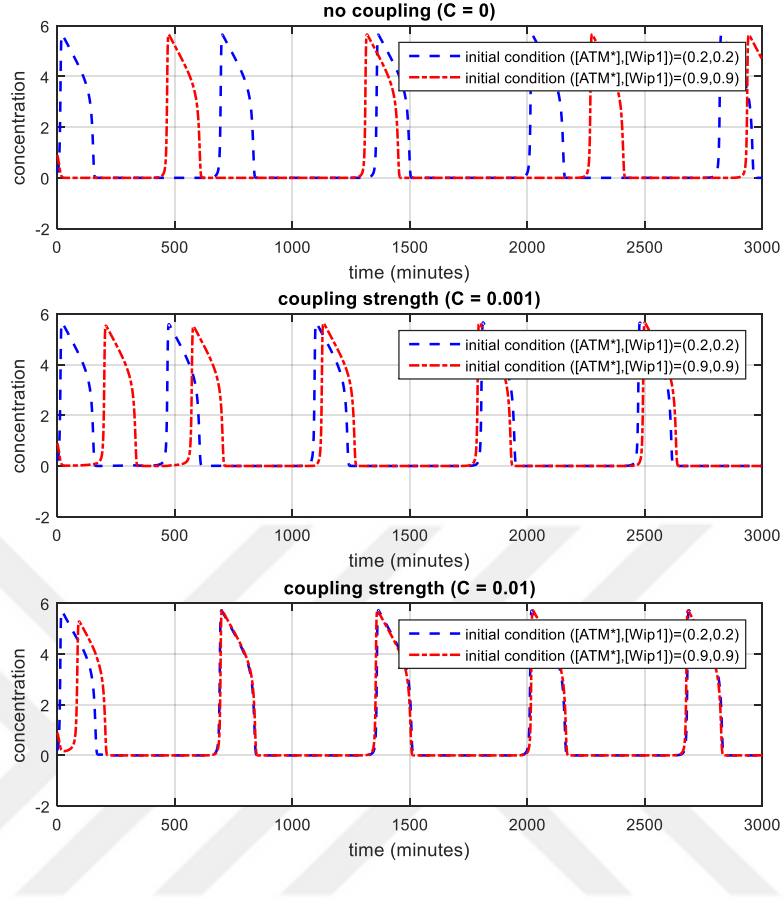
Figure 7.2 The simulation of coupling of the two RRO models for different coupling strengths and different initial conditions is shown

7.2 Coupling Confers Robustness against Noise

Noise is unavoidable in biological systems. Since the period of oscillation is crucial for reliable cell fate decisions, the coupling would help cells to maintain their periods under noise. For this, we design an *in silico* experiment. We consider the coupling of two identical PTCRO models for p53 network (Equations (7.1) and (7.2)): PTCRO-1 and PTCRO-2. We add noise to PTCRO-1 such that it loses its ability to oscillate in case of no coupling. When the two oscillators are coupled, PTCRO-1 regains its ability to oscillate and the two oscillators synchronizes (see Figure 7.3). We choose the noise (η) as normal distribution with mean of 1 and standard deviation of 1. The PTCRO-1 loses its ability to oscillate under such noise, while the period of the PTCRO -2 (the oscillator without noise) is about 9 hours as can be seen in Figure 7.3. Coupling these

two oscillator with a coupling strength of 2 rescues the noisy oscillator and its ability to oscillate is regained.
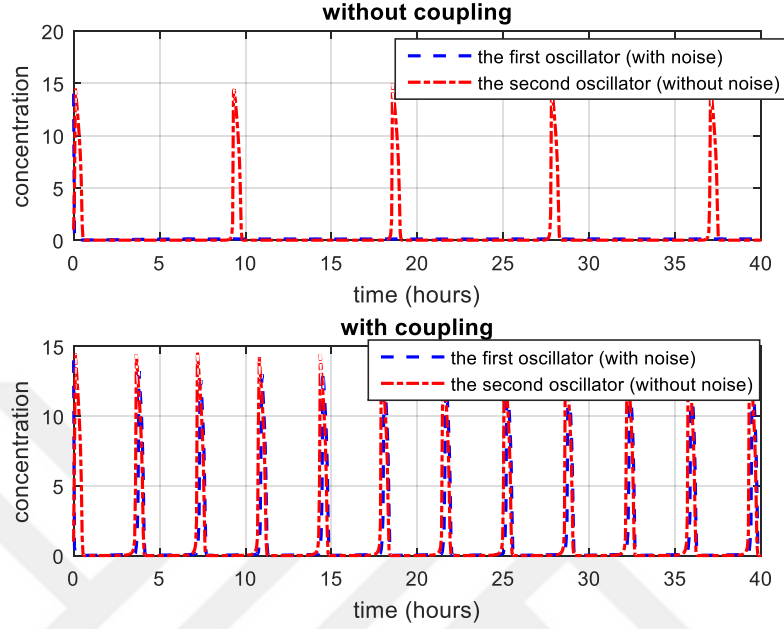
Figure 7.3 Coupling confers robustness against noise. The oscillator that lost its ability under noise is rescued by the help of another oscillator via coupling and the two oscillators synchronize. Coupling strength is 2

The experiment is modified for the RRO models for p53 network (Equations (7.3) and (7.4)). Two identical oscillators, RRO-1 and RRO -2, are used. We add noise to RRO-1 such that its frequency of oscillations changes drastically in case of no coupling. For this purpose, we choose the noise (η) as normal distribution with mean of 0.25 and standard deviation of 0.25. As can be seen in Figure 7.4, RRO-1 oscillates at a frequency at about four times of RRO-2's. When these oscillators are coupled with coupling strength of 0.1, these two oscillators synchronize.

For the coupling of the RRO model cases under noise, we could not find a parametric range where RRO-1 loses its ability to oscillate and coupling with RRO-2 rescues it. However, it must be noted that we are using a linear coupling as a mean field. Under more complex coupling conditions, this case can be searched as a future study. Nevertheless, the synchronization reduces the side effect of noise, which is the high frequency of RRO-1.
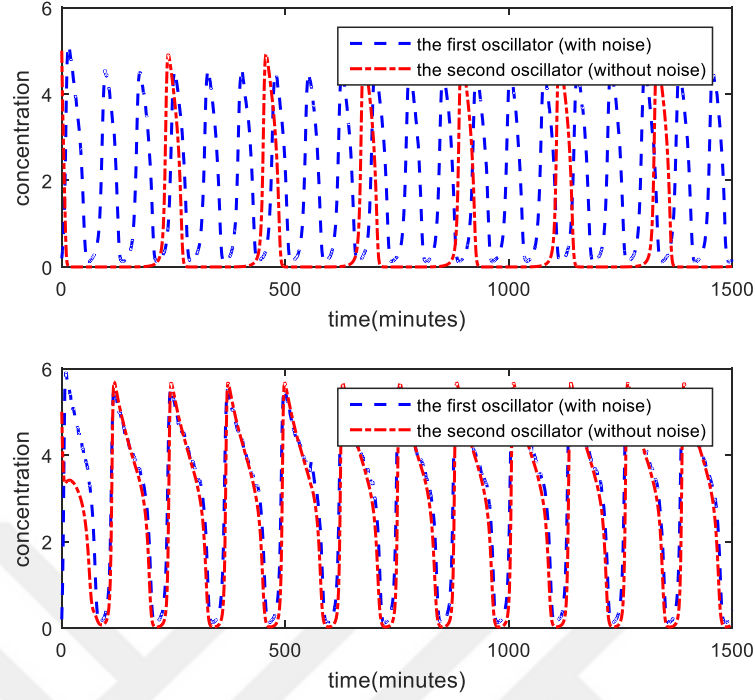
Figure 7.4 Coupling confers robustness against noise by synchronization. The RRO-1 oscillates at a higher frequency. Via coupling, the two oscillators synchronizes. Coupling strength is 0.1

7.3 Coupling Confers Robustness against Genetic Heterogeneity

In realistic systems, no two oscillations can have identical periods. The same is true for p53 network oscillations in cell. Every cell have different kinetic parameters due to genetic heterogeneity or environmental conditions. In this subsection, we show that coupling confers robustness against genetic heterogeneity by making cells with different periods oscillate in a common period. For this, we design an *in silico* experiment for the PTCRO model and the RRO model cases.

For the coupling experiment of PTCRO models (Equations (7.1) and (7.2)), we create 50 different parameter sets by randomly perturbing parameters as ($parameter = parameter + parameter * \xi$), where ξ is a random number drawn from a uniform distribution on the open interval (0,1) and selecting those parameters which results in oscillations. The variability of oscillations due to perturbation of parameters models the genetic heterogeneity resulting in different

96

period of oscillations. The constructed random parameter sets are given in Appendix-4. The period of the oscillations range from 3 hours to 17.6 hours. The mean of the periods are 6.14 whilst the standard deviation is 2.96. Note that the standard deviation of periods in our case is more than the standard deviation used in another coupling study done in mammalian circadian rhythm, which is 0.25 by (Locke, Westermark, Kramer, & Herzel, 2008).

50 different PTCRO models of Equations (7.1) and (7.2) without coupling and with coupling is numerically solved. We see that the coupling creates a uniform period, thus giving coherent oscillations of p53 network as in Figure 7.5.
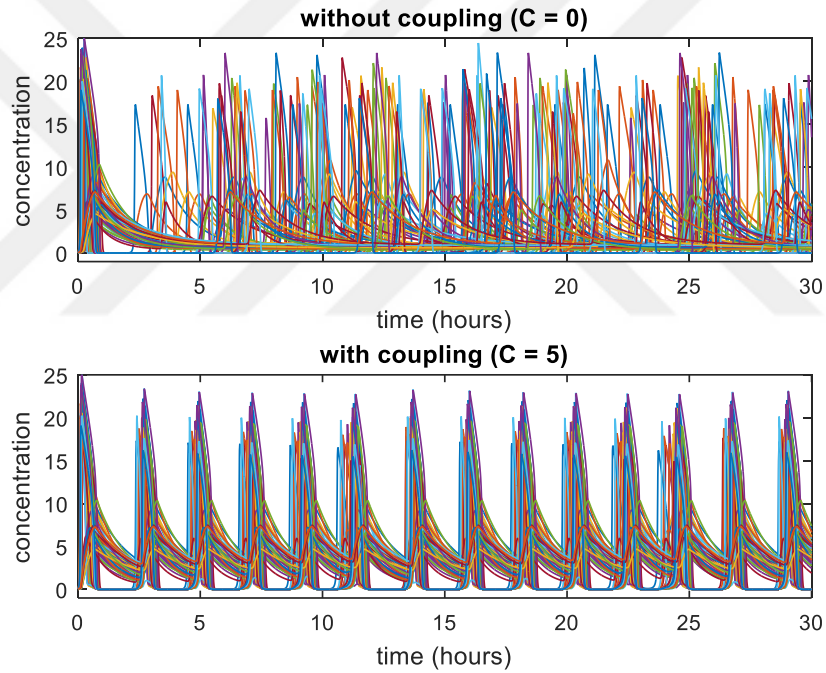
Figure 7.5 50 different PTCRO models with coupling and without coupling are numerically solved. In the uncoupled case, the period of oscillations are very different. When coupled, the oscillators synchronize

The same experiment is repeated for the RRO case. This time, we scaled Equations (7.3) and (7.4) with random timescales calculated with the formula $timescale = 1 + 5\,\xi$, where ξ is the random number drawn from the uniform distribution on the open

interval of (0,1). 50 RRO models with different periods without coupling are numerically solved. After coupling, 50 oscillators synchronizes.
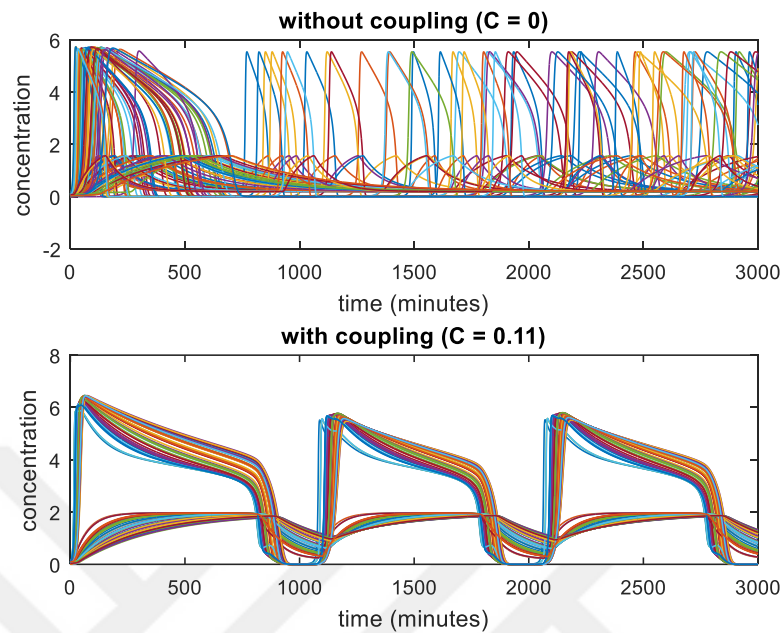
Figure 7.6 50 different RRO models with coupling and without coupling is numerically solved. In the uncoupled case, the period of oscillations are very different. When coupled, the oscillators synchronize

7.4 Future Study

Further study should be carried out to investigate the coupling and synchronization properties of p53 network. It must be noted that the current wet lab data is not sufficient to validate the coupling studies with experimental results, so logical reasoning is required (Kim & Jackson, 2013). It is known that non-irradiated cells are effected by irradiated neighbour cells, known as Radiation Inducer Bystander Effect (as we mentioned above) or Type 1 effect. This bystander effect is also seen in irradiated cells known as Type 2 and Type 3 effects (Mackonis et al., 2007). Type 2 effect is the increased cell survival when nearby cells receive a lethal dose whilst Type 3 effect causes an increase in cell survival when cells receive a high dose of radiation while nearby cells receive a low dose. It would be very interesting to investigate these bystander effects in the context of coupling of oscillators. Since radiation is used in radiotherapy, studies in this direction would be of great importance for developing more effective curing strategies.

CHAPTER EIGHT
A MATHEMATICAL FRAMEWORK FOR COUPLING OF P53 NETWORK AND CIRCADIAN CLOCK

In Chapter 1, a new modularity perspective of two-phase dynamics was introduced, where p53 network was considered as a collective system that has an oscillator in the center. According to this suggestion, several subsystems manipulate this oscillator to make an effect on outcomes of cell fate, namely normal cell cycle progression, cell cycle arrest, and apoptosis. We also showed that since there is a relaxation oscillator subsystem in p53 network, the interplay between proteins and this oscillator may be controversial (e.g. Mdm2). Thus, we suggest that to study the effects of a protein, a pathway, or another network on p53 network, three qualitative p53 network dynamics (low level, oscillations, and a sustained high level) must be investigated as well, for reliable results. However, the experiments that take into account the mentioned three qualitative behavior of p53 dynamics is restricted to only a few studies (Batchelor, Loewer, Mock, & Lahav, 2011; Lahav et al., 2004; Purvis et al., 2012), and those studies do not consider the circadian clock.

In Section 5.5, we discussed that the oscillations may be strengthened by increasing the amplitudes of ATM oscillation by another subsystem that have positive effect on the high stable steady state of ATM, since ATM oscillations occurred due to switching between the high stable steady state and the low steady state of ATM, as we had shown. In this chapter, we investigate whether one candidate system that provides such an interaction is circadian clock, holding on to the established information that circadian clock plays an important role in determining the strengths of cellular responses to DNA damage checkpoints (i.e. cell cycle arrest) and apoptosis (Sancar et al., 2010). In our case, we interpret the strengthening of cellular response to DNA damage as the increased amplitude of oscillations, the increased level of active p53 in apoptosis, and the easier initiation of apoptosis. In light of these interpretations, in this chapter we propose a framework confirming the positive effect of circadian clock on DNA damage response of the cell. The proposed framework can be seen as the first step of a systems-level approach for managing the tolerability of cancer therapy, which is

influenced up to several folds due to circadian effect (Ortiz-Tudela, Mteyrek, Ballesta, Innominato, & Lévi, 2013), in chronotherapy[5].

In the literature, there are some studies revealing the pathways that p53 network and circadian clock effect each other through, as will be reviewed in the next section. However, this information is not enough for the validation of a comprehensive modeling of interaction between circadian clock and p53 network under DNA damage in terms of dynamical behaviors. For the validation of such a modeling approach, experiments that investigate both the circadian clock and p53 dynamics (low steady state, oscillations, and high stable steady state) together are needed. However, to the best of our knowledge such experiments do not exist. Nevertheless, it is known that circadian clock has a positive effect on DNA damage response of the cell. Considering this body of information in the literature, in this chapter we realize an experiment to show how circadian clock might effect p53 dynamics, considering both circadian clock and p53 dynamics *in silico* by making some idealizations. We observe that, in the proposed framework, for some set of parameters circadian clock leads to increased amplitude of oscillations, increased level of p53 in apoptosis, and easier initiation of apoptosis.

The organization of this chapter is as follows. In Section 8.1, we review circadian clock in the context of systems biology. In Section 8.2, we collect as much information as possible about the interactions between circadian clock and p53 network from the literature and provide a plausible coupling framework for the study of circadian and p53 network coupling. With the realization of experiments *in silico*, we show that circadian clock have positive effect on DNA damage response.

8.1 Circadian Clock

Circadian clock is a self-sustaining oscillatory mechanism with the period of about 24 hours (Halberg, Halberg, Barnum, & Bittner J.J., 1959), which aligns biological rhythm of an organism with daily environmental changes (e.g. light and dark,

---

[5] Chronotherapy is the scheduling of drug delivery to a patient by considering circadian effect or other rhythmic hormones in an individual to maximize the effectiveness of the therapy.

temperature) (Sancar et al., 2010). The alignment with the environmental change and physiological functions of organism gives survival advantages (Beaver et al., 2002; Gaddameedhi, Reardon, Ye, Ozturk, & Sancar, 2012; Dodd et al., 2005; Sharma, 2003; Woelfle, Ouyang, Phanvijhitsiri, & Johnson, 2004). In humans, disruption of the circadian clock has been associated with many types of diseases including depression (Kripke, Elliott, Welsh, & Youngstedt, 2015), metabolic diseases (diabetes and obesity) (Marcheva, et al., 2010), and cancer (Hastings, Reddy, & Maywood, 2003; Sahar & Sassone-Corsi, 2009). Although circadian clock is autonomous and self-sustaining with a free-running rhythm, it is under the influence of the environmental inputs, and synchronizes to the environment, so called entrainment. The most obvious environmental cue that circadian clock entrains is the sun light (Hirschie Johnson, Elliott, & Foster, 2003).

Circadian clock is a time tracking system in organisms that synchronizes the organism to the environmental changes with a period of about 24 hours. The circadian clock works autonomously, i.e. it is self-sustaining. This means circadian clock is able to persist even in the absence of external cues (i.e. constant darkness). The period of the circadian rhythm in constant conditions is called free running rhythm and free running rhythm may not be 24 hours due to heterogeneity of the biochemical rates. Thus, circadian clock has developed an entrainment mechanism to overcome this problem. The circadian rhythm entrains (synchronizes) to the light and dark cycles of the environment. Even if it is shifted, the circadian rhythm will be reset in the next day.

Circadian clock structure consists of interlocked transcription-translation feedback loops (TTFLs) (Ko & Takahashi, 2006; Kim & Forger, 2012) as illustrated in Figure 8.1. According to this directed graph in Figure 8.1, the circadian clock model consists of a core negative feedback loop and an additional negative feedback loop (the Negative Negative Feedback Structure). Per1, Per2, Cry1, and Cry2 are repressors. These repressors inactivate the activators BMALs and CLOCK/NPAS2 (CLK) via a core negative feedback loop. In addition, these activators also inactivate their own transcription expression by inducing the Rev-erbs through the secondary negative

feedback loop. Although the expression on these loops have very large changes, the circadian rhythm is still about 24 hours, meaning it is robust (Dibner et al., 2009).
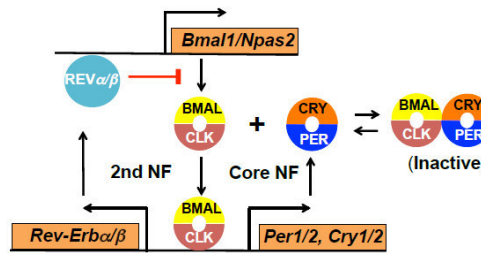
Figure 8.1 Interaction diagram of circadian clock through two negative feedback loops. The figure is taken from (Kim & Forger, 2012)

The mathematical models proposed so far has been used to understand how circadian system keeps its period and how it entrains to the environmental changes. We divide the mathematical models used in the literature into three groups: (1) Detailed biochemical models, (2) Limit cycle models and variants, (3) Phase oscillators. We will review the literature about mathematical models of circadian clocks according to this division.

Detailed biochemical models: These models are the detailed biochemical models that try to take every biochemical process (phosphorylation, Michaelis-Menten kinetics, etc.) and interacting proteins into account. The number of variables of the models range from 7 to 181 (Becker-Weimann, Wolf, Herzel, & Kramer, 2004; Forger & Peskin, 2003; Kim & Forger, 2012; Leloup & Goldbeter, 2003). Since these models can be full of details, they lack the intuitive understanding of the topological structure a human mind can grasp. The topological structure in mammalian and non-mammalian circadian rhythms are the same, with only a difference that instead of CLK protein, non-mammalians possess Timeless protein (Tim). The first molecular circadian models in literature has been proposed for *Drosophila* by (Leloup & Goldbeter, 1998), which consists of 16 variables. Similar kinetic models are used for mammalians (Leloup & Goldbeter, 2004; Relógio et al., 2011) and *Neurospora* (Sriram & Gopinathan, 2004).

Limit cycle models and variants: Since circadian clock is a robust timekeeper, the oscillations must come from a stable limit cycle oscillation. The candidate for such an oscillation is the 3 dimensional Goodwin model (Goodwin, 1965), which is originally posed to model oscillatory dynamics in enzymatic control processes. The model is a minimal model based on a delayed feedback loop, which resembles the simplified mechanism of circadian clock. The variants of Goodwin model has also been proposed since Goodwin model does not oscillate as it is supposed to do in the first original paper due to numerical artefacts. That is why (Griffith, 1968) corrected the model increasing the nonlinearity of the first equation with the variable n (see Figure 8.2). There are parameter sets that lead to oscillation only if $n > 8$. Goodwin models and their variants have been widely used to focus on topological structure rather than detailed biochemical processes to gain intuitive understanding. Although Goodwin model variables does not have a one-to-one link between circadian clock molecular mechanisms, they provide a basic description of circadian oscillator.

	Goodwin model 1965	Griffith model 1968
X ⊣ Y Z	$\dfrac{dX}{dt} = k_1 \dfrac{1}{K_I^n + Z^n} - k_2 X$ $\dfrac{dY}{dt} = k_3 X - k_4 Y$ $\dfrac{dZ}{dt} = k_5 Y - k_6 Z$	$\dfrac{dX}{dt} = k_1 \dfrac{1}{K_I^n + Z^n} - k_2 X$ $\dfrac{dY}{dt} = k_3 X - k_4 Y$ $\dfrac{dZ}{dt} = k_5 Y - k_6 Z$
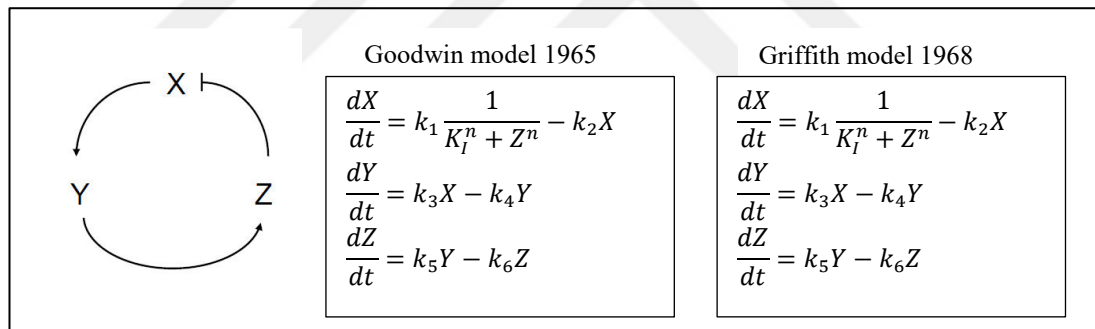
Figure 8.2 Interaction diagram of variables in Goodwin model (Goodwin, 1965). Goodwin model is later corrected by (Griffith, 1968)

Phase oscillators: Other widely used oscillators are phase oscillators. Since circadian oscillations are robust with respect to circadian period, in ideal conditions a phase oscillator can be used for modelling. Although phase oscillators are simple, all the main ingredients of a circadian clock such as 24 hour period, stability rate, frequency fluctuations with variance, and other noise effects can be embedded into the model so that frequency analysis, phase shifts with stochastic processes can be studied (Rougemont & Naef, 2008). Another advantage of using a phase oscillator is that, unlike Goodwin variants or detailed biochemical models, parameters corresponding to

period, amplitude, and phase shifts can be set accurately and separately. Disadvantage of using phase oscillators may be that the link between the biochemical process rates and parameters in phase oscillators are not clear. On the other hand, in ODE models which parameters are responsible for the stability, the frequency, or other properties is very hard to determine. An example of a phase oscillator is given in equations (3.1) and (3.2) by Granada & Herzel (2009). Equation (3.1) models the amplitude of oscillations whilst the second equation (3.2) models the phase. Thus, the solution is $r\,cos(\varphi)$. The equilibrium of the first equation is $r\;=\;1$. The parameter n in (3.1) controls the greediness of the system, when it is perturbed the transient time that the amplitude will converge to 1 again is determined by this variable. To change the oscillatory dynamics from sinusoidal to spiky, authors add a nonlinear term as $\varepsilon\cos^2(\varphi)$.

$$\frac{dr}{dt} = \lambda r^n (1 - r) \tag{3.1}$$

$$\frac{d\varphi}{dt} = f(\varphi) = \varepsilon\cos^2(\pi\varphi) \tag{3.2}$$

8.2 A Mathematical Framework for Interaction between P53 Network and Circadian Clock

Circadian clock and p53 network are two periodic regulatory mechanisms that can work independently of one another. However, these two systems interface and coupling is inevitable. There are evidences showing that circadian and p53 network has bidirectional coupling. It has been shown that p53 protein modulates circadian behavior by binding Per2 promoter, which BMAL1/Clock binds to promote Per2 expression. Thus, p53 blocks BMAL1/Clock binding to the Per2 promoter, leading to repression of Per2 expression (Beaver et al., 2002). We suggest that this interaction may be a key regulatory link between p53 network and circadian clock.

There is an inverse relationship between p53 and Per2. That is why P53^{-/-} mice have a shorter period length (22.8, for WT 23.3) (Beaver et al., 2002), since per2 concentration reaches high level faster. This demonstrates that there is a signal from p53 network via p53 protein to circadian clock. In addition, circadian clock sends a

signal to p53 network, as well, since it is established that under DSBs, ATM-Per acts via Chk2 on p53-ser20 phosphorylation (Caspari, 2000). This phosphorylation prevents the degradation of p53 by Mdm2. Also it has been shown by Gery et al. (2006) that Per1 may be required for the activation of ATM and overexpression of Per1 sensitized human cancer cells to DNA damage-induced apoptosis. Thus, this body of information reveals that circadian clock and p53 network has bidirectional binding. The schematic representation of idealized interplay between p53 network and circadian clock can be illustrated as in Figure 8.3. A model can be produced from this schematic diagram by elaborating on the interactions in the blocks. The added blocks of circadian clock to p53 network constitutes a negative feedback loop. Thus, there are two negative feedback loops in this proposed framework: Wip1 feedback loop and p53-BMAL/CLK-Per1/2 feedback loop.
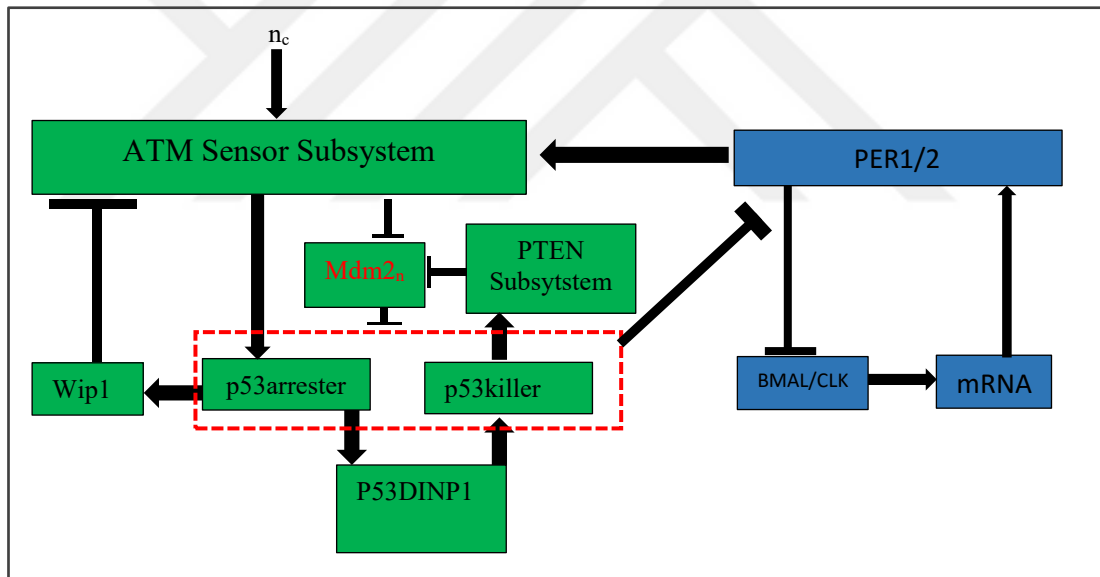
Figure 8.3 Schematic representation of a plausible coupling framework of p53 network and circadian clock

The effect of these two negative feedback loops on the frequency of oscillations of each network would provide information about how these networks keep or tune their oscillations, since it is known that coupling of oscillators usually quenches each other (Kamal, Sharma, & Shrimali, 2015). However, to study the coupling of these systems by combining two models via a coupling parameter blindly, whose parameters are

tuned for different purposes from different studies, is very unlikely that it will be informative. This is because mathematical models contain parameters estimated for an isolated experimental data but these parameters constitute only one set of parameter values in infinitely many possible set of parameters. Therefore, parameter estimation of combining two mathematical models from different experimental design areas would require the experimental data in which both these systems dynamics in terms of qualitative modes of oscillators (low steady state, oscillations, high steady state) are under investigation. However, to the best of our knowledge, such experiments do not exist. After the publication of such experiments, a more comprehensive modelling for coupling between these systems in terms of oscillator dynamics can be generated and validated.

We further simplify the framework by using 2-D oscillator model that we proposed (see Figure 8.4). This simplification provides the advantage of less parameters. Also, the simplified framework in Figure 8.4 allows for the investigation of coupling between these parameters in the context of coupling of oscillators. The coupling of oscillators is extensively studied in engineering and physics, but the lack of a low dimensional oscillator model made it less attractive for researchers. After the publication of this framework, we believe there will be more studies on the interaction between these two systems.
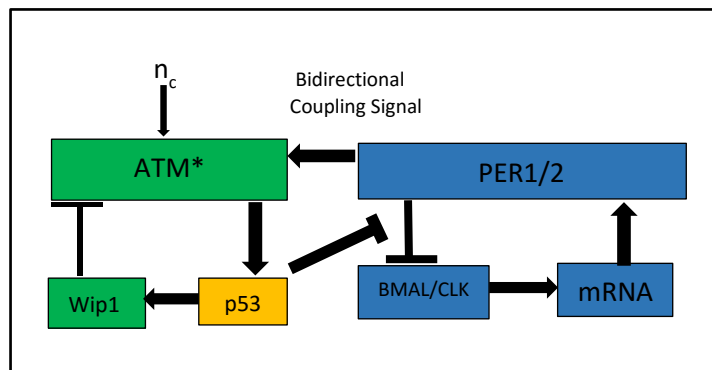
Figure 8.4 A coupling framework for p53 network and circadian clock oscillators as can be studied in the context of oscillator coupling

Figure 8.4 shows coupled oscillators, namely p53 network and circadian clock oscillators. The study of the coupling of these two systems is another challenge, since coupled oscillators exhibit some emergent dynamics such as amplitude death and oscillation death (Kamal, Sharma, & Shrimali, 2015). (In this thesis, we do not go into such deep analysis. We just provide a framework for further studies. Nevertheless, we study the framework to show the positive effect of circadian clock.) However, in healthy cells, it is known that p53 network is able to oscillate under circadian coupling. This means that p53 network and circadian clock are coupled under some conditions that they are both able to oscillate. Investigating these conditions would reveal valuable information about the design principles of these oscillators.

It is known that Per1 concentration is a representative signal of circadian clock, which is high at night and low during the day. Thus, the signal that goes out of Per1/2 to ATM sensor subsystem is known to oscillate. Since this signal is an observed signal, under some idealizations, we can model it as a sinusoidal signal and give it as an input to the 2-D oscillator model, and get results by looking from p53 network viewpoint (see Figure 8.5a,b). Since our aim is to find how p53 dynamics change under the circadian clock effect, this simplification here serves our aim.
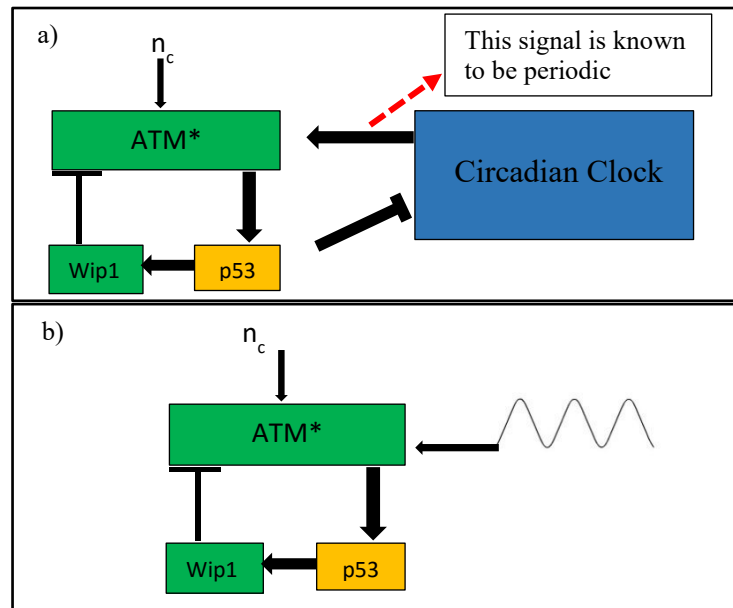
Figure 8.5 A simpler framework for studying the coupling from the perspective of p53 network. a) Circadian clock provides a sinusoidal signal to p53 network. b) Sinusoidal enhancing effect of circadian clock on p53 network through ATM

By giving a periodical input as circadian input to the ATM-Wip1 system, we numerically solve the proposed 2-D oscillator model in Table 3.1 for n_c = 20 throughout the simulation indicating a high DSBC activity, and sketch the solution in Figure 8.6. When it is mid-day (around 1000 minutes in Figure 8.6), the strength of oscillations (i.e. the amplitudes) increases to give a stronger cell cycle arrest signal. This strategy may exist for avoiding the risk of tumour formation in mid-day during which the sunlight has the most damaging effect.
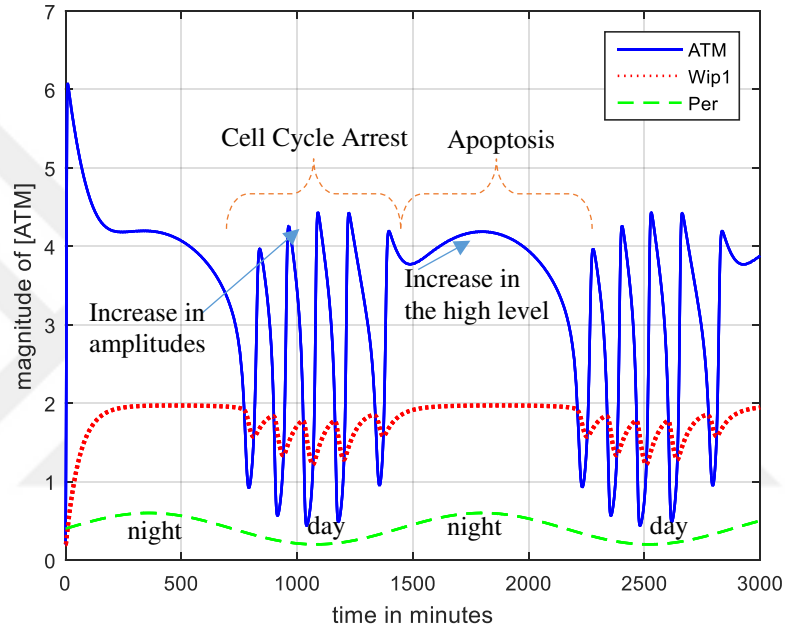
Figure 8.6 Per level is increased at night and decreased in day light. When Per is decreased and there is DNA damage, ATM-Wip1 oscillates indicating cell cycle arrest. If DNA damage is not repaired until night, then circadian system forces cell to apoptosis. The circadian signal is modelled as: $0.4 + 0.2sin(\frac{2\pi}{24}t)$

As can be seen in Figure 8.6, during the mid-night if there is still DSBC activity going on, circadian clock increases the highest level of p53 in apoptosis to ensure the easier initiation of apoptosis. Note that, in this simulation, Wip1 feedback loop is still on, and $Mdm2_n$ effect is not included. In Chapter 1 and 2, the apoptosis was initiated by distracting Wip1 feedback loop to stop p53 network oscillator and by decreasing $Mdm2_n$ level after the distraction. Herein, we show that p53 network oscillator can be stopped by a strong circadian signal, even if Wip1 feedback loop is on. The simulation result indicates that a strong circadian signal can mediate a higher sustained p53 level,

thus an easier initiation of apoptosis especially during night hours. This prediction here seems logical, however it needs to be proven by wet lab experiments.

Circadian system forces cells to initiate apoptosis during night hours (see Figure 8.6). Although some mathematical models rely on an integration term to apoptosis (He & Liu, 2014; Li et al., 2011; Zhang et al. 2011), herein under strong influence of circadian clock, p53 network may initiate apoptosis, thus an accumulating term may not be needed. This is especially important for cancer patients that cannot initiate apoptosis due to a deficiency in integration blocks (e.g. P53DINP1). Thus, with this coupling study, we show that a periodic input, like circadian rhythm, would force the oscillator to stop and initiate apoptosis (Figure 8.6).

CHAPTER NINE
CONCLUSION

This thesis develops two reduced oscillator models of 2-dimension for p53 dynamics by identifying an oscillator subsystem in p53 network and analyze them with the aim of uncovering the mechanisms that aid p53 network dynamics or implement a biological function.

To explore the oscillatory dynamics of p53 network, in Chapter 2 we re-conceptualize p53 network as a system that contains an oscillator in it (Figure 2.5). Holding on to that perspective, in Chapter 3 we introduced a 2-dimensional explanatory oscillator model by reducing the known 17-dimensional two-phase dynamics of p53 network (Table 3.1). The resulting model is a nonlinear relaxation oscillator that is capable of showing qualitative p53 dynamics (stable steady state at a low level, oscillatory regime, and a stable steady state at a high level) (Figure 3.1). This reduction also provided many novel fruitful understandings and new perspectives into two-phase dynamics of p53 network. With the help of the introduced 2-D model, it was possible (i) to think p53 network as a modular system whose core module consists of an excitable oscillator (Figure 2.5), (ii) to show that oscillations are of relaxation type (Figure 3.2, Sections 3.2, 3.3, and 3.4), (iii) to pose outcomes of cell fate as a phase space problem, which in turn brings a new perspective to understanding some situations that may lead to cancer (Chapter 5).

We applied local stability analysis and graphical methods on the explanatory 2-dimensional (2-D) model that was obtained by reducing two-phase dynamics model. The analysis of the introduced 2-D reduced oscillator model revealed a set of determinants of p53 network (Chapter 4), confirmed some known biological findings, and provided predictions to be validated as explained in the sequel.

We showed that $Mdm2_n$ (nuclear Mdm2 protein), known as the main negative regulator of p53, have different effects on the first and second phases of the p53 dynamics. Decreasing of $[Mdm2_n]$ (i.e. the concentration of $Mdm2_n$ protein) results in

110

a smaller amplitude of p53 level oscillations (the first phase), whereas it causes an increase in the high steady state level of p53 in apoptosis (the second phase). So, for oscillation with sufficient size of amplitudes, $Mdm2_n$ level should not be decreased. However, in apoptosis (i.e. second phase) where a higher level of p53 is needed, decreasing of $Mdm2_n$ level has a positive effect (Section 3.5, Figure 3.8, and Figure 4.1).

We found that the oscillations in p53 network is due to an underlying oscillator that is of relaxation type, which means p53 network has more complex dynamics than a simple static feedforward model of suppressor-effector interaction (Sections 3.2, 3.3, 3.4).

We found out that Wip1 and P53DINP1 regulators have profound effects on the cell fate due to their certain roles in the oscillator. Wip1 dynamics is observed to have a strong effect on the frequency and amplitude of oscillations and P53DINP1 is understood to be an Oscillation Accumulation Triggered Genetic Switch (OATGS) (He & Liu, 2014) which shuts off Wip1 feedback loop to provide sustained level of [p53*] (active p53 protein) to drive the cell to apoptosis. These findings may pave the way for some alternative approaches towards developing new therapeutic drugs (Chapter 4).

The presented work contributes to the systems-level understanding of p53 network, providing a better interpretation of wet lab experiments and suggests specific targets, namely Wip1 and P53DINP1, for curing strategies of cancer to be investigated further with drug developers (Chapter 4).

We showed that mutations such as Wip1 overexpression and ATM deficiency drastically change the phase space of the reduced 2-D oscillator model of p53 network and result in malfunctioning of the oscillator. We showed mathematically that the oscillatory phase space can be recovered. Thus, apoptosis can be initiated, in the types of cancer cell caused by Wip1 overexpression or ATM deficiency as with suppression of Wip1 overexpression and degradation of Wip1, respectively. Therefore, it is

observed that such a phase space analysis of Wip1 and ATM dynamics provides a tool to manipulate the cancer cells pharmacologically (Sections 5.1, 5.2, and 5.3; Figure 5.1).

We identified that decreasing p53 inhibitors, e.g. Mdm2, to activate p53 function to initiate apoptosis for possible medical purposes (e.g. as a cancer therapeutic approach), may have a serious side effect: It may result in weak oscillations of p53 causing problems in arresting cell cycle, which may cause cancer. We speculate that this may be one of the reasons for the complexity of p53 network (Section 5.4, Figure 5.2).

We suggest that the oscillator constituting the core subsystem of p53 network may be considered as a potential cancer therapeutic target to control cell fate (Section 5.5). We showed that, in two-phase dynamics model, cell fate can be determined by modulating this 2-D oscillator. By using the developed reduced 2-D oscillator model, we were able to pose some cancer types as a phase space problem, which is a new kind of mechanistic explanation to those cancer types that result from deficient cell cycle arrest (Chapter 5).

We showed that complexity of cancer may be due to a relaxation type oscillator embedded in p53 network. For instance, we revealed an interesting phenomenon about p53 inhibitors: the abundance of p53 inhibitors (e.g. $Mdm2_n$) may increase the amplitudes of p53 oscillations due to the relaxation type oscillator having p53 in its feedback loop (Sections 5.4 and 5.5). This may be one of the reason for the complexity of p53 network. To qualitatively manipulate the p53 network, e.g. to drive the cell to apoptosis, one has to manipulate this core oscillator as a first step. Any other intervention strategies that do not address the working of the oscillator may give controversial results. Further research employing similar system level approaches on p53 network may lead to development of novel therapeutic strategies. Another potential significance of the introduced 2-D oscillator model for p53 network is the possibility of modelling and studying the couplings between p53 network and other oscillators such as circadian network (as done to some extent in Chapter 8).

Taken as a whole, the presented work in Chapters 2, 3, 4, and 5 contributes to the systems-level understanding of p53 network dynamics, providing a better interpretation of wet lab experiments. Proposing such a comprehensive 2-D oscillator model for p53 network that controls the cell fate is valuable for measuring the significance of the feedback loops, regulators, and uncovering the essential working principles underlying the two-phase dynamics.

In Chapter 6, we proposed a 2-dimensional canonical relaxation oscillator model with polynomial terms for p53 network dynamics. This oscillator is a new oscillator for biological systems. The proposed simple model is rich in dynamics and valuable for intuitive understanding of p53 dynamics.

By using the proposed canonical model, we stressed the importance of Wip1 degradation term (Section 6.3.2) and showed in mathematical terms that this parameter is critical for recovering the cell's ability to oscillate in case of mutations such as ATM deficiency and Wip1 overexpression (Section 6.4). The results obtained by the introduced model emphasizes the importance of ATM and Wip1 in p53 dynamics. Due to its simplicity, the model has the potential of being used in further analytical studies of p53 network in the context of nonlinear systems theory.

The analyses on the canonical model revealed that the production rate of Wip1 and sensitivity of ATM to DNA damage are critical parameters that are related to cancer (Section 6.4). Wip1 feedback loop is important for different behaviours of p53 dynamics. Thus, Wip1 feedback loop may be a control element for adjusting P53 dynamics. This perspective is important since it hypothesizes that cancer treatment strategies might use Wip1 feedback loop as a target to control mutated cells, encouraging experimentalists to go in this direction.

We showed that the proposed canonical oscillator model is a relaxation oscillator (Section 6.3.6). We give an analytical range on the parameters that result in oscillations. This analytical range also includes the time-scale separation property. The

findings emphasize the importance of time scale separation in the dynamics of relaxation oscillations (Section 6.3.2).

We developed a novel coupling framework based on a literature search to investigate the synchronization properties of p53 network by using the two proposed oscillators of 2-dimension (Section 7.1). By using the developed framework, we realized *in silico* experiments with the aim of revealing the advantages of coupling properties. Results show that the coupling makes cells robust against noise (Section 7.2) and genetic heterogeneity (Section 7.3). By using the developed framework, future work should extend these studies to investigate the bystander effects in cells (e.g. Radiation Induced Bystander Effect).

We developed a coupling framework for circadian clock and p53 network based on literature search (Section 8.2). We showed that the circadian clock may favor the DNA damage response in some time intervals through the day. For example, circadian clock may favor the DNA damage response during the day-light to minimize the effects of irradiations to the cells. To prevent possible tumor formations, the circadian clock may ease the initiation of apoptosis. The understanding of the analytical conditions in which circadian clock has positive effect on DNA damage response is very crucial for chronotherapy. Finding a drug that can enhance the DNA damage response is very hard and requires commitment of hard work of companies and several researchers. Instead, why don't we use the natural enhancer that is already built in organism and look for those clues? Chapter 8 of this thesis provides such a framework to be used in the context of control and coupling of oscillators to be used in further research. The mathematical approaches to these two networks will pave the way for more effective scheduling in chronotherapy.

REFERENCES

Alon, U. (2003). Biological Networks: The Tinkerer as an Engineer. *Science*, 1866-1867.

Alon, U. (2006). *An Introduction to Systems Biology: Design Principles of Biological Circuits.* Boca Raton: CRC Press.

Avcu, N., Alyürük, H., Demir, G. K., Pekergin, F., Cavas, L., & Güzeliş., C. (2015). Determining the bistability parameter ranges of artificially induced lac operon using the root locus method. *Computers in Biology and Medicine*, 75-91.

Avcu, N., Demir, G., Pekergin, F., Alyürük, H., Çavaş, L., & Güzeliş, C. (2016). Discriminant-based bistability analysis of a TMG-induced lac operon model supported with boundedness and local stability results. *Turkish Journal of Electrical Engineering & Computer Sciences*, 719-732.

Bakkenist, C., & Kastan, M. (2003). DNA damage activates ATM through intermolecular autophosphorylation and dimer dissociation. *Nature*, 499.

Bar-Or, Lev, R., Maya, R., Segel, L. A., Alon, U., Levine, A. J., & M., O. (2000). Generation of oscillations by the p53-Mdm2 feedback loop: a theoretical and experimental study. *Proceedings of the National Academy of Sciences*, 11250-11255.

Batchelor, E., Loewer, A., & Lahav, G. (2009). The ups and downs of p53: Understanding protein dynamics in single cells. *Nature Reviews Cancer*, 371-377.

Batchelor, E., Loewer, A., Mock, C., & Lahav, G. (2011). Stimulus-dependent dynamics of p53 in single cells. *Molecular Systems Biology*, 488.

Batchelor, E., Mock, C. S., Bhan, I., Loewer, A., & Lahav, G. (2008). Recurrent initiation: a mechanism for triggering p53 pulses in response to DNA damage. *Molecular Cell*, 277-289.

Batchelor, E., Mock, C. S., Bhan, I., Loewer, A., & Lahav, G. (2008). Recurrent initiation: a mechanism for triggering p53 pulses in response to DNA damage. *Molecular Cell*, 277-289.

Beaver, L. M., Gvakharia, B. O., Vollintine, T. S., Hege, D. M., Stanewsky, R., & Giebultowicz, J. M. (2002). Loss of circadian clock function decreases reproductive fitness in males of Drosophila melanogaster. *Proceedings of the National Academy of Sciences*, 2134-2139.

Becker-Weimann, S., Wolf, J., Herzel, H., & Kramer, A. (2004). Modeling feedback loops of the mammalian circadian oscillator. *Biophysical Journal*, 3023-3034.

Belova, G. I., Demidov, O., Fornace, A. J., & Bulavin, D. V. (2005). Chemical inhibition of Wip1 phosphatase contributes to suppression of tumorigenesis. *Cancer Biology & Therapy*, 1154-1158.

Bensussen, A., & Díaz, J. (2012). Dynamical aspects of apoptosis. *Current Topics in Ionizing Radiation Research*, 243-268.

Bernard, S. G., Čajavec, B., Herzel, H., & Kramer, A. (2007). Synchronization-induced rhythmicity of circadian oscillators in the suprachiasmatic nucleus. *PLoS Computational Biology*, 667-679.

Braithwaite, A. W., & Prives., C. L. (2006). p53: more research and more questions. *Cell Death & Differentiation*, 877-880.

Branzei, D., & Foiani, M. (2008). Regulation of DNA repair throughout the cell cycle. *Nature Reviews*, 297.

Bray, D. (1995). Protein molecules as computational elements in living cells. *Nature*, 307-312.

Brigandt, I. (2013). Systems biology and the integration of mechanistic explanation and mathematical explanation. *Studies in History and Philosophy of Science Part C: Studies in History and Philosophy of Biological and Biomedical Sciences*, 477-492.

Brown, D. R., Thomas, C. A., & Deb, S. P. (1998). The human oncoprotein MDM2 arrests the cell cycle: elimination of its cell-cycle-inhibitory function induces tumorigenesis. *The EMBO Journal*, 2513-2525.

Bulavin, D. V., Demidov, O. N., Saito, S., Kauraniemi, P., Phillips, C., Amundson, S. A., . . . Appella, E. (2002). Amplification of PPM1D in human tumors abrogates p53 tumor-suppressor activity. *Nature Genetics*, 210-215.

Burdak-Rothkamm, S., & Prise, K. (2009). New molecular targets in radiotherapy: DNA damage signalling and repair in targeted and non-targeted cells. *European Journal of Pharmacology*, 151-155.

Caspari, T. (2000). Checkpoints: How to activate p53. *Current Biology*, R315-R317.

Castellino, R. C., Bortoli, M. D., Lu, X., Moon, S.-H., Nguyen, T.-A., Shepard, M. A., . . . Kim, J. Y. (2008). Medulloblastomas overexpress the p53-inactivating oncogene WIP1/PPM1D. *Journal of Neuro-oncology*, 245-256.

Chen, J., Yue, H., & Ouyang, Q. (2014). Correlation between oncogenic mutations and parameter sensitivity of the apoptosis pathway model. *PLOS Computational Biology*, e1003451.

Chou, I.-C., & Voit, E. O. (2009). Recent developments in parameter estimation and structure identification of biochemical and genomic systems. *Mathematical Biosciences*, 57-83.

Ciliberto, A., Novák, B., & Tyson, J. J. (2005). Steady states and oscillations in the p53/Mdm2 network. *Cell Cycle*, 488-493.

Craver, C. F. (2006). When mechanistic models explain. *Synthese*, 355-376.

Dang, J., Kuo, M.-L., Eischen, C. M., Stepanova, L., Sherr, C. J., & Roussel, M. F. (2002). The RING domain of Mdm2 can inhibit cell proliferation. *Cancer Research*, 1222-1230.

Darlington, Y., Nguyen, T., Moon, S., Herron, A., Rao, P., Zhu, C., . . . Donehower, L. (2012). Absence of Wip1 partially rescues Atm deficiency phenotypes in mice. *Oncogene*, 1155-1165.

Deguin-Chambon, V., Vacher, M., Jullien, M., May, E., & Bourdon, J. (2000). Direct transactivation of c-Ha-Ras gene by p53: evidence for its involvement in p53 transactivation activity and p53-mediated apoptosis. *Oncogene*, p.5831.

Delia, D., Fontanella, E., Ferrario, C., Chessa, L., & Mizutani, S. (2003). DNA damage-induced cell-cycle phase regulation of p53 and p21waf1 in normal and ATM-defective cells. *Oncogene*, 7866-7869.

Devi, G., Alam, M., & Singh, R. (2015). Synchronization in stress p53 network. *Mathematical Medicine and Biology: a journal of the IMA*, 437-456.

Dibner, C., Sage, D. U., Bauer, C., d'Eysmond, T., Naef, F., & Schibler, U. (2009). Circadian gene expression is resilient to large fluctuations in overall transcription rates. *The EMBO journal*, 123-134.

Dodd, A. N., Salathia, N., Hall, A., Kévei, E., Tóth, R., Nagy, F., . . . Webb, A. (2005). Plant circadian clocks increase photosynthesis, growth, survival, and competitive advantage. *Science*, 630-633.

Doumont, G., Martoriati, A., Beekman, C., Bogaerts, S., Mee, P., Bureau, F., . . . Scanziani, E. (2005). G1 checkpoint failure and increased tumor susceptibility in mice lacking the novel p53 target Ptprv. *The EMBO Journal*, 3093-3103.

El-Deiry, W. (1998). January. Regulation ofp53downstream genes. *Seminars in Cancer Biology*, 345-357.

Erdrich, P., & Ralf Steuer, S. K. (2015). An algorithm for the reduction of genome-scale metabolic network models to meaningful core models. *BMC Systems Biology*, 48.

Essmann, F., Engels, I. H., Totzke, G., Schulze-Osthoff, K., & Jänicke, R. U. (2004). Apoptosis resistance of MCF-7 breast carcinoma cells to ionizing radiation is

independent of p53 and cell cycle control but caused by the lack of caspase-3 and a caffeine-inhibitable event. *Cancer Research*, 7065-7072.

FitzHugh, R. (1961). Impulses and physiological states in theoretical models of nerve membrane. *Biophysical journal*, 445.

Forger, D., & Peskin, C. (2003). A detailed predictive model of the mammalian circadian clock. *Proceedings of the National Academy of Sciences*, 14806-14811.

Fuku, T., Semba, S., Yutori, H., & Yokozaki, H. (2007). Increased wild-type p53-induced phosphatase 1 (Wip1 or PPM1D) expression correlated with downregulation of checkpoint kinase 2 in human gastric carcinoma. *Pathology International*, 566-571.

Fumiko, S.-O., Imoto, I., Inoue, J., Hosoi, H., Nakagawara, A., Sugimoto, T., & Inazawa, J. (2003). PPM1D is a potential target for 17q gain in neuroblastoma. *Cancer Research*, 1876-1883.

Gaddameedhi, S., Reardon, J. T., Ye, R., Ozturk, N., & Sancar, A. (2012). Effect of circadian clock mutations on DNA damage response in mammalian cells. *Cell Cycle*, 3481-3491.

Gartel, A. L., & Radhakrishnan, S. K. (2005). Lost in transcription: p21 repression, mechanisms, and consequences. *Cancer research*, 3980-3985.

Gery, S., Komatsu, N., Baldjyan, L., Yu, A., Koo, D., & Koeffler, H. (2006). The circadian gene per1 plays an important role in cell growth and DNA damage control in human cancer cells. *Molecular Cell*, 375-382.

Geva-Zatorsky, N., Rosenfeld, N., Itzkovitz, S., Milo, R., Sigal, A., Dekel, E., . . . Alon, U. (2006). Oscillations and variability in the p53 system. *Molecular Systems Biology*, *2*(1).

Ghosh, S., Ghosh, A., & Krishna, M. (2015). Role of ATM in bystander signaling between human monocytes and lung adenocarcinoma cells. *Mutation Research/Genetic Toxicology and Environmental Mutagenesis*, 39-45.

Gillespie, D. T. (1977). Exact stochastic simulation of coupled chemical reactions. *The Journal of Physical Chemistry*, 2340-2361.

Goloudina, A., Tanoue, K., Hammann, A., Fourmaux, E., Le Guezennec, X., Bulavin, D., . . . Demidov, O. (2012). Wip1 promotes RUNX2-dependent apoptosis in p53-negative tumors and protects normal tissues during treatment with anticancer agents. *Proceedings of the National Academy of Sciences*, E68-E75.

Gonze, D., Bernard, S., Waltermann, C., Kramer, A., & Herzel, H. (2005). Spontaneous synchronization of coupled circadian oscillators. *Biophysical Journal*, 120-129.

Goodwin, B. (1965). Oscillatory behavior in enzymatic control processes. *Advances in enzyme regulation*, 425IN1429IN3431-428IN2430IN6437.

Granada, A., & Herzel, H. (2009). How to achieve fast entrainment? The timescale to synchronization. *PLoS One*, p.e7057.

Green, D. R., & Evan, G. I. (2002). A matter of life and death. *Cancer cell*, 19-30.

Griffith, J. (1968). Mathematics of cellular control processes I. Negative feedback to one gene. *Journal of Theoretical Biology*, 202-208.

Grudziński, K., & Żebrowski, J. J. (2004). Modeling cardiac pacemakers with relaxation oscillators. *Physica A: Statistical Mechanics and its Applications*, 153-162.

Halberg, F., Halberg, E., Barnum, C., & Bittner J.J. (1959). Physiologic 24-hour periodicity in human beings and mice, the lighting regimen and daily routine, , Washington DC, 1959. *Photoperiodism and Related Phenomena in Plants and Animals*, 803-878.

Hartwell, L. H., Hopfield, J. J., Leibler, S., & Murray, A. W. (1999). From molecular to modular cell biology. *Nature*, C47-C52.

Hastings, M. H., Reddy, A. B., & Maywood, E. S. (2003). A clockwork web: Circadian timing in brain and periphery, in health and disease. *Nature Reviews Neuroscience*, 649-661.

Hat, B., Kochańczyk, M., Bogdał, M., & Lipniacki, T. (2016). Feedbacks, bifurcations, and cell fate decision-making in the p53 system. *PLoS computational biology, 12*(2), 1004787.

He, Q., & Liu, Z. (2014). Investigation of oscillation accumulation triggered genetic switch in gene regulatory networks. *Journal of theoretical biology* , 61-66.

Hirschie Johnson, C., Elliott, J., & Foster, R. (2003). Entrainment of circadian programs. *Chronobiology international*, 741-774.

Hünten, S., Siemens, H., Kaller, M., & Hermeking, H. (2013). The p53/microRNA network in cancer: experimental and bioinformatics approaches. In *MicroRNA Cancer Regulation* (pp. 77-101). Springer Netherlands.

IARC TP53 Database. (2017, August 24). Retrieved from The p53 Web Site: http://p53.iarc.fr/

Jaiswal, H., & Lindqvist, A. (2015). Bystander communication and cell cycle decisions after DNA damage. *Frontiers in genetics*, 6.

Jonak, K., Kurpas, M., Szoltysek, K., Janus, P., Abramowicz, A., & Puszynski, K. (2016). A novel mathematical model of ATM/p53/NF-κ B pathways points to the importance of the DDR switch-off mechanisms. *BMC systems biology, 10*(1), 75.

Jonathan R. Karr, ,. K. (2015). The principles of whole-cell modeling. *Current opinion in microbiology*, 18-24.

Kaluza, P., & Meyer-Ortmanns, H. (2010). On the role of frustration in excitable systems. *Chaos: An Interdisciplinary Journal of Nonlinear Science*, 043111.

Kamal, N., Sharma, P., & Shrimali, M. (2015). Oscillation suppression in indirectly coupled limit cycle oscillator. *Physical Review E*, p.022928.

Kang, T., & Sancar, A. (2009). Circadian regulation of DNA excision repair: implications for chrono-chemotherapy. *Cell cycle*, 1665-1667.

Kim, J. K., & Forger, D. B. (2012). A mechanism for robust circadian timekeeping via stoichiometric balance. *Molecular Systems Biology*, 630.

Kim, J., & Jackson, T. (2013). Mechanisms that enhance sustainability of p53 pulses. *PloS one* , p.e65242.

Ko, C., & Takahashi, J. (2006). Molecular components of the mammalian circadian clock. *Human Molecular Genetics*, R271-R277.

Ko, C., Yamada, Y., Welsh, D., Buhr, E., Liu, A., Zhang, E., . . . Takahashi, J. (2010). Emergence of noise-induced oscillations in the central circadian pacemaker. *PLoS Biology*, p.e1000513.

Kochańczyk, M., Kocieniewski, P., Kozłowska, E., Jaruszewicz-Błońska, J., Sparta, B., Pargett, M., . . . Lipniacki, T. (2017). Relaxation oscillations and hierarchy of feedbacks in MAPK signaling. *Scientific Reports*, p.38244.

Kong, W., Jiang, X., & Mercer, W. (2009). Downregulation of Wip-1 phosphatase expression in MCF-7 breast cancer cells enhances doxorubicin-induced apoptosis through p53-mediated transcriptional activation of Bax. *Cancer Biology & Therapy*, 555-563.

Kozyreff, G., & Erneux, T. (2014). Singular Hopf bifurcation in a differential equation with large state-dependent delay. *The Royal Society*, Vol. 470, No. 2162, p. 20130596.

Krinsky, V. I., & Kholopov, A. V. (1967). Echo in excitable tissue. *Biofizika*, 524-528.

Kripke, D., Elliott, J., Welsh, D., & Youngstedt, S. (2015). Photoperiodic and circadian bifurcation theories of depression and mania. *F1000Research*.

Krishna, S., Semsey, S., & Jensen, M. H. (2009). Frustrated bistability as a means to engineer oscillations in biological systems. *Physical Biology*, 036009.

Kurz, E. U., & Lees-Miller, S. P. (2004). DNA damage-induced activation of ATM and ATM-dependent signaling pathways. *DNA Repair*, 889-900.

Lahav, G. (2004). The strength of indecisiveness: oscillatory behavior for better cell fate determination. *Science Signaling*, pe55-pe55.

Lahav, G., Rosenfeld, N., Sigal, A., Geva-Zatorsky, N., Levine, A. J., Elowitz, M. B., & Alon, U. (2004). Dynamics of the p53-Mdm2 feedback loop in individual cells. *Nature Genetics*, 147-150.

Lambros, M., Natrajan, R., Geyer, F., Lopez-Garcia, M., Dedes, K., Savage, K., . . . Ashworth, A. (2010). PPM1D gene amplification and overexpression in breast cancer: a qRT-PCR and chromogenic in situ hybridization study. *Modern Pathology*, 1334-45.

Lavin, M., & Kozlov, S. (2007). TM activation and DNA damage response. *Cell Cycle*, 931-942.

Lazebnik, Y. (2002). Can a biologist fix a radio?—Or, what I learned while studying apoptosis. *Cancer Cell*, 179-182.

Leloup, J., & Goldbeter, A. (1998). A model for circadian rhythms in Drosophila incorporating the formation of a complex between the PER and TIM proteins. *Journal of Biological Rhythms*, 70-87.

Leloup, J., & Goldbeter, A. (2003). Toward a detailed computational model for the mammalian circadian clock. *Proceedings of the National Academy of Sciences*, 7051-7056.

Leloup, J., & Goldbeter, A. (2004). Modeling the mammalian circadian clock: sensitivity analysis and multiplicity of oscillatory mechanisms. *Journal of Theoretical Biology*, 541-562.

Li, Q., & Wang, Y. (2007). Coupling and internal noise sustain synchronized oscillation in calcium system. *Biophysical Chemistry*, 23-28.

Li, Z., Ni, M., Li, J., Zhang, Y., Ouyang, Q., & Tang, C. (2011). Decision making of the p53 network: Death by integration. *Journal of theoretical biology*, 205-211.

Lillacci, G., & Khammash, M. (2009). Parameter estimation and model selection in computational biology. *PLoS Computational Biology*, e1000696.

Liu, A. C., Welsh, D. K., Ko, C. H., Tran, H. G., Zhang, E. E., Priest, A. A., . . . Doyle, F. J. (2007). Intercellular coupling confers robustness against mutations in the SCN circadian clock network. *Cell*, 605-616.

Locke, J. C., Westermark, P. O., Kramer, A., & Herzel, H. (2008). Global parameter search reveals design principles of the mammalian circadian clock. *BMC Systems Biology*, 22.

Lord, C. J., & Ashworth, A. (2012). The DNA damage response and cancer therapy. *Nature*, 287.

Lotka, A. (1910). Contribution to the theory of periodic reactions. *Journal of Physical Chemistry*, 271-274.

Lowe, J., Cha, H., Lee, M.-O., Mazur, S. J., Appella, E., & Jr., A. J. (2012). Regulation of the Wip1 phosphatase and its effects on the stress response. *Frontiers in bioscience: a journal and virtual Library*, 1480.

Lu, X., Ma, O., Nguyen, T., Jones, S., Oren, M., & Donehower, L. (2007). The Wip1 Phosphatase acts as a gatekeeper in the p53-Mdm2 autoregulatory loop. *Cancer cell, 12*(4), 342-354.

Ma, L., Wagner, J., Rice, J. J., Hu, W., Levine, A. J., & Stolovitzky., G. A. (2005). A plausible model for the digital response of p53 to DNA damage. *Proceedings of the National Academy of Sciences of the United States of America*, 14266-14271.

Mackonis, E., Suchowerska, N., Zhang, M., Ebert, M., McKenzie, D., & Jackson, M. (2007). Cellular response to modulated radiation fields. *Physics in Medicine and Biology*, 5469.

Manfredi, J. J. (2010). The Mdm2–p53 relationship evolves: Mdm2 swings both ways as an oncogene and a tumor suppressor. *Genes & development*, 1580-1589.

Marchenko, N. D., Zaika, A., & Moll, U. M. (2000). Death signal-induced localization of p53 protein to mitochondria a potential role in apoptotic signaling. *Journal of Biological Chemistry*, 16202-16212.

Marcheva, B., Ramsey, K., Buhr, E., Kobayashi, Y., Su, H., Ko, C., . . . Lopez, J. (2010). Disruption of the clock components CLOCK and BMAL1 leads to hypoinsulinaemia and diabetes. *Nature*, 627-631.

Marín, A., Martín, M., Liñán, O., Alvarenga, F., López, M., Fernández, L., . . . Cerezo, L. (2015). Bystander effects and radiotherapy. *Reports of Practical Oncology & Radiotherapy*, 12-21.

Marino, S., Hogue, I., Ray, C., & Kirschner, D. (2008). A methodology for performing global uncertainty and sensitivity analysis in systems biology. *Journal of Theoretical Biology*, 178-196.

Mayo, L., Dixon, J., Durden, D., Tonks, N., & Donner, D. (2002). PTEN protects p53 from Mdm2 and sensitizes cancer cells to chemotherapy. *Journal of Biological Chemistry*, pp.5484-5489.

Michael, D., & Oren, M. (2003). The p53–Mdm2 module and the ubiquitin system. *Seminars in Cancer Biology* (pp. 49-58). Academic Press.

Mihara, M., Erster, S., Zaika, A., Petrenko, O., Chittenden, T., Pancoska, P., & Moll, U. M. (2003). p53 has a direct apoptogenic role at the mitochondria. *Molecular Cell*, 577-590.

Miles MacLeod, & Nersessian, N. J. (2015). Modeling systems-level dynamics: Understanding without mechanistic explanation in integrative systems biology. *Studies in History and Philosophy of Science Part C: Studies in History and Philosophy of Biological and Biomedical Sciences* , 1-11.

Monk, N. A. (2003). Oscillatory expression of Hes1, p53, and NF-κB driven by transcriptional time delays. *Current Biology*, 1409-1413.

Mouri, K., Nacher, J. C., & Akutsu, T. (2009). A mathematical model for the detection mechanism of DNA double-strand breaks depending on autophosphorylation of ATM. *PLoS One*, e5131.

Murray-Zmijewski, F., Slee, E. A., & Lu, X. (2008). A complex barcode underlies the heterogeneous response of p53 to stress. *Nature reviews Molecular cell biology*, 702-712.

Murray-Zmijewski, F., Slee, E., & Lu, X. (2008). A complex barcode underlies the heterogeneous response of p53 to stress. *Nature Reviews Molecular Cell Biology*, 702-712.

Nakamura, Y., & Arakawa, H. (2008, May 13). *U.S. Patent No. 7,371,835.*

Nurse, P. (2008). Life, logic and information. *Nature*, 424-426.

Okamura, S., Arakawa, H., Tanaka, T., Nakanishi, H., Ng, C. C., Taya, Y., . . . Nakamura, Y. (2001). p53DINP1, a p53-inducible gene, regulates p53-dependent apoptosis. *Molecular Cell*, 85-94.

Ongusaha, P., Kim, J., Fang, L., Wong, T., Yancopoulos, G., Aaronson, S., & Lee, S. (2003). p53 induction and activation of DDR1 kinase counteract p53-mediated apoptosis and influence p53 regulation through a positive feedback loop. *The EMBO Journal*, 1289-1301.

Ortiz-Tudela, E., Mteyrek, A., Ballesta, A., Innominato, P., & Lévi, F. (2013). Cancer chronotherapeutics: experimental, theoretical, and clinical aspects. In Circadian clocks. *Springer Berlin Heidelberg*, 261-288.

Pandita, T., Lieberman, H., Lim, D., Dhar, S., Zheng, W., Taya, Y., & Kastan, M. (2000). Ionizing radiation activates the ATM kinase throughout the cell cycle. *Oncogene*, 1386.

Purvis, J. E., Karhohs, K. W., Mock, C., Batchelor, E., Loewer, A., & Lahav, G. (2012). p53 dynamics control cell fate. *Science*, 1440-1444.

Purvis, J., & Lahav, G. (2013). Encoding and decoding cellular information through signaling dynamics. *Cell*, 945-956.

Rao, S., Schaft, A. v., Eunen, K. v., Bakker, B. M., & Jayawardhana, B. (2013). Model-order reduction of biochemical reaction networks. *Control Conference*, (pp. 4502-4507).

Rauta, J., Alarmo, E.-L., Kauraniemi, P., Karhu, R., Kuukasjärvi, T., & Kallioniemi., A. (2006). The serine-threonine protein phosphatase PPM1D is frequently activated through amplification in aggressive primary breast tumours. *Breast Cancer Research and Treatment*, 257-263.

Rayter, S. E., Jones, K., Linardopoulos, S., Workman, P., Aherne, W., & Lord, C. (2008). A chemical inhibitor of PPM1D that selectively kills cells overexpressing PPM1D. *Oncogene*, 1036-1044.

Reifenberger, G., Liu, L., Ichimura, K., Schmidt, E., & Collins, V. (2003). Amplification and overexpression of the MDM2 gene in a subset of human malignant gliomas without p53 mutations. *Cancer Research*, 2736-2739.

Relógio, A., Westermark, P., Wallach, T., Schellenberg, K., Kramer, A., & Herzel, H. (2011). Tuning the mammalian circadian clock: Robust synergy of two loops. *PLoS Computational Biology*, 1002309.

Richter, M., Dayaram, T., Gilmartin, A., Ganji, G., Pemmasani, S., Van Der Key, H., . . . Kumar, R. (2015). WIP1 phosphatase as a potential therapeutic target in neuroblastoma. *PLoS One*, e0115635.

Rosenfeld, N., Elowitz, M. B., & Alon, U. (2002). Negative autoregulation speeds the response times of transcription networks. *Journal of Molecular Biology*, 785-793.

Rothkamm, K., Krüger, I., Thompson, L., & Löbrich, M. (2003). Pathways of DNA double-strand break repair during the mammalian cell cycle. *Molecular and cellular biology*, 5706-5715.

Rougemont, J., & Naef, F. (2008). Stochastic phase oscillator models for circadian clocks. In *Cellular Oscillatory Mechanisms* (pp. 141-149). New York: Springer.

Rzeszowska-Wolny, J., Przybyszewski, W., & Widel, M. (2009). Ionizing radiation-induced bystander effects, potential targets for modulation of radiotherapy. *European Journal of PHarmacology*, 156-164.

Sahar, S., & Sassone-Corsi, P. (2009). Metabolism and cancer: The circadian clock connection. *Nature Reviews Cancer*, 886-896.

Saito-Ohara, F., Imoto, I., Inoue, J., Hosoi, H., Nakagawara, A., Sugimoto, T., & Inazawa, J. (2003). PPM1D is a potential target for 17q gain in neuroblastoma. *Cancer Research*, 1876-1883.

Samuel, T., Weber, H., & Funk, J. (2002). Linking DNA damage to cell cycle checkpoints. *Cell Cycle*, 161-167.

Sancar, A., Lindsey-Boltz, L. A., Kang, T. H., Reardon, J. T., Lee, J. H., & Ozturk, N. (2010). Circadian clock control of the cellular response to DNA damage. *FEBS letters*, 2618-2625.

Sedelnikova, O., Nakamura, A., Kovalchuk, O., Koturbash, I., Mitchell, S., Marino, S., . . . Bonner, W. (2007). DNA double-strand breaks form in bystander cells after microbeam irradiation of three-dimensional human tissue models. *Cancer Research*, 4295-4302.

Sharma, V. K. (2003). Adaptive significance of circadian clocks. *Chronobiology International*, 901-919.

Shreeram, S., Demidov, O., Hee, W., Yamaguchi, H., Onishi, N., Kek, C., . . . Minami, Y. (2006). Wip1 phosphatase modulates ATM-dependent signaling pathways. *Molecular Cell*, 757-764.

Shreeram, S., Hee, W. K., Demidov, O. N., Kek, C., Yamaguchi, H., Fornace, A. J., & Bulavin, D. V. (2006). Regulation of ATM/ P53-dependent suppression of myc-induced lymphomas by Wip1 phosphatase. *The Journal of Experimental MEdicine*, 2793-2799.

Soliman, S., & Heiner, M. (2010). A unique transformation from ordinary differential equations to reaction networks. *PloS One*, e14284.

Sriram, K., & Gopinathan, M. (2004). A two variable delay model for the circadian rhythm of Neurospora crassa. *Journal of Theoretical Biology*, 23-38.

Stewart, R. D. (2001). Two-lesion kinetic model of double-strand break rejoining and cell killing. *Radiation Research*, 365-378.

Sun, T., & Cui, J. (2015). Dynamics of P53 in response to DNA damage: Mathematical modeling and perspective. *Progress in Biophysics and Molecular Biology*, 175-182.

Sun, T., & Cui, J. (2015). Dynamics of P53 in response to DNA damage: Mathematical modeling and perspective. *Progress in biophysics and molecular biology* , 175-182.

Sunnåker, M., Cedersund, G., & Jirstrand, M. (2011). A method for zooming of nonlinear models of biochemical systems. *BMC Systems Biology*, 140.

Szymańska, P., Martin, K., MacKeigan, J., Hlavacek, W., & Lipniacki, T. (2015). Computational analysis of an autophagy/translation switch based on mutual inhibition of MTORC1 and ULK1. *Plos One*, 0116550.

Tan, D., Lambros, M., Rayter, S., Natrajan, R., Vatcheva, R., Gao, Q., . . . Fenwick, K. (2009). PPM1D is a potential therapeutic target in ovarian clear cell carcinomas. *Clinical Cancer Research*, 2269-2280.

Teschl, G. (2012). *Ordinary Differential Equations and Dynamical Systems.* Providence: American Mathematical Society.

Tiana, G., Jensen, M. H., & Sneppen, K. (2002). Time delay as a key to apoptosis induction in the p53 network. *The European Physical Journal B-Condensed Matter and Complex Systems*, 135-140.

Toettcher, J., Loewer, A., Ostheimer, G., Yaffe, M., Tidor, B., & Lahav, G. (2009). Distinct mechanisms act in concert to mediate cell cycle arrest. *Proceedings of the National Academy of Sciences*, 785-790.

Tyson, J. J., & Novak, B. (2015). Bistability, oscillations, and traveling waves in frog egg extracts. *Bulletin of Mathematical Biology*, 796-816.

Tyson, J. J., Chen, K. C., & Novak, B. (2003). Sniffers, buzzers, toggles and blinkers: dynamics of regulatory and signaling pathways in the cell. *Current Opinion in Cell Biology*, 221-231.

Van der Pol, B. (1926). On relaxation-oscillations. *The London, Edinburgh, and Dublin Philosophical Magazine and Journal of Science*, 978-992.

Van der Pol, B., & Mark, J. V. (1928). The heartbeat considered as a relaxation oscillation, and an electrical model of the heart. *The London, Edinburgh, and Dublin Philosophical Magazine and Journal of Science*, 763-775.

Voit, E., & Chou, I.-C. (2010). Parameter estimation in canonical biological systems models. *International Journal of Systems and Synthetic Biology*, 1-19.

Volterra, V. (1927). Variazioni e fluttuazioni del numero d'individui in specie animali conviventi. *C. Ferrari*.

Vousden, K., & Lane, D. (2007). p53 in health and disease. *Molecular Cell Biology*, 275.

Wang, H., Liu, Z., Qiu, L., Guo, J., Li, Y., Zhang, J., . . . Liu, X. (2015). Knockdown of Wip1 enhances sensitivity to radiation in hela cells through activation of p38 MAPK. *Oncology Research Featuring Preclinical and Clinical Cancer Therapeutics*, 225-233.

Woelfle, M., Ouyang, Y., Phanvijhitsiri, K., & Johnson, C. (2004). The adaptive value of circadian clocks: an experimental assessment in cyanobacteria. *Current Biology*, 1481-1486.

Xia, Y., Ongusaha, P., Lee, S., & Liou, Y. (2009). Loss of Wip1 sensitizes cells to stress-and DNA damage-induced apoptosis. *Journal of Biological Chemistry*, 17428-17437.

Xu, Y., & Baltimore, D. (1996). Dual roles of ATM in the cellular response to radiation and in cell growth control. *Genes & Development*, 2401-2410.

Yamaguchi, H., Durell, S., Feng, H., Bai, Y., Anderson, C., & Appella, E. (2006). Development of a substrate-based cyclic phosphopeptide inhibitor of protein phosphatase 2Cδ, Wip1. *Biochemistry*, 13193-13202.

Yi, W., Hu, X., Chen, Z., Liu, L., Tian, Y., Chen, H., . . . Zhang, Z. (2015). Phosphatase Wip1 controls antigen-independent B-cell development in a p53-dependent manner. *Blood*, 620-628.

Yoda, A., Toyoshima, K., Watanabe, Y., Onishi, N., Hazaka, Y., Tsukuda, Y., . . . Minami, Y. (2008). Arsenic trioxide augments Chk2/p53-mediated apoptosis by inhibiting oncogenic Wip1 phosphatase. *Journal of Biological Chemistry*, 18969-18979.

Zhang, T., Brazhnik, P., & Tyson., J. J. (2007). Exploring mechanisms of the DNA-damage response: p53 pulses and their possible relevance to apoptosis. *Cell Cycle*, 85-94.

Zhang, X.-P., Liu, F., & Wang, W. (2011). Two-phase dynamics of p53 in the DNA damage response. *Proceedings of the National Academy of Sciences*, 8990-8995.

Zhou, T., Zhang, J., Yuan, Z., & Chen, L. (2008). Synchronization of genetic oscillators. *Chaos: An Interdisciplinary Journal of Nonlinear Science*, p.037126.

APPENDICES

Appendix-1: Two-phase Model by Zhang et al. (2011)

$$\frac{d[ATM_2]}{dt} = 0.5k_{dim}[ATM]^2 - k_{undim}[ATM_2] \tag{A.6}$$

$$\frac{d[ATM^*]}{dt} = k_{acatm}\frac{n_c}{n_c + j_{nc}}[ATM^*]\frac{[ATM]}{([ATM] + j_{acatm})}$$
$$- k_{deatm}(1 + Wip1)\frac{[ATM^*]}{([ATM^*] + j_{deatm})} \tag{A.7}$$

$$[ATM] = ATM_{tot} - 2[ATM_2] - [ATM^*] \tag{A.8}$$

$$k_{dmdm2n} = k_{dmdm2n0} + \frac{k_{dmdm2n1}[ATM^*]}{[ATM^*] + j_{atm}} \tag{A.9}$$

$$k_{acp53} = k_{acp531} * \frac{[ATM^*]}{([ATM^*] + j_{atm})} \tag{A.10}$$

$$\frac{d[p53^*]}{dt} = k_{acp53}[p53] - k_{dep53}[p53^*] - k_{dp53s}[Mdm2_n]\frac{[p53^*]}{j_{1p53n} + [p53^*]} \tag{A.11}$$

$$\frac{d[p53]}{dt} = k_{sp53} - k_{dp53n}[p53] - k_{dp53}[Mdm2_n]\frac{[p53]}{j_{1p53n} + [p53]} - k_{acp53}[p53]$$
$$+ k_{dep53}[p53^*] \tag{A.12}$$

$$\frac{d[Mdm2_c]}{dt} = k_{smdm20} + k_{smdm2}\frac{[P53^*]^4}{(j_{smdm2}{}^4 + [P53^*]^4)} - k_{dmdm2c}[Mdm2_c]$$
$$+ k_{1mdm2s}\frac{[Mdm2_{cp}]}{(j_{1mdm2s} + [Mdm2_{cp}])}$$
$$- k_{mdm2s}[Akt^*]\frac{[Mdm2_c]}{(j_{mdm2s} + [Mdm_{2c}])} \tag{A.13}$$

$$\frac{d[Mdm2_{cp}]}{dt} = k_{mdm2s}[Akt^*]\frac{[Mdm2_c]}{(j_{mdm2s} + [Mdm2_c])}$$
$$- k_{1mdm2s}\frac{[Mdm2_{cp}]}{(j_{1mdm2s} + [Mdm2_{cp}])} - k_i[Mdm2_{cp}]$$
$$+ k_0[Mdm2_n] - k_{dmdm2c}[Mdm2_{cp}] \tag{A.14}$$

$$\frac{d[Mdm2_n]}{dt} = k_i[Mdm2_{cp}] - k_0[Mdm2_n] - k_{dmdm2n}[Mdm2_n] \tag{A.15}$$

$$\frac{d[Akt^*]}{dt} = k_{acakt} * [PIP3] * \frac{[Akt]}{[Akt] + j_{acakt}} - k_{deakt} * \frac{[Akt^*]}{[Akt^*] + j_{deakt}} \tag{A.16}$$

$$[Akt] = Akt_{tot} - [Akt^*] \tag{A.17}$$

$$\frac{d[PIP3]}{dt} = k_{p2}\frac{[PIP2]}{[PIP2] + j_{p2}} + k_{p3}[PTEN]\frac{[PIP3]}{[PIP3] + j_{p3}} \tag{A.18}$$

$$PIP2 = PIP_{tot} - PIP3 \tag{A.19}$$

$$\frac{d[p53k]}{dt} = k_{p46} * [P53DINP1] * \frac{[p53A]}{j_{p46} + [P53A]} - k_{dp46} * [Wip1]$$
$$* \frac{[p53k]}{j_{dp46} + [p53k]}$$

(A.20)

$$[p53_{arrester}] = [p53^*] - [p53_{killer}]$$

(A.21)

$$\frac{d[Wip1]}{dt} = k_{swip10} + k_{swip1} \frac{[p53Arrester]^3}{(j_{swip1}{}^3 + [p53Arrester]^3)} - k_{dp21}[Wip1]$$

(A.22)

$$\frac{d[p53DINP1]}{dt} = k_{sdinp10} + \frac{k_{sdinp11}[p53_{arrester}]^3}{J^3_{sdinp11} + [p53arrester]^3} d$$
$$+ \frac{k_{sdinp12}[p53killer]^3}{[p53killer]^3 + J^3_{sdinp12}} - k_{ddinp1}[p53DINP1]$$

(A.23)

$$\frac{d[PTEN]}{dt} = k_{spten0} + k_{spten} \frac{[P53_{killer}]^3}{[P53_{killer}]^3 + j_{spten}{}^3} - k_{dpten}[PTEN]$$

(A.24)

$$\frac{d[p21]}{dt} = k_{sp210} + k_{sp21} - \frac{[p53_{arrester}]^3}{J^3_{sp21} + [p53_{arrester}]^3} - k_{dp21}[p21]$$

(A.25)

$$\frac{d[p53AIP1]}{dt} = k_{saip10} + \frac{k_{saip1}[p53_{killer}]^3}{J^3_{saip1} + [p53_{killer}]^3} - k_{daip1}[p53AIP1]$$

(A.26)

$$\frac{d[CytoC]}{dt} = k_{accytoc0} + \frac{k_{accytoc1}[p53AIP1][Casp3]^4}{[Casp3]^4 + j^4_{casp3}} (CytoC_{tot} - [CytoC])$$
$$- k_{decytoc}[CytoC]$$

(A.27)

$$\frac{d[Casp3]}{dt} = \left(k_{accasp30} + \frac{k_{accasp31}[Cytc]^4}{([Cytc]^4 + j^4_{cytoc})} \right) (Casp3_{tot} - [Casp3])$$
$$- k_{decasp3}[Casp3]$$

(A.28)

Appendix-2: Gillespie Algorithm Implementation for 2-lesion Kinetic Model

```
%Gillespie Algorithm Implementation of 2-Lesion Kinetic Model
% References for 2-Lesion Kinetic Model
% 1) Stewart, R. D. (2001). Two-lesion kinetic model of double-strand break
% rejoining and cell killing. Radiation Research, 365-378.
% 2) Ma, L., Wagner, J., Rice, J. J., Hu, W., Levine, A. J.,
% & Stolovitzky., G. A. (2005). A plausible model for the digital response
% of p53 to DNA damage. Proceedings of the National Academy of Sciences of
% the United States of America, 14266-14271.
% 3)Zhang, X.-P., Liu, F., & Wang, W. (2011). Two-phase dynamics of p53 in
% the DNA damage response. Proceedings of the National Academy of Sciences,
% 8990-8995.
% Author: Gökhan Demirk?ran
% Electrical and Electronics Engineering / Yasar University
% email: gokhan.demirkiran@yasar.edu.tr
% Website:  gdemirkiran.yasar.edu.tr
% 28 July 2017, last revision: 28 July 2017
clc,clear
    IRy=5; % IRy:=IR dose. Change it to 3 or 5
                    meanValue=35*IRy;
                  nrp= 20; nfrp=20;   %number of free repair proteins
%                  nd0=poissrnd(meanValue);
                  nd0=300;
                  nd1=round(0.7*nd0) ; %Simple DSB repair, 0.7
                  nd2=round(0.3*nd0) ; %Complex DSB repair, 0.3
%
  nc1=0;   % boolean state C, tamir DSB-Protein Complex
  nc2=0;   %
  nf1=0;   % boolean F state, Fixed.
  nf2=0;   %
  kfb1=2;  %Association rate of repair proteins in fast kinetics
  kfb2=0.2;%Association rate of repair proteins in slow kinetics

  krb1=0.5;%Dissociation rate of repair proteins in fast kinetics
  krb2= 0.05;%Dissociation rate of repair proteins in slow kinetics
  kcross= 0.001;%DSB binary mismatch rate
  kfix1= 0.03;%DSB ligation rate in fast kinetics
  kfix2= 0.003;%DSB ligation rate in slow kinetics

RP=20; % maximum number of repair proteins available
time = 0;
nd=0;k=2;nf=0;
% for k = 2:3000

while (nf (k-1) < nd0)
   pd1c1=(RP-nc1-nc2)*(kfb1 + kcross*(nd1 + nd2))*nd1;
            pc1d1=krb1*nc1;
```

```matlab
pc1f1=kfix1*nc1;
pc2d2=krb2*nc2;
pd2c2=(RP-nc1-nc2)*(kfb2 + kcross*(nd1+nd2))*nd2;
pc2f2=kfix2*nc2;


% r=rand(1,4);
a0_=[pd1c1 pc1d1 pc1f1 pc2d2 pd2c2 pc2f2];
% index=find(a0_ ~=inf );
a0=sum(a0_);
r_=rand(1,6);
%   taus=-log(r)./a0_;
  taus=-log(r_)./a0_;
%   index=find(taus ==-inf );
%   taus(index)=inf;
  [tau , mu]=min(taus);
  %   [tau mu]=min(taus);
%    r=r_(2);t=k+1;
%                 if r<p1 && nrp>0   % 0<r2p1 d1c1
if  tau==inf
   tau=1;
end
if mu ==1 && nrp>0 && nd1>0
%

                    nrp = nrp-1;
                    nc1=nc1+1;
                    nd1=nd1-1;



%                 elseif p1<r && r < p2 && nc1>0 %p1<r2p2 c1d1
elseif mu==2 && nc1>0
                    nrp = nrp+1;
                    nc1=nc1-1;
                     nd1=nd1+1;

%                 elseif p1+ p2 <r && r<p3 && nc1>0 % p2<r2p3 c1f1
elseif mu==3 && nc1>0
                %C1 den D1 e geçti
                    nrp = nrp+1;
                    nf1=nf1+1;
                    nc1=nc1-1;



%                 elseif p1+p2+p3<r && r<p4 && nc2>0 % c2d2
elseif mu==4 && nc2>0
                    % C1 den F1 e geçti
                     nrp = nrp+1;
                    nc2=nc2-1;
```

135

```matlab
                        nd2=nd2+1;

%                    elseif p1+p2+p3+p4<r && r<p5 && nd2>0% d2c2
elseif mu==5 && nd2>0
                        nrp = nrp+1;
                        nc2=nc2+1;
                        nd2=nd2-1;

%                    elseif p1+p2+p3+p4+p5<r && r<p6 &nc2>0%c2f2
elseif mu==6 && nc2>0
                        nrp = nrp+1;
                        nf2=nf2+1;
                        nc2=nc2-1;
                        disp('here')

end


                    nd(k)=nd1+nd2;
                    nc(k)=nc1+nc2;
                    nf(k)=nf1+nf2;
%                    time(k+1)=time(k) + tau;
            time(k)=time(k-1) + tau;
    k = k + 1;
end
%% Figure
figure
plot(time,nc,'b'), hold on, grid on
xlabel('minutes'),ylabel('n_c the number of DSBCs')

figure
plot(time,nd,'r.-','Linewidth',1), hold on, grid on
plot(time,nf,'g:','Linewidth',2)
xlabel('minutes'),%ylabel('the number')
legend('the number of DSBs in DNA','the number of DSBs repaired')
```

Appendix-3: Reduction Process of 6-dimensional Oscillator Subsystem

ATM sensor subsystem consists of two differential equations, as shown by equations S1 and S2, while S3 is an algebraic expression.

$$\frac{d[ATM_2]}{dt} = 0.5 k_{dim}[ATM]^2 - k_{undim}[ATM_2] \tag{S1}$$

$$\frac{d[ATM^*]}{dt} = k_{acatm} \frac{n_c}{n_c + j_{nc}}[ATM^*]\frac{[ATM]}{([ATM] + j_{acatm})}$$

$$- k_{deatm}(1 + Wip1)\frac{[ATM^*]}{([ATM^*] + j_{deatm})} \tag{S2}$$

$$[ATM] = ATM_{tot} - 2*[ATM_2] - [ATM^*] \tag{S3}$$

Since ATM* is an active protein that effects downstream modules, we eliminate ATM₂ by quasi-steady state assumption and keep ATM* as a variable. Thus, equating (S1) to zero, $\frac{d[ATM_2]}{dt} = 0$, then we can obtain [ATM₂] as an algebraic expression as below:

$$[ATM_2] = 0.5 * \frac{k_{dim}}{k_{undim}} * [ATM]^2$$

Then, putting $[ATM_2]$ expression into Equation (S3) to obtain:

$$[ATM] = ATM_{tot} - 2*0.5\frac{k_{dim}}{k_{undim}}[ATM]^2 - [ATM^*]$$

$$[ATM] + 2*0.5*\frac{k_{dim}}{k_{undim}}*[ATM]^2 = ATM_{tot} - [ATM^*]$$

Where $k_{dim} = 10$ and $k_{undim} = 1$. Replacing the values of k_{dim} and k_{undim} and after a few arrangements in the equation, we obtain [ATM] as in (S6):

$$[ATM] + 10*[ATM]^2 = ATM_{tot} - [ATM^*] \tag{S4}$$

$$10*[ATM]^2 \cong ATM_{tot} - [ATM^*] \tag{S5}$$

$$[ATM] = \sqrt{0.1*(ATM_{tot} - [ATM^*])} \tag{S6}$$

Putting the Equation (S6) in appropriate places in Equation (S2), then Equations (S1)-(S3) turn into one reduced differential equation as below (S7).

$$\frac{d[ATM^*]}{dt} =$$

$$k_{acatm} \frac{n_c}{(n_c + j_{nc})}[ATM^*]\frac{\sqrt{0.1*(ATM_{tot} - [ATM^*])}}{(\sqrt{0.1*(ATM_{tot} - [ATM^*])} + jacatm)} - kdeatm*(1 +$$

$$Wip1)\frac{[ATM^*]}{([ATM^*] + j_{deatm})} \tag{S7}$$

After eliminating ATM sensor subsystem into one dimension, now we eliminate p53 subsystem completely writing it as an algebraic equation. p53 subsystem equations are written as below (S8) – (S10):

$$k_{acp53} = k_{acp531} \frac{[ATM^*]}{([ATM^*] + j_{atm})} \tag{S8}$$

$$\frac{d[p53^*]}{dt} = k_{acp53}[p53] - k_{dep53}[p53^*] - k_{dp53s}[Mdm2_n] \frac{[p53^*]}{j_{1p53n} + [p53^*]} \tag{S9}$$

$$\frac{d[p53]}{dt} = k_{sp53} - k_{dp53n}[p53] - k_{dp53}[Mdm2_n] \frac{[p53]}{j_{1p53n} + [p53]}$$
$$- k_{acp53}[p53] + k_{dep53}[p53^*] \tag{S10}$$

Equation (S8) is an algebraic expression while (S9) and (S10) are differential equations. Since p53* is the active protein, we want to write [p53*] as an algebraic equation by embedding (S8) and (S10) into (S9).

The rational term $\frac{[p53]}{j_{1p53n}+[p53]}$ in (S10) makes it hard to write [p53] as an algebraic expression. Thus, we eliminate this term by linearizing. $j_{1p53n} = 0.1$ and [p53] changes between 0.4 and 1.4 in the oscillation phase. Thus, an appropriate elimination is:

$$\frac{[p53]}{0.1 + [p53]} \cong 0.1333 * [P53] + 0.7467$$

Putting this linearized expression into Equation (S9) and then equating (S9) to zero, then [p53] becomes a function of $[Mdm2_n]$ and $[p53^*]$ as shown in Equation (S11):

$$[p53_{linearized}] = \frac{(k_{sp53} - k_{dp53}[Mdm2n]\ 0.7467 + k_{dep53} *[P53^*])}{k_{dp53n} + k_{dp53}[Mdm2n]\ 0.1333 + k_{acp53}(ATM^*)} \tag{S11}$$

Replacing [p53] in Equation (S9) with p53$_{linearized}$, (S9) becomes:

$$\frac{d[p53^*]}{dt} = k_{acp53}(ATM^*)[p53_{linearized}] - k_{dep53}[P53^*] - k_{dp53s}[Mdm2_n] \frac{[P53^*]}{(j_{1p53n} + [P53^*])}$$

To write (S9) as an algebraic equation with quasi-steady state assumption, we need to linearize the rational term $\frac{[P53^*]}{(j_{1p53n}+[P53^*])}$:

$$\frac{[p53^*]}{0.1 + [p53^*]} \cong 0.667 * [p53^*]$$

Replacing the linearized term, (S9) becomes:

$$\frac{d[p53^*]}{dt} = k_{acp53}(ATM^*)[p53_{linearized}] - k_{dep53}[p53^*] - k_{dp53s}[Mdm2_n]0.667[p53^*]$$

Equating $\frac{d[p53^*]}{dt} = 0$ and after several simplifications linearized [p53*] equation is found as:

$$[p53^*] = [ATM^*](1.5 - 3.947 * [Mdm2_n])$$ (S12)

Note that in the oscillator model, [p53*] consists of [p53arrester] since [p53killer] appears in the second phase. Thus Equation (S13) can also be written for [p53arrester]:

$$[p53arrester] = [ATM^*](1.5 - 3.947 * [Mdm2_n])$$ (S13)

So far, we have obtained [ATM*] dynamics as one dimensional differential (S7) as in Equation 1 of Table 3, [p53arrester] equation as an algebraic equation (S13) as in Equation 3 of Table 3. We keep the Wip1 dynamics as in the 17-dimensional model of two-phase dynamics by (Zhang, Liu, & Wang, 2011) without changing it, which is the Equation 2 of Table 3 and shown below:

$$\frac{d[Wip1]}{dt} = k_{swip10} + k_{swip1}\frac{[p53Arrester]^3}{(j_{swip1}^3 + [p53Arrester]^3)} - k_{dwip1}[Wip1]$$

Appendix-4: 50 Different Parameter Sets for Canonical Model

No	a	b	c	d	m	n	z	τ_1	τ_2
1	5.0209	17.12	27.79	126.1	1.9378	0.955	0.9689	1.8657	1.6416
2	5.0535	10.642	22.372	99.108	1.2959	1.0538	0.5301	1.0347	1.8762
3	8.7593	10.839	17.838	138.66	2.2641	1.1356	0.6244	1.6531	1.5783
4	9.1103	12.306	17.493	130.72	1.8097	1.2742	0.6398	1.3109	1.8913
5	8.2067	12.652	25.14	135.31	2.0498	1.4931	0.9099	1.7331	1.4492
6	5.6706	11.089	29.631	99.129	2.3581	1.5042	0.9812	1.9084	1.6169
7	5.5745	10.999	16.195	75.366	1.6907	1.4969	0.8856	1.1036	1.7844
8	6.4169	11.481	26.243	108.04	1.5568	1.0424	0.9725	1.269	1.4662
9	5.3024	15.441	19.245	104.85	1.2763	1.1886	0.8707	1.0197	1.081
10	9.2123	13.203	16.457	138.13	1.439	1.2103	0.5696	1.5723	1.0267
11	5.9189	10.88	17.139	135.65	2.3805	1.5236	0.8279	1.6314	1.7493
12	7.2253	10.689	15.021	132.81	2.1227	1.5568	0.6729	1.0928	1.5578
13	5.0515	15.863	27.142	125.67	2.0571	1.2064	0.6549	1.9249	1.0387
14	5.2968	19.503	24.189	128.15	1.8677	1.2867	0.7677	1.4982	1.4182
15	5.3466	10.636	20.874	128	1.5263	1.4012	0.703	1.7573	1.2291
16	9.8628	10.531	28.875	123.84	2.304	1.4156	0.8358	1.3264	1.1789
17	8.4851	10.769	23.066	125.95	1.7307	1.269	0.6507	1.3919	1.8143
18	7.1407	15.283	16.929	136.94	2.1734	1.3604	0.9142	1.0978	1.9888
19	5.0812	12.731	20.776	121.36	1.5864	1.1525	0.6687	1.6537	1.3597
20	7.1089	13.441	20.572	108.89	1.7636	1.4713	0.5115	1.9452	1.1387
21	8.2516	11.69	20.461	111.75	2.07	1.1941	0.7524	1.4182	1.9613
22	5.0151	17.634	28.197	131.7	1.4261	1.3127	0.6729	1.5713	1.9192
23	6.9617	15.356	29.715	138.33	2.0306	1.1856	0.7252	1.4996	1.2341
24	5.8301	11.86	26.428	94.577	1.7061	1.2836	0.5235	1.7615	1.5143
25	7.8975	10.737	25.766	133.23	2.3792	0.8742	0.7135	1.3052	1.4573
26	6.0818	13.974	29.208	138.39	1.8361	0.8353	0.9341	1.2738	1.4292
27	5.5719	11.778	26.681	108.87	2.4673	1.4248	0.62	1.8025	1.6174
28	6.8383	11.661	25.078	121.36	1.7059	0.9424	0.8664	1.2608	1.3351
29	5.8388	17.214	15.002	121.4	2.0977	1.5446	0.8059	1.4089	1.453
30	5.3446	17.84	25.828	110.95	2.019	1.2055	0.6046	1.0415	1.1061
31	7.9395	13.235	28.649	139.83	1.3076	1.4879	0.8207	1.98	1.953
32	5.4353	13.375	20.663	123.3	1.7794	1.1154	0.8753	1.357	1.5556
33	5.3232	14.714	15.089	103.68	1.6175	0.9615	0.7052	1.8081	1.1067
34	7.3545	11.069	29.768	119.32	2.1178	1.1811	0.9609	1.3665	1.131
35	5.921	11.868	23.621	136.7	1.3123	0.9463	0.8032	1.3352	1.5205
36	5.923	15.52	18.281	115.04	1.5717	0.9473	0.6165	1.4021	1.4503
37	9.2254	10.327	26.125	117.87	1.5772	1.389	0.773	1.2926	1.456
38	8.4171	10.746	25.425	134.71	1.989	0.8123	0.7816	1.3968	1.5504
39	5.4594	13.896	21.802	95.995	1.2891	1.4556	0.8569	1.7038	1.7871
40	7.8192	10.072	27.887	130.63	1.4354	1.0149	0.6757	1.0578	1.8924

41	7.3576	17.659	16.837	139.6	2.1269	1.5634	0.6312	1.0651	1.9401
42	6.7013	13.336	28.884	138.98	2.3738	1.5457	0.627	1.0751	1.1369
43	8.7309	12.818	21.682	128.92	1.2863	1.3213	0.684	1.6192	1.0259
44	7.8115	11.771	16.074	124.96	2.2419	1.2606	0.8541	1.5298	1.2733
45	6.4779	15.933	23.787	130.25	1.3619	0.8699	0.7971	1.3681	1.5901
46	5.8083	11.208	17.098	91.068	2.2725	1.2668	0.753	1.7667	1.1483
47	5.5116	11.126	23.337	84.206	1.5012	0.9302	0.5632	1.6161	1.8808
48	5.1722	17.254	28.05	137.07	1.6459	1.4892	0.6163	1.5661	1.7827
49	8.0961	10.481	19.835	129.93	1.5057	0.9452	0.8977	1.6292	1.305
50	6.8875	10.022	18.605	119.65	1.6656	0.9891	0.83	1.2855	1.62